


For Reference

NOT TO BE TAKEN FROM THIS ROOM

Ex LIBRIS
UNIVERSITATIS
ALBERTAENSIS





Digitized by the Internet Archive
in 2023 with funding from
University of Alberta Library

<https://archive.org/details/Green1973>

copy

THE UNIVERSITY OF ALBERTA

RELEASE FORM

NAME OF AUTHOR: Peter Watson Green

TITLE OF THESIS: A study of the Gamma-Ray Decay of The
Low-Lying Levels of ^{64}Cu

DEGREE FOR WHICH THESIS IS PRESENTED: Doctor of Philosophy

Permission is hereby granted to THE UNIVERSITY OF ALBERTA LIBRARY to reproduce single copies of this thesis and to lend or sell such copies for private, scholarly or scientific research purposes only.

The author reserves other publication rights, and neither the thesis nor extensive extracts from it may be printed or otherwise reproduced without the author's written permission.

THE UNIVERSITY OF ALBERTA

A STUDY OF THE GAMMA-RAY DECAY
OF THE LOW-LYING LEVELS OF ^{64}Cu

by



Peter Watson Green

A THESIS

SUBMITTED TO THE FACULTY OF GRADUATE STUDIES AND RESEARCH
IN PARTIAL FULFILMENT OF THE REQUIREMENTS FOR THE DEGREE
OF DOCTOR OF PHILOSOPHY

DEPARTMENT OF PHYSICS

EDMONTON, ALBERTA

FALL, 1973

THE UNIVERSITY OF ALBERTA
FACULTY OF GRADUATE STUDIES AND RESEARCH

The undersigned certify that they have read, and
recommend to the Faculty of Graduate Studies and Research,
for acceptance, a thesis entitled A Study of the Gamma-Ray
Decay of The Low-Lying Levels of ^{64}Cu
submitted by Peter Watson Green
in partial fulfilment of the requirements of the degree of
Doctor of Philosophy.

ABSTRACT

This work deals with a study of the levels of the odd-odd nucleus ^{64}Cu , using the $^{64}\text{Ni}(p,n\gamma)^{64}\text{Cu}$ reaction. Spin assignments, γ -ray multipole mixing ratios and γ -decay branching ratios have been determined for the levels below 1 MeV excitation energy. The experimental level scheme is also compared with the predictions of the Intermediate Coupling model.

Properties of the low-lying excited states of ^{64}Cu were determined by measuring the angular distributions, linear polarization angular distributions and angular triple correlations of the γ rays emitted by these levels. Spin assignments and γ -ray multipole mixing ratios were determined by comparing the experimental data with the predictions of the Statistical Compound Nuclear model. The phase of the mixing ratio employed in this study is consistent with that of Rose and Brink; an extension of their phase consistent formalism to include linear polarization angular distributions and $\gamma - \gamma$ triple angular correlations is presented in an Appendix.

The following spin-parity assignments have been deduced for levels in ^{64}Cu : 159 keV ($J = 2$), 278 keV ($J^\pi = 2^{(+)}$), 344 keV ($J^\pi = 1^+$), 362 keV ($J = 3$), 574 keV ($J = 4(2)$), 609 keV ($J^\pi = 2^{(+)}$), 663 keV ($J = 1$), 739 keV ($J = (2,3)$), 746 keV ($J = 3$), 878 keV ($J = 0$), 895 keV ($J = 3$) and 927 keV ($J = 1(3)$). Multipole mixing ratios have also been determined for most of the γ decays between these levels. The results obtained in this experiment are compared with previous works.

The properties of the low-lying energy levels of ^{64}Cu have been calculated using the Intermediate Coupling model. The results of these calculations are in reasonable agreement with the excitation energies and single particle spectroscopic factors for many of the levels below 1 MeV excitation, although there are some aspects of the experimental spectrum which are not well reproduced. Suggestions are made for possible improvements to the calculation.

ACKNOWLEDGEMENTS

I would like to express my appreciation to my supervisor, Dr. D.M. Sheppard, for his encouragement and assistance throughout all phases of this project.

I am grateful to Dr. W.C. Olsen for his support, and for many helpful discussions, concerning not only this project but many other aspects of nuclear physics as well.

I wish to thank all of my colleagues who helped with the data collection; Ed Wong, Georges Corola, Peter Johnson, Woon Chung, and especially Mark Drum, who initiated the work on ^{64}Cu , and was always available when help was needed most.

I am very grateful to Dr. Barry Robertson, for many enlightening discussions, and for his assistance during the initial stages of this project.

A special thanks goes to "Uncle Jock" Elliott, for his patient and seemingly endless explanations of the ins and outs of van de Graaffitti (usually at four o'clock in the morning), and for generally making life at the NRC exciting. Thanks also to the entire technical and secretarial staff of the NRC.

I am grateful to Dr. W.K. Dawson and Jim Easton for their assistance and advice in computer programming, and for proving to me that computers do, in fact, do what they are told.

I would like to express my appreciation to Dr. Helmy Sherif, whose comments and criticisms regarding the theoretical portion of this work were extremely helpful.

A very special thanks goes to my wife, Lisa, who did such an excellent job of typing the manuscript, in spite of many last-minute changes and unreasonable deadlines.

The financial assistance of the National Research Council of Canada and the University of Alberta is gratefully acknowledged.

To Lisa,

June, 1973.

TABLE OF CONTENTS

CHAPTER		PAGE
1.	MOTIVATION	1
2.	THEORY	5
2.1	Phase Consistency in γ Decay	5
2.2	Angular Correlation Theory	6
	γ -Ray Angular Distribution (Double Correlation)	6
	γ -Ray Linear Polarization Double Correlation ..	8
	γ -Ray Triple Correlations	9
2.3	Measurement of Linear Polarization Using Compton Scattering	11
2.4	The Statistical Compound Nuclear Model	13
2.5	Data Analysis	16
3.	EXPERIMENTAL PROCEDURE	18
3.1	General	18
3.2	Angular Distribution Measurements	19
3.3	Linear Polarization Measurements	20
	Description of the Polarimeter	20
	Linear Polarization Electronics	25
	Experimental Measurements	26
3.4	$\gamma - \gamma$ Angular Correlation Measurements	29
	Choice of Geometries	29

CHAPTER	PAGE
Electronics	30
Data Collection	32
3.5 Data Analysis	33
4. EXPERIMENTAL RESULTS	37
4.1 Branching Ratios	39
4.2 The Levels of ^{64}Cu	41
The 159 and 278 keV Levels	44
The 344 keV Level	48
The 362 keV Level	52
The 574 keV Level	52
The 609 keV Level	56
The 663 keV Level	60
The 739 and 746 keV Levels	64
The 878 keV Level	64
The 895 and 927 keV Levels	69
5. THE INTERMEDIATE COUPLING MODEL	75
5.1 Motivation	75
5.2 Basis for the Model	77
5.3 Formulation of the Model	79
5.4 Application of the Model to ^{64}Cu	82
Energy Levels of ^{63}Cu	82
Energy Levels of ^{64}Cu	85
Spectroscopic Factors	94
5.5 Discussion of the Results	94

CHAPTER	PAGE
6. CONCLUSIONS	98

REFERENCES	100
APPENDIX A. A PHASE CONSISTENT DEVELOPMENT OF γ -RAY POLARIZATION TRIPLE CORRELATIONS	104
APPENDIX B. CUPPLE-1. A DESCRIPTION OF CALCULATIONS IN THE INTERMEDIATE COUPLING MODEL	140

LIST OF TABLES

Table		Page
I	Angles specifying the seven $\gamma - \gamma$ angular correlation geometries of Ferguson (Fe 65).	30
II	A summary of the γ -decay branching ratios for levels below 1 MeV in ^{64}Cu . The results of the present experiment are compared with those of Shera and Bolotin (Sh 68) and Drum (Dr 70).	40
III	Experimental a_2 and a_4 coefficients for the γ ray angular distributions.	42
IV	Experimental a_2 and a_4 coefficients for the A1 and C1 geometries of the $\gamma - \gamma$ triple correlations.	43
V	A summary of the spin assignments and multipole mixing ratios determined in this work.	54
VI	A comparison between the spin assignments determined in the present experiment and those of previous works.	55
VII	A comparison between the mixing ratios determined in the present experiment and those of Davidson <u>et al</u> (Da 70).	63
VIII	Expansion coefficients for the states $ E(\text{keV}); I^\pi\rangle$ in ^{63}Cu .	86
IX	Expansion coefficients for the states $ E(\text{keV}); I^\pi\rangle$ in ^{64}Cu .	89
X	Parameters used in the Intermediate Coupling model calculations.	93
XI	Spectroscopic factors $(2J + 1)S$ for the $^{63}\text{Cu} (d,p) ^{64}\text{Cu}$ reaction, calculated from the Intermediate Coupling model. The calculated values are compared with the experimental results of Park and Daehnick (Pa 69).	95
XII	Reduced matrix elements for the boson creation operators.	158
XIII	Input cards for CUPPLE-I.	159

LIST OF FIGURES

Figure	Page
1. The Compton scattering angle ψ_{MAX} for which the asymmetry ratio R is a maximum, and the value of R for $\psi = \psi_{MAX}$, plotted as a function of the energy of the incident γ ray.	14
2. A typical γ -ray singles spectrum, taken at a proton bombarding energy of 3.75 MeV and an angle of $\theta = 55^\circ$, with the 48 cc detector.	21
3. A schematic diagram of the Compton polarimeter used for the linear polarization measurements.	23
4. A comparison between the asymmetry ratio R_{IDEAL} for a Compton polarimeter consisting of point detectors, and the asymmetry ratio R_{ACTUAL} taking into account finite size effects. The data points are measurements for the ^{60}Co γ rays.	24
5. A block diagram of the electronics used for the linear polarization measurements. The portion inside the dashed line was duplicated for the $\phi = 90^\circ$ analyzing crystal.	27
6. A typical sum-coincidence spectrum, taken at an energy of 3.30 MeV and an angle of $\theta = 90^\circ$.	28
7. A block diagram of the electronics used for the $\gamma - \gamma$ triple correlation measurements. The portion inside the dashed line was duplicated for the NaI crystal in the Al geometry.	31
8. A typical $\gamma - \gamma$ coincidence spectrum, showing γ rays detected in the Ge(Li) which are in coincidence with the 278 keV transition in ^{64}Cu . This spectrum was obtained for the Al geometry at $\theta = 55^\circ$.	34
9. Efficiency curve for the 48cc Ge(Li), measured with ^{57}Co , ^{22}Na , ^{137}Cs , ^{54}Mn and ^{60}Co sources.	35
10. Level scheme for ^{64}Cu , showing spin-parity assignments and γ -decay branching ratios determined in this experiment.	38

11. χ^2 curves for the $278 \rightarrow 0$ angular distribution, showing the dependence of the angular distribution on the parity of the initial state in the decay. 45
12. The 159 keV level: (a) χ^2 curves and (b) angular distribution for the $159 \rightarrow 0$ transition. The 278 keV level: (c) χ^2 curves and (d) angular distribution for the $278 \rightarrow 0$ transition. 46
13. The 278 keV level: (a) χ^2 curves and (b) linear polarization distribution for the 278 keV γ ray. The solid lines in (b) show the expected polarization distributions for values of J^π and δ which gave good fits to the angular distribution 47
14. The 344 keV level: (a) χ^2 curves, (b) angular distribution for the 185 keV γ ray, (c) Al geometry and (d) Cl geometry of the $344 \rightarrow 159 \rightarrow 0$ angular correlation. 49
15. The 344 keV level: (a) χ^2 curves and (b) angular distribution for the $344 \rightarrow 0$ transition. The 362 keV level: (c) χ^2 curves and (d) angular distribution for the $362 \rightarrow 159$ transition. 50
16. The 344 keV level: (a) χ^2 curves and (b) linear polarization distribution for the 344 keV γ ray. 51
17. The 574 keV level: (a) χ^2 curves, (b) angular distribution for the 212 keV γ ray, (c) Al geometry and (d) Cl geometry of the $574 \rightarrow 362 \rightarrow 159$ angular correlation. 53
18. The 609 keV level: (a) χ^2 curves, (b) angular distribution for the 450 keV transition, (c) Al geometry and (d) Cl geometry of the $609 \rightarrow 159 \rightarrow 0$ angular correlation. 57
19. The 609 keV level: (a) χ^2 curves and (b) angular distribution for the 609 keV γ ray. (c) χ^2 curves and (d) angular distribution for the $609 \rightarrow 344$ transition. For (c) and (d), J refers to the spin of the 344 keV level. 58
20. The 609 KeV level: (a) χ^2 curves and (b) linear polarization distribution for the 609 keV γ ray. 59

Figure	Page
21. The 663 keV level: (a) χ^2 curves, (b) angular distribution for the 385 keV transition, (c) Al geometry and (d) Cl geometry for the $663 \rightarrow 278 \rightarrow 0$ angular correlation.	61
22. The 663 keV level: (a) χ^2 curves and (b) angular distribution for the 663 keV transition. (c) χ^2 curves and (d) angular distribution for the $663 \rightarrow 344$ transition.	62
23. The 739 keV level: (a) χ^2 curves, (b) angular distribution for the 580 keV γ ray (c) Al geometry and (d) Cl geometry of the $739 \rightarrow 159 \rightarrow 0$ angular correlation.	65
24. The 739 keV level: (a) χ^2 curves, (b) angular distribution for the 461 keV γ ray (c) Al geometry and (d) Cl geometry of the $739 \rightarrow 278 \rightarrow 0$ angular correlation.	66
25. The 739 keV level: (a) χ^2 curves and (b) angular distribution for the $739 \rightarrow 362$ transition.	67
26. The 746 keV level: (a) χ^2 curves, (b) angular distribution for the 468 keV γ ray (c) Al geometry and (d) Cl geometry of the $746 \rightarrow 278 \rightarrow 0$ angular correlation.	68
27. The 878 keV level: (a) χ^2 curves and (b) angular distribution for the $878 \rightarrow 0$ transition. (c) χ^2 curves and (d) angular distribution for the $878 \rightarrow 159$ transition.	70
28. The 878 keV level: (a) χ^2 curves, (b) angular distribution for the 534 keV γ ray, (c) Al geometry and (d) Cl geometry of the $878 \rightarrow 344 \rightarrow 0$ angular correlation.	71
29. The 895 keV level: (a) χ^2 curves and (b) angular distribution for the $895 \rightarrow 278$ transition. (c) χ^2 curves and (d) angular distribution for the $895 \rightarrow 159$ transition.	72
30. The 927 keV level: (a) χ^2 curves, (b) angular distribution for the 649 keV γ ray (c) Al geometry and (d) Cl geometry of the $927 \rightarrow 278 \rightarrow 0$ angular correlation.	73

Figure	Page
31. The Intermediate Coupling model: Energy levels of the $^{62}\text{Ni} + p$ system as a function of the coupling strength ξ . The best fit to the levels of ^{63}Cu occurs for $\xi = 2.12$.	83
32. A comparison between the experimental energy spectrum of ^{63}Cu , and the level scheme calculated from the Intermediate Coupling model.	84
33. The Intermediate Coupling model: Energy levels of the $^{63}\text{Cu} + n$ system as a function of the coupling strength ξ . The best fit to the levels of ^{64}Cu occurs for $\xi = 1.5$.	87
34. A comparison between the experimental level scheme of ^{64}Cu and the energy levels predicted by the Intermediate Coupling model.	88
35. The Intermediate Coupling model: Energy levels of the $^{64}\text{Ni} + p$ system as a function of the coupling strength ξ . The best fit to the levels of ^{65}Cu occurs for $\xi = 2.10$.	91
36. A comparison between the experimental energy spectrum of ^{65}Cu and the level scheme calculated from the Intermediate Coupling model.	92
37. The Euler angles (α, β, γ) of the rotation R which takes the co-ordinate system S (x, y, z) to $S'(x', y', z')$. This transformation is accomplished by a rotation of angle α about the z axis (to S''), followed by a rotation of angle β about the y'' axis (to S'''), followed by a rotation of angle γ about the z''' axis (to S').	134
38. A schematic diagram of the γ ray cascade $ J_1 M_1\rangle \rightarrow J_2 M_2\rangle \rightarrow J_3 M_3\rangle$.	134

CHAPTER 1

MOTIVATION

The odd-odd nucleus ^{64}Cu has been the subject of several experimental investigations in recent years. The (d,p) and (d, α) measurements of Park and Daehnick (Pa 69) established the level scheme up to about 3 MeV excitation, and measurement of the charged particle angular distributions resulted in the assignment of J^π limits for most of the low-lying excited states. The (n, γ) capture work of Shera and Bolotin (Sh 68) established the γ -decay scheme for the levels below 1322 keV excitation in ^{64}Cu , and provided tentative spin assignments for most of these levels based on the assumption that the predominant mode of decay is via M1 radiation.

Several authors (Ve 61, Mi 62, Ko 65, Ko 69) have carried out measurements on the circular polarization of the γ rays from ^{64}Cu following the capture of polarized thermal neutrons by ^{63}Cu . These measurements generally did not lead to unique spin assignments, and often produced results which were in serious disagreement with other works.

In the last few years, several authors have exploited the $^{64}\text{Ni}(p,n\gamma)^{64}\text{Cu}$ reaction to study the low-lying levels of ^{64}Cu . Davidson et al (Da 70) and Drum (Dr 70) have studied the double correlation (often called the angular distribution) of the γ rays from levels of ^{64}Cu populated in the $^{64}\text{Ni}(p,n)$ reaction, and have presented

spin assignments based on the comparison of the data with the predictions of the Statistical Compound Nuclear model (Sh 63, Sh 65). In several cases, it was not possible to make unique spin assignments on the basis of the angular distribution alone (see Section 2.2.1), and for many of the γ decays, the multipole mixing ratio could not be uniquely determined. While the results of these two studies are generally consistent with each other, several spin assignments do not agree with previous works. Wellborn et al (We 71) have studied $\gamma - \gamma$ triple correlations from ^{64}Cu , again using the $^{64}\text{Ni}(p,n)$ reaction to excite the states of interest. Their results are in agreement with those of Davidson et al (Da 70) and Drum (Dr 70), but this work dealt mainly with the states below 400 keV excitation. Mischenko et al (Mi 72) have studied (n,γ) correlations following the $^{64}\text{Ni}(p,n\gamma)^{64}\text{Cu}$ reaction, and have deduced spin assignments for the first four excited states of ^{64}Cu .

In spite of the wealth of experimental data available for the low-lying states of ^{64}Cu , the situation regarding spin assignments for these levels, especially the levels above 400 keV excitation, and multipole mixing ratios for the γ decays is still somewhat uncertain. For this reason, we decided to re-investigate the γ decay of this nucleus, using a combination of double correlation, linear polarization double correlation and $\gamma - \gamma$ triple correlation measurements to attempt to resolve the present ambiguities.

We have also chosen the $^{64}\text{Ni}(p,n)$ reaction to excite this nucleus, for several reasons. The relatively large cross-section for this reaction will permit measurements to be performed for many of the

weaker γ transitions, and will provide a high enough yield for the coincidence experiments to be feasible. In this region of the periodic table, the mechanism of the (p,n) reaction can be described by the Statistical Compound Nuclear Theory, which can be used to calculate the substate population parameters of the γ -decaying level provided that this state is not populated by a cascade transition from a higher excited state. The endothermic nature of the reaction ($Q = -2.461$ MeV) allows the state of interest to be excited close to threshold, thereby eliminating complications due to cascade feeding. Moreover, the usual target contaminants, carbon and oxygen, have very large negative Q -values for protons, which results in a fairly "clean" γ -ray spectrum.

From a theoretical standpoint, there have been no attempts to apply any of the usual nuclear models to ^{64}Cu . Shell model calculations, in particular, would be exceedingly difficult, due to the prohibitively large configuration space which would be necessary. On the other hand, there is no evidence that nuclei in this region of the periodic table are permanently deformed, so Nilsson model calculations have little chance of success.

The most promising approach to a theoretical study of ^{64}Cu is probably via the Intermediate Coupling model (Ch 54, Ch 67). The even-even nucleus ^{62}Ni shows a characteristic vibrational-type spectrum, and both Gomez (Go 71) and Markham (Ma 71) have given a description of ^{63}Cu as a single proton coupled to this vibrating core.

The success of these calculations for ^{63}Cu suggests that it might be possible to describe low-lying states in ^{64}Cu in terms of two particles (a proton and a neutron) coupled to the surface vibrations of ^{62}Ni .

CHAPTER 2

THEORY

2.1 Phase Consistency in γ Decay

The technique of observing the angular distribution or angular triple correlation of the γ rays emitted by excited nuclear states is a widely used source of information on the properties of these states. In particular, such measurements can be used to determine the multipole mixing ratios (i.e. ratios of reduced matrix elements for different multipoles) of the decay, which are sensitive to the detailed structure of the nuclear wave functions.

The theory of γ -ray angular correlations has been presented by many authors (Bi 53, De 57, Bi 60, Fe 65, Po 65), but these earlier formulations all suffered from the lack of an explicit definition of the phase of the mixing ratio. This in turn made it extremely difficult to compare the sign of a measured mixing ratio with the predictions of a nuclear theory. This problem has been overcome with the development of the theory by Rose and Brink (Ro 67), who adopted the convention that the electromagnetic transition multipole operators $T_{LM}^{<\pi>}$ should transform under time reversal according to the rule

$$\theta T_{LM}^{<\pi>} \theta^{-1} = (-)^{L-M} T_{L-M}^{<\pi>} \quad (2-1)$$

where θ is the time reversal operator.

The work of Rose and Brink (Ro 67) included only the development of the angular distribution formula. In order to make use of their phase consistent theory in the present work, their formalism has been extended to include linear polarization and angular triple correlations as well (Gr 72). This development is given in Appendix A.

The next section contains a brief discussion of the three different measurements which were performed in this experiment, with particular emphasis on what new information can be obtained from each. A detailed derivation of the formulae used can be found in Appendix A.

2.2 Angular Correlation Theory

2.2.1 γ -Ray Angular Distribution (Double Correlation)

The angular distribution of a γ ray refers to the relative intensity of the γ ray yield as a function of angle, and can be expressed in the form

$$W(\theta) = \sum_k a_k P_k(\cos \theta) \quad (2-2)$$

where θ is the angle between the direction of emission and the z-axis. The a_k coefficients in (2-2) depend on the spins of the initial and final nuclear states, the relative amplitudes of the different multipoles contributing to the decay, and the mechanism of the reaction leading to the formation of the initial state.

The amount of useful information which can be extracted from an angular distribution measurement is governed by the number of a_k coefficients present in the expansion (2-2), and this is limited by

the following considerations.

i) If the initial and final states are states of definite parity, and if parity is conserved by the electromagnetic interaction, then the summation over k is limited to even values only.

ii) The subscript k must satisfy the triangle conditions $\Delta(L', L', k)$ and $\Delta(J_1, J_1, k)$, where L' is the highest multipole in the transition, and J_1 is the spin of the initial state. The symbol $\Delta(a, b, c)$ means $|a-b| \leq c \leq a+b$.

Except in very rare cases (see e.g. Li 64), it is a good assumption that multipoles with $L \geq 3$ do not contribute significantly to the decay. It is therefore possible to extract, at most, the a_2 and a_4 coefficient from the data (a_0 is just a normalization factor). Usually, the final spin in the decay is known, so the unknown parameters are the initial spin, a single quadrupole/dipole mixing ratio (δ), and the substate population parameters.

The angular distribution formula (2-2) assumes that the radiation is observed by a point detector. In practice, detectors always have a finite angular spread, and the result of averaging the angular distribution over the solid angle of the detector is to reduce the measured anisotropy of the distribution. Provided that the detector has cylindrical symmetry, one can correct for this effect exactly by multiplying each term in (2-2) by an "attenuation coefficient" Q_k (Ro 53), and the measured angular distribution is

$$W_E(\theta) = \sum_k a_k Q_k P_k(\cos \theta) \quad (2-3)$$

In certain instances, it is possible to adjust the conditions of the experiment so that the population parameters can be calculated from a reaction theory. In the present work, the Statistical Compound Nuclear model has been used, and a brief discussion of the assumptions of this model will be presented in Section 2.4. Even with this additional tool, however, it is often impossible to uniquely determine both the spin and mixing ratio from an angular distribution measurement alone, and it is then necessary to resort to other techniques, such as linear polarization or triple correlation measurements in order to resolve these ambiguities.

2.2.2 γ -Ray Linear Polarization Double Correlation

The electromagnetic multipole fields of order L can be divided into two classes, the electric multipoles (with parity $(-)^L$) and the magnetic multipoles (with parity $(-)^{L+1}$). At large distances from the source of the radiation, the only difference between the electric and magnetic multipole fields is that the electric and magnetic vectors of the radiation are both rotated through an angle of $\pi/2$ about the direction of propagation. In order to measure the parity of the radiation, it is therefore necessary to determine the direction of the electric (or magnetic) vector.

The linear polarization of a γ ray is defined as the direction of the electric vector. If ϕ is the angle between the reaction plane (the plane containing both the z -axis and the γ ray) and the

polarization direction of the radiation, the angular distribution of linearly polarized photons is given by

$$W(\theta, \phi) = \sum_k \{ a_k P_k(\cos \theta) + (-)^{\pi'} \cos 2\phi a_k' P_k^2(\cos \theta) \} \quad (2-4)$$

where the index π' is zero if the L' radiation is electric and one if it is magnetic. The degree of linear polarization is defined as

$$\begin{aligned} p(\theta) &= \frac{W(\theta, 0^\circ) - W(\theta, 90^\circ)}{W(\theta, 0^\circ) + W(\theta, 90^\circ)} \\ &= \frac{1}{W(\theta)} \sum_k (-)^{\pi'} a_k' P_k^2(\cos \theta) \end{aligned} \quad (2-5)$$

since this limits $p(\theta)$ to lie between +1 and -1, with $p(\theta) = 0$ for an unpolarized γ ray.

Apart from the dependence of the linear polarization double correlation on the parity of the radiation (and hence on the relative parities of the initial and final nuclear states), the measurement of the coefficients a_k' in (2-5) can give further information on the spins and mixing ratio. For example, there are certain values of δ for which the angular distribution will be isotropic, but the γ ray may nevertheless be strongly polarized (Gr 71), and a measurement of $p(\theta)$ can eliminate some possible spin assignments.

2.2.3 γ -Ray Triple Correlations

A third method of obtaining additional information about the decay is through the measurement of two γ rays in coincidence. The $\gamma - \gamma$ triple correlation can be expressed in the form

$$W(\theta_1, \theta_2, \phi) = \sum_{k_1 k_2 k_3} a_{k_1 k_2 k_3} P_{k_1 k_2 k_3}(\theta_1, \theta_2, \phi) \quad (2-6)$$

and, as before, the $a_{k_1 k_2 k_3}$ coefficients are functions of the spins and multipoles involved in each of the decays, and also of the population parameters of the initial state. The subscripts k_1 , k_2 and k_3 are limited to even values only, and are also governed by the restrictions $\Delta(J_1, J_1, k_1)$, $\Delta(L_1', L_1', k_2)$, $\Delta(L_2', L_2', k_3)$, $\Delta(J_2, J_2, k_3)$ and $\Delta(k_1, k_2, k_3)$. If multipoles higher than quadrupole do not contribute to either decay, there are a maximum of 19 coefficients which can be determined experimentally, and although the number of unknown parameters is increased, there are enough measurements possible to overdetermine the problem.

In practice, the number of unknowns in the problem is unlikely to exceed about five, and it is therefore unnecessary to measure all of the 19 coefficients in equation (2-6). Instead, it is usually sufficient to determine certain linear combinations of these coefficients, by measuring the correlation in one or more "geometries", in which two of the three angles θ_1 , θ_2 , ϕ are held fixed, and the third is allowed to vary. If the fixed angles are chosen properly, it is possible to write the correlation as an ordinary Legendre polynomial series, by using the expansion

$$P_{k_1 k_2 k_3}(\theta_1, \theta_2, \phi) = \sum_k \alpha_{k_1 k_2 k_3}^k P_k(\cos \theta) \quad (2-7)$$

where θ is the single variable angle. The index k takes on even values only, and is limited to $0 \leq k \leq 4$ if multipoles higher than quadrupole

are not included. Finite geometry effects are taken into account by multiplying each term in equation (2-6) by the factor $Q_{k_2} Q_{k_3}$, where Q_{k_2} is the attenuation coefficient for the detector of the first γ ray in the cascade, and Q_{k_3} is the attenuation coefficient for the detector of the second radiation.

2.3 Measurement of Linear Polarization Using Compton Scattering

In order to measure the linear polarization of a γ ray it is necessary to make use of a process which is sensitive to the direction of the electric vector of the radiation. Although several processes have been suggested (Fa 59), the most commonly used has been Compton scattering, because of the relatively large cross-section and the high sensitivity to linear polarization over an energy range containing most nuclear γ rays of interest.

In practice, the polarization of the scattered quantum is not observed, and the differential cross-section for the Compton scattering of a linearly polarized photon is (Fa 59)

$$\frac{d\sigma}{d\Omega\zeta} = \frac{r_0^2}{2} \left(\frac{k}{k_0}\right)^2 \left(\frac{k}{k_0} + \frac{k_0}{k} - 2 \sin^2\psi \cos^2\zeta\right) \quad (2-8)$$

where $r_0 = e^2/m_0c^2$ is the classical radius of the electron, ψ is the Compton scattering angle, and ζ is the angle between the polarization direction of the incident radiation and the scattering plane. k_0 is the energy (in units of m_0c^2) of the incident radiation, and $k = k_0/\{1 + k_0(1 - \cos\psi)\}$ is the energy of the scattered photon.

The linear polarization $p(\theta)$ is measured by observing the number of quanta N_0 and N_{90} which are scattered parallel to the reaction plane and perpendicular to the reaction plane respectively. Neglecting solid angle effects, these numbers are given by (Tw 70)

$$\begin{aligned} N_0 &= W(\theta, 0) d\sigma_0 + W(\theta, 90) d\sigma_{90} \\ N_{90} &= W(\theta, 0) d\sigma_{90} + W(\theta, 90) d\sigma_0 \end{aligned} \quad (2-9)$$

where $d\sigma_0$ and $d\sigma_{90}$ are respectively the Compton cross-sections for scattering parallel to and perpendicular to the plane defined by the propagation direction of the incident γ ray (k_0) and its electric vector. The linear polarization (equation 2-5) can then be calculated from the expression

$$\begin{aligned} p(\theta) &= \frac{1}{R} \left(\frac{N_{90} - N_0}{N_{90} + N_0} \right) \\ R &= \frac{d\sigma_{90} - d\sigma_0}{d\sigma_{90} + d\sigma_0} = \frac{\sin^2 \psi}{\frac{k}{k_0} + \frac{k_0}{k} - \sin^2 \psi} \end{aligned} \quad (2-10)$$

where R , the asymmetry ratio, gives the response of the process to linear polarization.

At low energies, the asymmetry ratio approaches unity for $\psi = 90^\circ$, indicating that Compton scattering exhibits ideal response to linear polarization. Although R decreases quite rapidly with increasing γ -ray energy, Compton scattering has been used successfully for polarization measurements on γ rays of energy as high as 8 MeV (Su 59).

As the photon energy increases, the "best" Compton scattering angle ψ_{MAX} decreases. Suffert et al (Su 59) have shown that, for experiments which are limited primarily by counting statistics, the

best scattering angle is that which maximizes the quantity

$$S(\psi) = R^2 \overline{\sigma}_C \quad (2-11)$$

where $\overline{\sigma}_C$ is the Compton cross-section averaged over polarization.

Figure 1 shows a plot of this angle ψ_{MAX} as a function of energy, as well as the asymmetry ratio R for $\psi = \psi_{MAX}$.

The value of R given by equation (2-10) is an upper limit. In practice, the finite solid angles of the detectors used to measure the linear polarization will reduce the actual asymmetry R of a polarimeter. These effects will be discussed further in Section 3.3.1.

2.4 The Statistical Compound Nuclear Model

The Statistical Compound Nuclear (SCN) model has been used with great success to describe the $(p, n\gamma)$ reaction on medium weight nuclei (Pi 70, Tw 70, Da 70, Mc 70, Ro 71). Since the model has been treated in detail elsewhere (Sh 63, Sh 65, Vo 68), only a general outline will be given here.

On quite general grounds, the differential cross-section for going from a reaction channel α to another channel α' is given by (Vo 68)

$$\begin{aligned} \left(\frac{d\sigma}{d\Omega}\right)_{\alpha\alpha'} &= \frac{1}{k_\alpha^2} \sum_{L=0}^{\infty} P_L(\cos \theta) \sum_i \frac{(-)^{s-s'}}{4(2i+1)(2i'+1)} i^{l_1-l_2-L} Z(l_1 J_1 l_2 J_2; sL) \\ &\times i^{l_1'-l_2'-L} Z(l_1' J_1' l_2' J_2'; s'L) \operatorname{Re}\{(\delta_{\alpha\alpha'} \delta_{l_1 l_1'} \delta_{s s'} - U_{\alpha' s' l_1'}^{J_1} ; \alpha s l_1)^* \\ &\times (\delta_{\alpha\alpha'} \delta_{s s'} \delta_{l_2 l_2'} - U_{\alpha' s' l_2'}^{J_2} ; \alpha s l_2)\} \end{aligned} \quad (2-12)$$

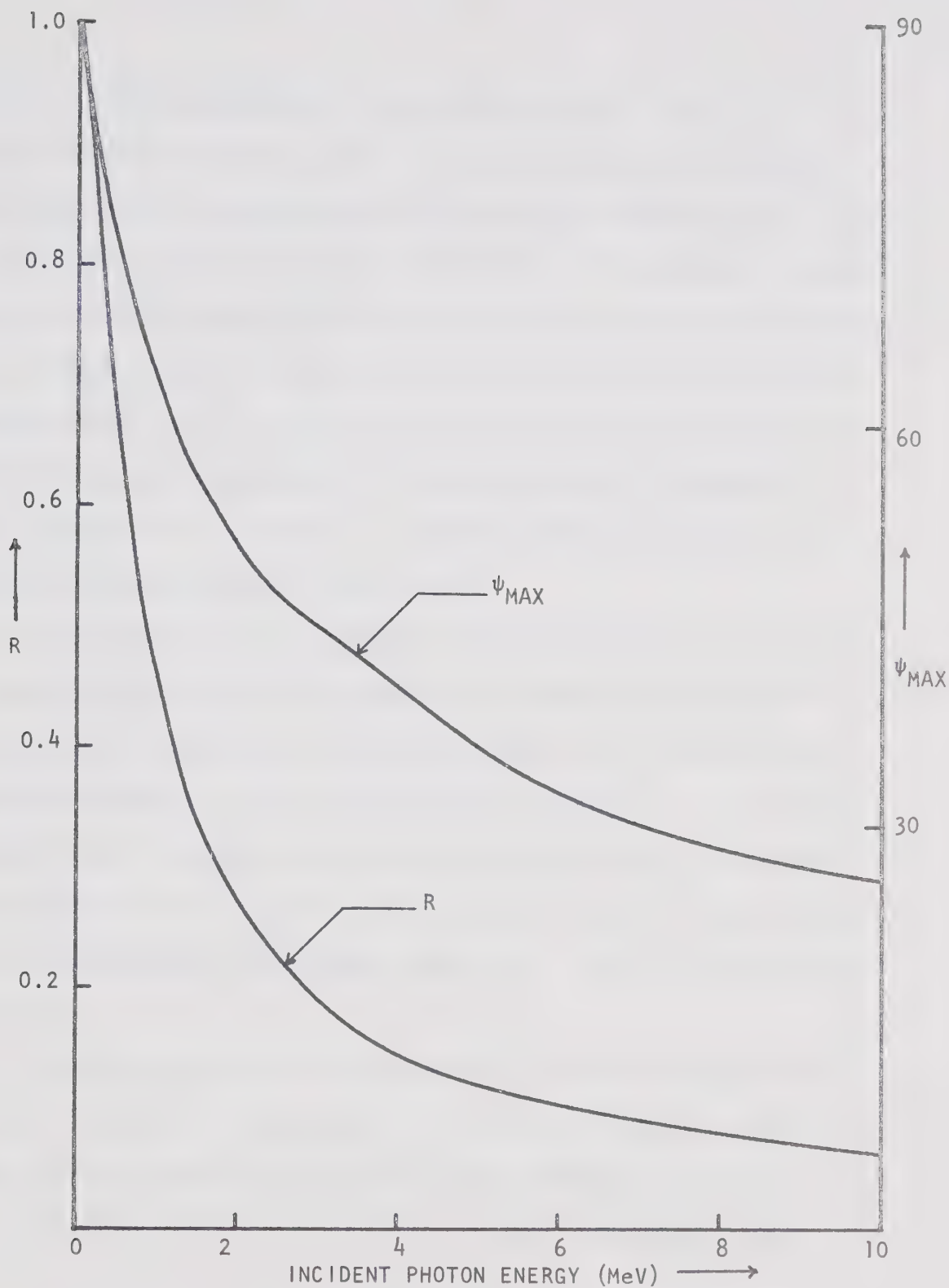


Figure 1. The Compton scattering angle ψ_{MAX} for which the asymmetry ratio R is a maximum, and the value of R for $\psi = \psi_{MAX}$, plotted as a function of the energy of the incident γ ray.

where l is the target spin, i the projectile spin. $s = |\vec{l} + \vec{i}|$ is the initial state channel spin, ℓ is the relative orbital angular momentum of the two particles α in the initial state and $J = |\vec{s} + \vec{\ell}|$ is the total angular momentum of the system. The primed variables refer to similar quantities in the exit channel, and the sum is over all of these indices, as well as the projections m_s and $m_{s'}$ of the channel spins. $U_{\alpha's'\ell';\alpha s\ell}^J$ is an element of the collision matrix, which connects the amplitude of the outgoing wave in channel α' to the incoming wave in channel α . The Z-coefficients contain only angular momentum coupling coefficients.

For compound nuclear processes, it is assumed that the (complex) numbers U vary rapidly with energy about a mean value of zero, and if we therefore average the cross-section over a sufficiently large energy interval, all terms linear in U will vanish. It is further assumed that the energy variations of different components of the scattering matrix are uncorrelated, and the only terms in (2-12) which survive are squares of the matrix elements. This is the statistical assumption.

The compound nucleus assumption states that the decay of the compound nucleus is independent of its mode of formation, and hence each absolute square of a collision matrix element can be written as a formation probability multiplied by a decay branching ratio.

$$U_{\alpha's'\ell';\alpha s\ell}^J = T_{\ell s J}(\alpha) \frac{T_{\ell's'J}(\alpha')}{\sum_{\alpha''s''\ell''} T_{\ell''s''J}(\alpha'')} \quad (2-13)$$

where $T_{\ell SJ}(\alpha) \equiv 1 - |e^{2i\delta_{\alpha\ell}}|^2$ is the optical model transmission coefficient.

Consider specifically the $(p,n\gamma)$ reaction near threshold. Since the quantization axis is chosen along the beam direction, the projection of the incoming orbital angular momentum ℓ is zero, and for the state J in the compound nucleus, only substates with $M \leq l + 1/2$ can be populated. Since the emerging neutron can be emitted in all directions, the projection of its orbital angular momentum is not necessarily zero, but if the neutrons are of low energy, $\ell' = 0$ partial waves will predominate, and only the contributions due to the particle spin can de-align the final state. For $(p,n\gamma)$ reactions near threshold, it is therefore expected that magnetic substates for $M \leq l + 1$ will be very nearly equally populated, and the populations of higher substates will be substantially smaller. If all possible substates in the final nucleus are equally populated, the resulting γ -ray angular distribution will be isotropic, and it is expected therefore that states with final spin $\leq l + 1$ will have isotropic decays.

2.5 Data Analysis

Spin-parity assignments and multipole mixing ratios are determined by comparing the experimental data with the predictions of equations (2-2), (2-5) and (2-6). A quantitative measure of the "goodness of fit" is obtained by calculating the quantity

$$S = \sum_i \frac{(W_i - Y_i)^2}{\sigma_i^2} \quad (2-14)$$

where W_i is the theoretically predicted result for a measurement at the angle θ_i , Y_i is the value actually measured, and σ_i^2 is the variance in Y_i . The measurements Y_i have the Poisson distribution, which approximates the normal distribution if the Y_i are large enough (say ≥ 30). If this approximation is justified, then the minimum value of S has the χ^2 distribution with $N-p$ degrees of freedom, where N is the number of data points, and p the number of parameters which were varied to minimize S . For a single angular distribution measurement, p is equal to 2, since an a_0 coefficient and a mixing ratio δ are fitted to the data.

Spin and mixing ratio combinations are accepted as possible solutions if the minimum value of the statistic S falls below the 0.1% confidence limit of the χ^2 distribution. The meaning of this confidence limit is that, if the theory used is the correct one (i.e. if the assumed spin and mixing ratio are correct), there is only one chance in 1,000 that S would be larger than this value.

For each possible spin and mixing ratio combination, the error in the mixing ratio is then calculated using the 10% confidence limit of the F distribution, as suggested by Cline and Lesser (Cl 70).

CHAPTER 3

EXPERIMENTAL PROCEDURE

3.1 General

In this experiment, targets of Ni metal (enriched to 98% in ^{64}Ni) were prepared by combining the powdered metal with a mixture of polyurethane and benzene, and smearing the resulting glue onto a piece of 0.005" Ta. Targets prepared in this manner were about 2 mg/cm² thick, and the resulting energy loss of ~ 100 keV for the incident protons was assumed to provide sufficient energy averaging over compound nuclear resonances to allow the Statistical Compound Nuclear model to be used.

The targets were bombarded with protons from the University of Alberta CN van de Graaff accelerator, with the beam collimated to a diameter of 1.5 mm at the target position. Beam currents were typically about 300 na.

After a preliminary study of the yield curve to determine the decay scheme of the low-lying levels of ^{64}Cu , four bombarding energies were chosen for further measurements. These energies were 2.75, 3.00, 3.30 and 3.75 MeV, and were chosen to eliminate complications arising from cascade feeding of the levels of interest from higher excited states. Many authors (Pi 69, Da 70, Dr 70) have stated that it is advisable to excite the γ -decaying state near threshold, and hence

ensure that the exit neutrons are essentially pure s-wave, in order to maintain the alignment of the compound nuclear state. We have found, however, that the decrease in alignment at higher bombarding energies (say 500 keV above threshold) is not critical, and the increase in γ -ray yield favours this procedure.

3.2 Angular Distribution Measurements

For the runs at 2.75, 3.00 and 3.30 MeV, the γ rays were detected in a 38 cc Ge(Li) detector*, which had a resolution of typically 3 keV (FWHM) for the 1.332 MeV γ ray from ^{60}Co . Pulses from the detector were fed through an amplifier**, and then into an analog to digital converter[†] which was interfaced to a Honeywell DDP-516 computer. For the runs at 3.75 MeV, a 48 cc detector^{††} was used, which had a resolution of 2.5 keV (FWHM) at 1.332 MeV.

For the runs at 3.30 and 3.75 MeV, measurements were taken at angles of 0° , 31° , 55° , 70° and 90° , since these angles are suitable for rapid extraction of the a_2 and a_4 coefficients from the experimental data (Gr 72a). For the runs at the two lower energies, measurements were taken at $\theta = 45^\circ$ instead of $\theta = 55^\circ$. All angles were repeated once. Since measurements made at the same angle are statistically independent, they were used as separate points in the χ^2 analysis of the data, and were not averaged to give a single point.

* Nuclear Diodes, Inc., model LGCC 5.7 - 2.3

** ORTEC, model 450

† TMC, model 217A

†† ORTEC, model 8101-0724

A typical γ -ray spectrum, taken at a bombarding energy of 3.75 MeV, is shown in Figure 2. γ rays corresponding to transitions in ^{64}Cu are labelled with the energies of the initial and final states in the decay, while contaminant peaks are indicated by the nucleus or the reaction responsible for the transition. The major contaminant peaks are the ^{181}Ta lines at 136, 165 and 301 keV, the ^{23}Na γ ray at 439 keV, the $^{74,72}\text{Ge}(n,n')$ lines at 596 and 692 keV, and the $^{64}\text{Ni}(p,\gamma\gamma)^{65}\text{Cu}$ peaks at 770 and 1115 keV.

For the runs at 2.75, 3.00 and 3.30 MeV, the 770 keV γ ray from the $J = 1/2$ first excited state of ^{65}Cu was used as an internal monitor. At 3.75 MeV, this transition could not be used since it was obscured by the $927 \rightarrow 159$ transition in ^{64}Cu , so one of the previously measured isotropic decays from a low-lying state of ^{64}Cu was used for an internal monitor.

3.3 Linear Polarization Measurements

3.3.1 Description of the Polarimeter

The polarimeter used in this experiment was based on the Compton scattering process. In its simplest form, such a polarimeter consists of a Compton scatterer, and an analyzer to detect the Compton scattered radiation, but in practice, it is usual to also measure the energy deposited in the scatterer and hence reduce background by recording coincidences between the two detectors. A Ge(Li) detector was used as a scatterer in the polarimeter, and a 3" x 3" NaI(Tl)* detector

* Harshaw "Integral line assembly" type 12S 12/3

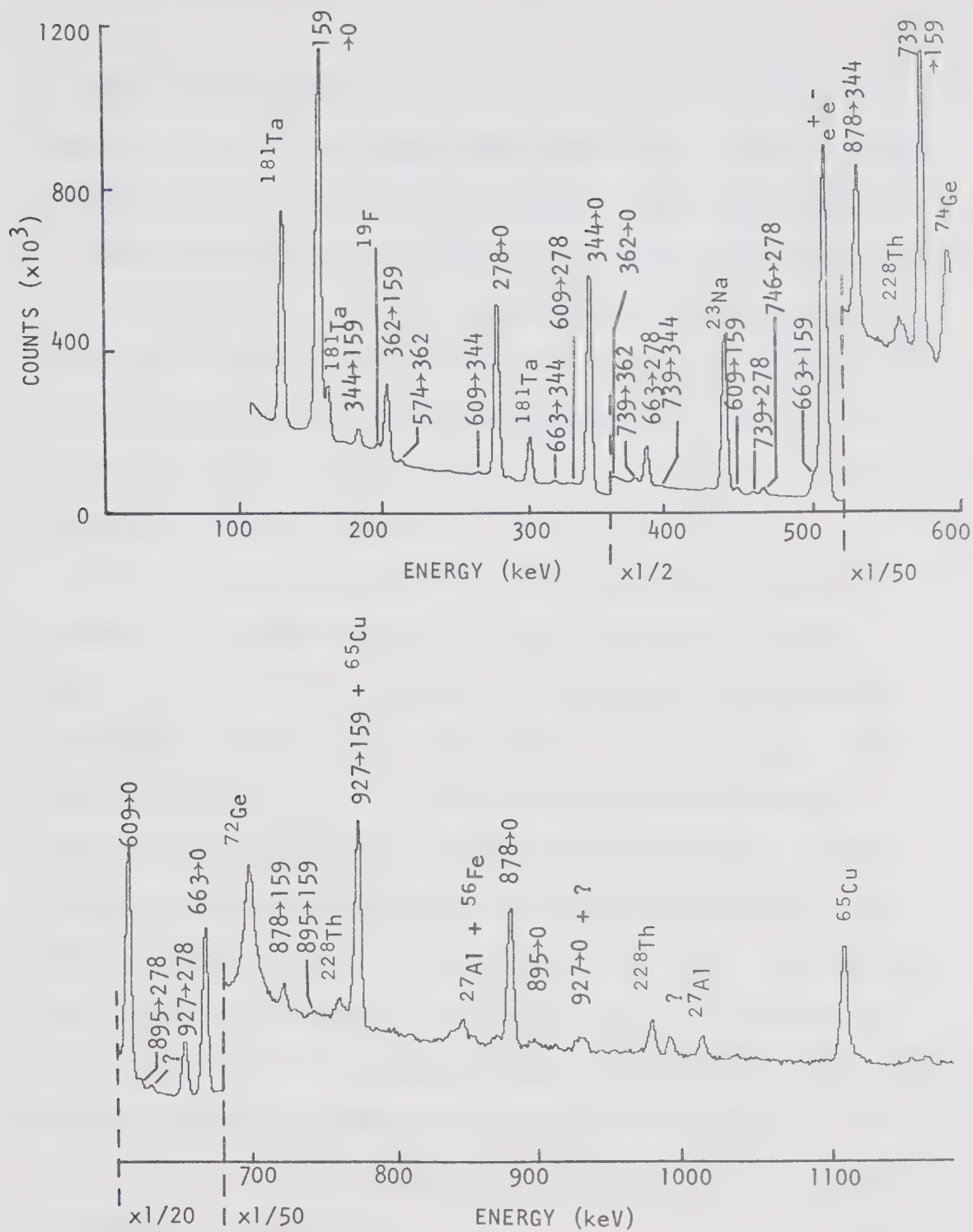


Figure 2. A typical γ -ray singles spectrum, taken at a proton bombarding energy of 3.75 MeV and an angle of $\theta=55^\circ$, with the 48 cc. detector.

was used as an analyzing crystal. .5" of lead were used to shield the analyzing crystal from primary target radiation. The mean Compton scattering angle from scatterer to analyzer was chosen as $\psi = 82^\circ$.

Measurements of the polarization are usually made at two angles, $\phi = 0^\circ$ and $\phi = 90^\circ$. In order to reduce data collection time and errors due to repositioning of the analyzing crystal, the polarimeter was constructed with two analyzing detectors, so that the 0° and 90° measurements could be made simultaneously. A schematic diagram of the polarimeter is shown in Figure 3.

For an ideal polarimeter (i.e. point scatterer and point analyzers), the asymmetry ratio is given by equation (2-10). In practice, the finite solid angles of the detectors must be taken into account, and the ideal value of R is never realized. The actual asymmetry ratio R for the polarimeter was calculated by numerical integration over the scattering and analyzing crystals, following the method outlined by Taras and Matas (Ta 68). The results of these calculations are shown in Figure 4. For energies above 1.5 MeV, the effect of the finite sizes of the detectors is small, but as the incident photon energy decreases, the error incurred by neglecting finite geometry effects becomes progressively larger, and for energies around 300 keV (which is the range we are interested in) can become as large as 30%.

The actual asymmetry of the polarimeter was determined at two energies by measuring the polarization of the ^{60}Co γ rays. The results of these measurements are also shown in Figure 4. The measured values agree with the calculated asymmetry to within 10%,

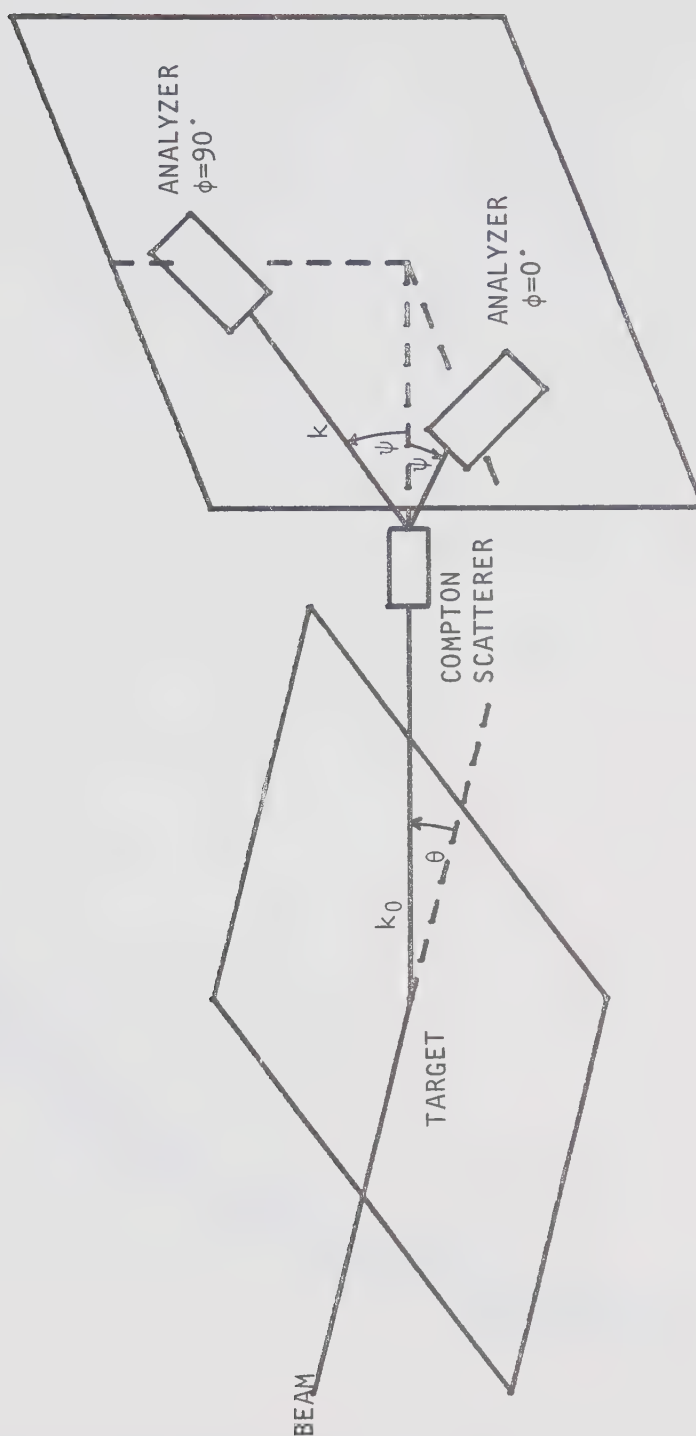


Figure 3. A schematic diagram of the Compton polarimeter used for the linear polarization measurements.

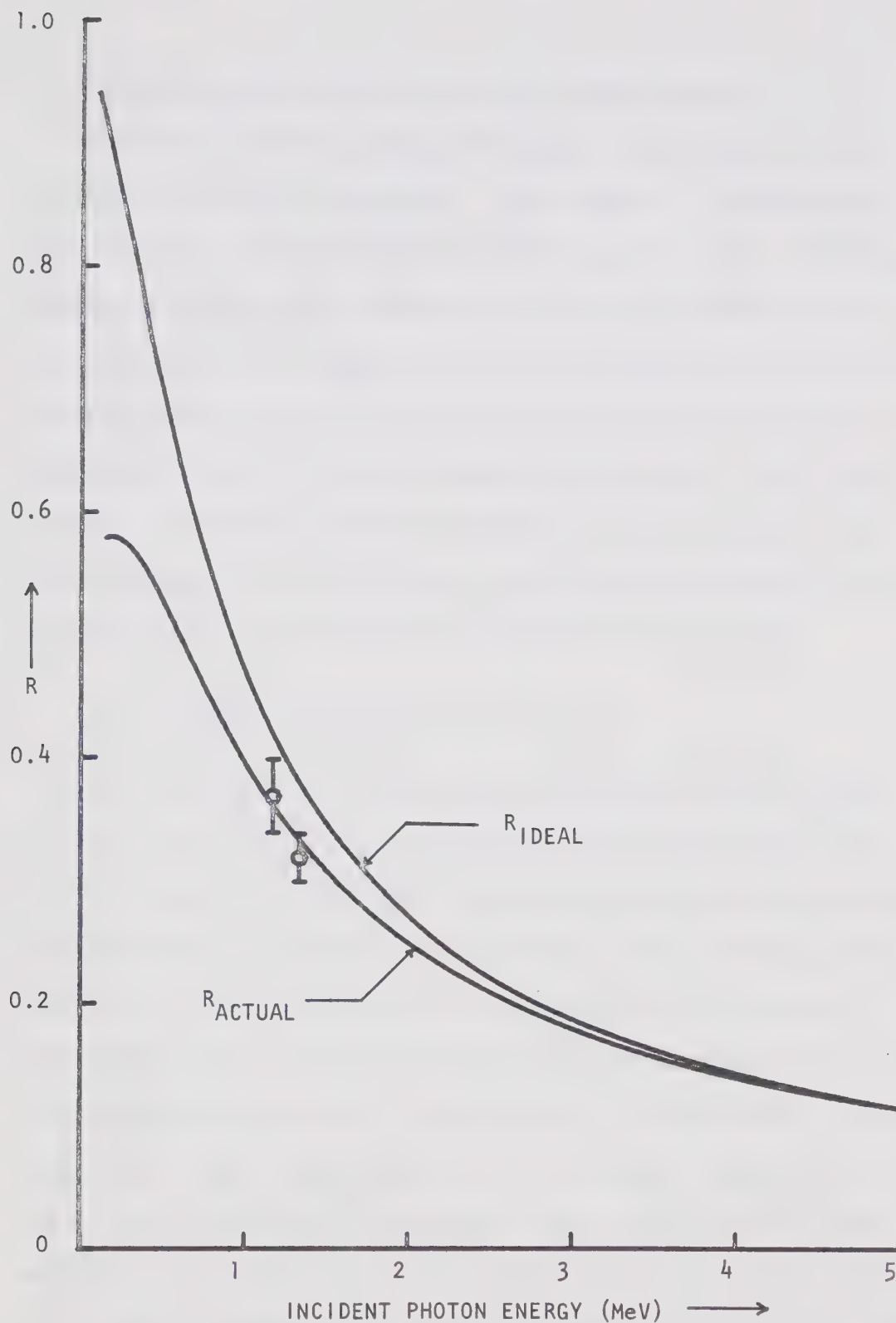


Figure 4. A comparison between the asymmetry ratio R_{IDEAL} for a Compton polarimeter consisting of point detectors, and the asymmetry ratio R_{ACTUAL} taking into account finite size effects. The data points are measurements for the ^{60}Co γ rays.

which was the experimental error in the measurements.

The effects of two consecutive Compton scatterings have been ignored in this calculation of R . This effect is expected to be most important at lower incident photon energies, since the Compton scattering cross-section decreases for increasing photon energy. The agreement (within experimental error) between the calculated results and measured values of R for the ^{60}Co γ rays indicates that this effect is probably small for incident energies greater than 1 MeV, but it is difficult to estimate the contribution from this process at lower photon energies. For the linear polarization measurements in ^{64}Cu , the calculated values of R were assigned an error of 10%.

3.3.2 Linear Polarization Electronics

A sum-coincidence circuit (Co 56, Ho 58) was used for each NaI-Ge(Li) pair, in which the parameter actually recorded is the sum of the energies deposited in the scattering and analyzing crystals. Recording the total energy for each event, rather than the energy deposited in one or the other of the detectors, has important advantages in the increased resolution obtained, especially if the analyzing crystal subtends a large angle at the scatterer. Even though, for a valid coincidence event, the energy deposited in one of the crystals varies with the Compton scattering angle, the sum of the energies is of course a constant, and the resolution is then limited only by the inherent resolution of the detectors (in this case, the NaI crystal).

A schematic diagram of the sum-coincidence electronics used in this experiment is shown in Figure 5. A fast timing signal for the Ge(Li) is obtained by feeding the output through a timing filter amplifier (TFA) and a constant fraction of pulse height trigger (CFPHT). This timing signal is delayed, and used to stop a time to amplitude converter (TAC). Start pulses for the TAC are obtained by feeding the output from the NaI through a double delay line amplifier (DDL) and a timing single channel analyzer (TSCA), which was also used to place an energy window on the scattered γ rays. The TAC output is then fed through an SCA, to provide a coincidence gate for the sum spectrum. The timing resolution from this circuit was about 20 ns FWHM.

The portion of the electronics shown inside the dashed line was duplicated for the 90° NaI detector. As well as the two sum spectra and associated time spectra, the Ge(Li) singles spectrum was also recorded for the angular distribution measurements.

3.3.3 Experimental Measurements

Linear polarization measurements were carried out at a proton bombarding energy of 3.3 MeV. Measurements were taken at angles of 0° , 31° , 55° , 70° and 90° .

A typical sum-coincidence spectrum is shown in Figure 6. The spectra shown in this figure have been corrected for the different efficiencies of the two analyzing crystals by normalizing the results at $\theta = 0^\circ$, where the γ rays are unpolarized. The peaks at 278, 344, and 609 keV are due to transitions in ^{64}Cu , and these were the only

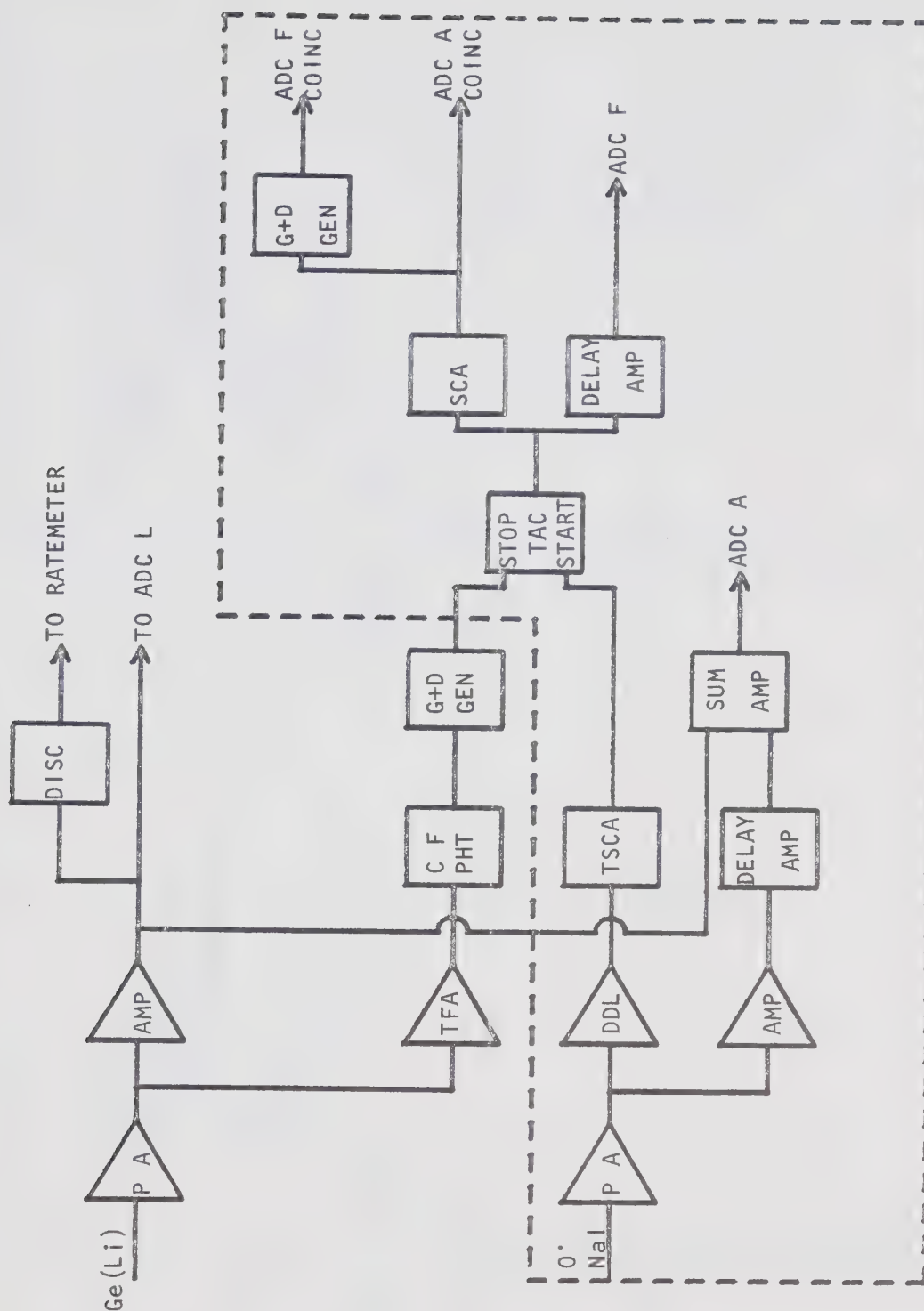


Figure 5. A block diagram of the electronics used for the linear polarization measurements. The portion inside the dashed line was duplicated for the $\phi=90^\circ$ analyzing crystal.

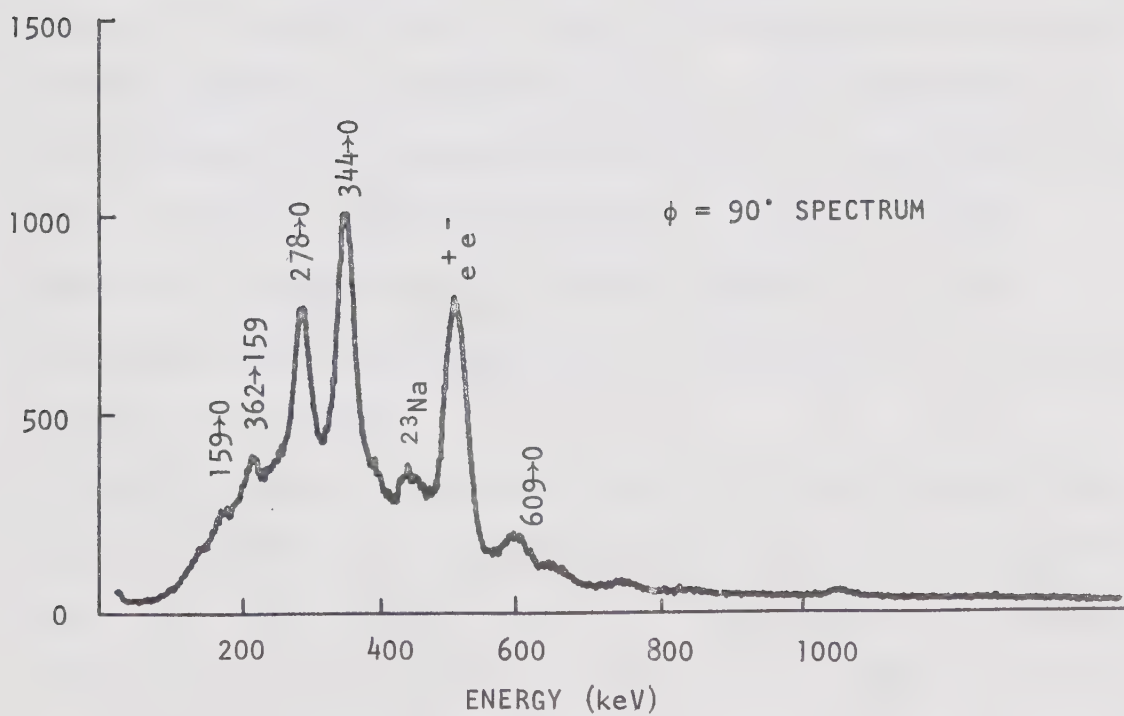
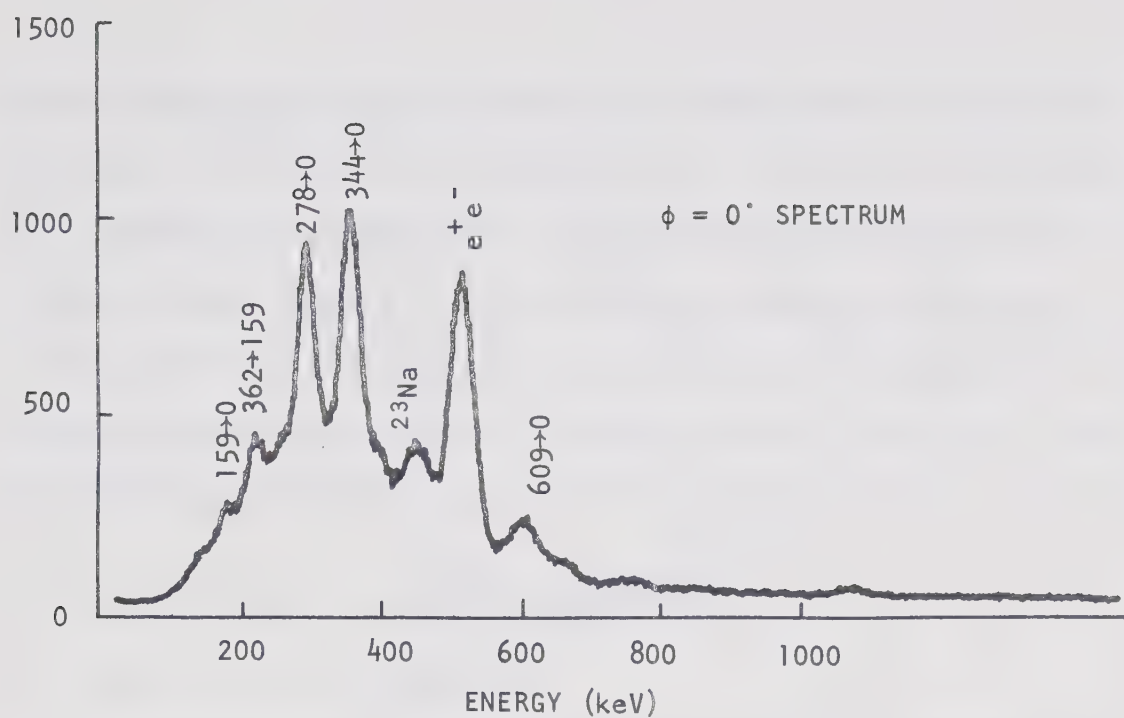


Figure 6. A typical sum-coincidence spectrum, taken at a bombarding energy of 3.30 MeV and an angle of $\theta=90^\circ$.

three transitions for which polarization measurements were possible. The peaks at 439 and 511 keV are due to the $^{23}\text{Na}(p,p'\gamma)$ reaction and e^+e^- annihilation respectively. The strong 159 keV γ ray in ^{64}Cu does not appear clearly in the sum spectrum, because of the poor timing qualities of the Ge(Li) detector at such low energies (the Compton scattered electron has an energy of only 34 keV), so it was not possible to perform a polarization measurement for this transition.

3.4 $\gamma - \gamma$ Angular Correlation Measurements

3.4.1 Choice of Geometries

As was mentioned in Section 2.2.3, it is usually unnecessary to measure all 19 coefficients of the $\gamma - \gamma$ triple correlation, and one therefore measures the correlation in one or more "geometries", in which two out of the three angles specifying the correlation are held fixed. A list of the angles specifying the seven "standard" geometries of Ferguson (Fe 65) is given in Table I. In this experiment, the A1 and C1 geometries of the correlation were measured for each γ ray cascade.

The C1 geometry is especially useful for resolving ambiguities in spin and mixing ratio from the angular distribution measurements in ^{64}Cu . The target nucleus ^{64}Ni has a 0^+ ground state spin, and hence nearly isotropic γ -ray angular distributions are expected for states with $J = 0$ or 1 (Section 2.4). For $J = 2$ states, there will be two specific values of δ for which the a_2 coefficient vanishes (regardless of the degree of alignment), and if the corresponding a_4 coefficient is small, these angular distributions will appear isotropic as well.

Table 1 Angles specifying the seven $\gamma - \gamma$ angular correlation geometries of Ferguson (Fe 65).

Geometry	θ_1	θ_2	ϕ
A1	Variable	90°	180°
A2	90°	Variable	180°
B1	Variable	0°	0°
B2	0°	Variable	0°
C1	Variable	90°	90°
C2	90°	Variable	90°
D	90°	90°	Variable

It is therefore expected that, if the angular distribution is isotropic, possible fits will be found for $J = 0, 1$ or 2 . This behavior is clearly evident in Figure 15 for the 344 keV transition. For the decay of a spherically symmetric initial state, the angular correlation of two succeeding γ rays depends only on the relative angle between the two γ rays. In the C1 geometry, this relative angle is constant at 90° , and hence the C1 geometry will appear isotropic for a weakly aligned state. This measurement can then serve to accept or eliminate the $J = 2$ assignment.

3.4.2 Electronics

A schematic diagram of the electronics circuit for the angular correlation measurements is shown in Figure 7. The timing circuits for both the Ge(Li) and the NaI are identical with those described in Section 3.3.2 for the linear polarization measurements. The timing

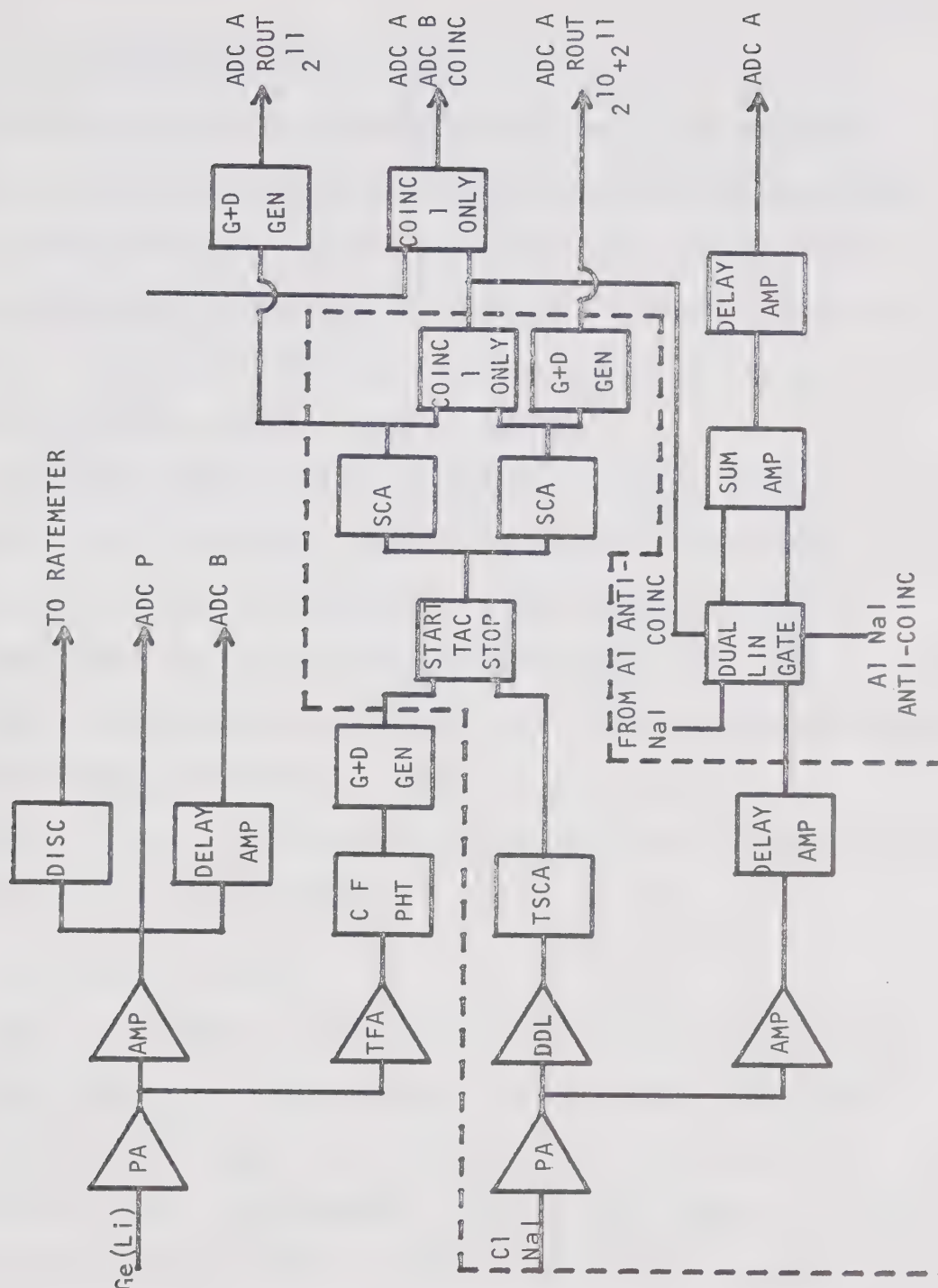


Figure 7. A block diagram of the electronics used for the γ - γ triple correlation measurements. The portion inside the dashed line was duplicated for the NaI crystal in the A1 geometry.

resolution was again about 20 ns FWHM.

The TAC output was fed through two SCA's, one corresponding to real + random coincidences, the other to random coincidences only. The SCA outputs were then used to generate routing signals for the NaI spectrum in ADC A, and were OR'd to give a coincidence gate for the NaI. The two NaI coincidence gates were then OR'd to give a general coincidence gate for ADC A and ADC B.

Due to the organization of the computer software, it was necessary to put the signals from both NaI detectors into ADC A. The NaI analog signals were therefore first fed through a summing amplifier, which acted as an impedance matching device. The coincidence pulse for each NaI detector was used as an anticoincidence pulse to prevent the accidental summing of pulses from the two detectors. The portion of the circuit shown inside the dashed lines was repeated for the NaI detector in the Al geometry.

3.4.3 Data Collection

The on-line computer allowed sorting of the Ge(Li) spectrum in ADC B according to the ADC A spectrum. Four windows were set on each of the four NaI spectra in ADC A (one real + random and one random spectrum for each detector), giving sixteen spectra of γ rays in coincidence with the 159, 278, 344 and 203 keV transitions from the first four excited states of ^{64}Cu . Runs were taken at Ge(Li) angles of 0° , 31° , 55° , 70° and 90° , all angles being repeated once. Each run was typically 5 - 6 hours long.

A typical coincidence spectrum is shown in Figure 8, showing γ rays feeding the 278 keV level. This spectrum shows the Al geometry of the angular correlation, taken at a proton bombarding energy of 3.75 MeV and an angle of 55° . The real coincidences with the 331 keV, 385 keV, 461 keV, 468 keV and 649 keV transitions can be clearly seen.

3.5 Data Analysis

γ -ray intensities were obtained directly from the computer display, using the program SUMMIT (Gr 71A), which fits either a linear or quadratic function to the background in the immediate vicinity of the peak, and subtracts this fitted background to obtain the peak sum.

Branching ratios were determined by first fitting these peak intensities to the function

$$W(\theta) = a_0(1 + a_2P_2(\cos \theta) + a_4P_4(\cos \theta)) \quad (3-1)$$

taking into account absorbtion of the γ rays in the 0.005" Ta backing and the 0.055" Al plate, which were at an angle of 30° with respect to the beam axis. The a_0 coefficient of this expansion was then corrected for the efficiency of the Ge(Li) detector, which was measured using ^{57}Co , ^{22}Na , ^{137}Cs , ^{54}Mn and ^{60}Co sources of known intensity. The efficiency curve for the 48 cc detector is shown in Figure 9.

The population parameters of the initial state in the γ decay were calculated from the Statistical Compound Nuclear computer code AK (Gr 71b) which is based on the code MANDY of Sheldon and Strang (Sh 69), but expanded to include calculation of the γ -ray

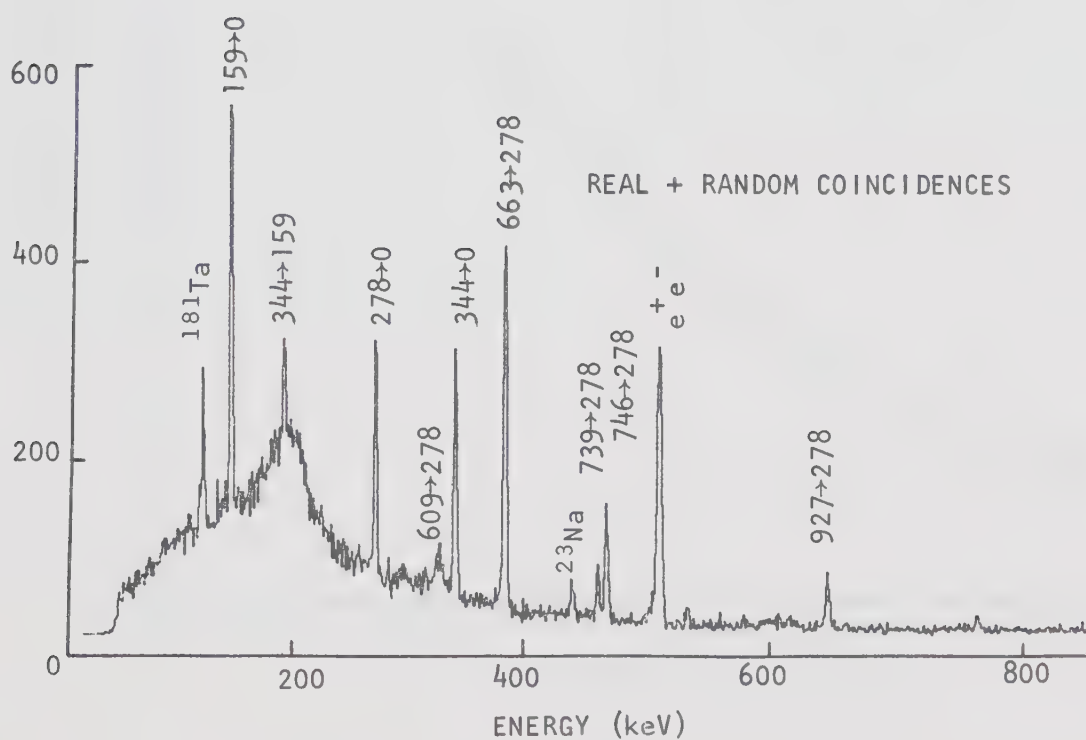
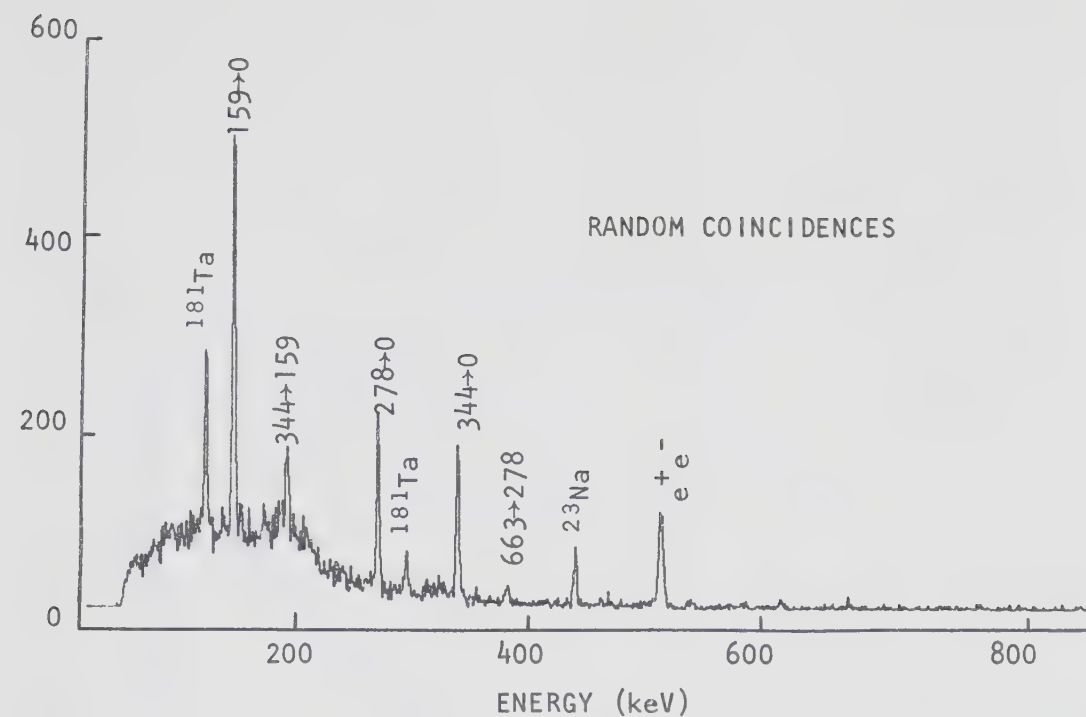


Figure 8. A typical $\gamma - \gamma$ coincidence spectrum, showing γ rays detected in the Ge(Li) which are in coincidence with the 278 keV transition in ^{64}Cu . This spectrum was obtained for the A1 geometry, at $\theta=55^\circ$.

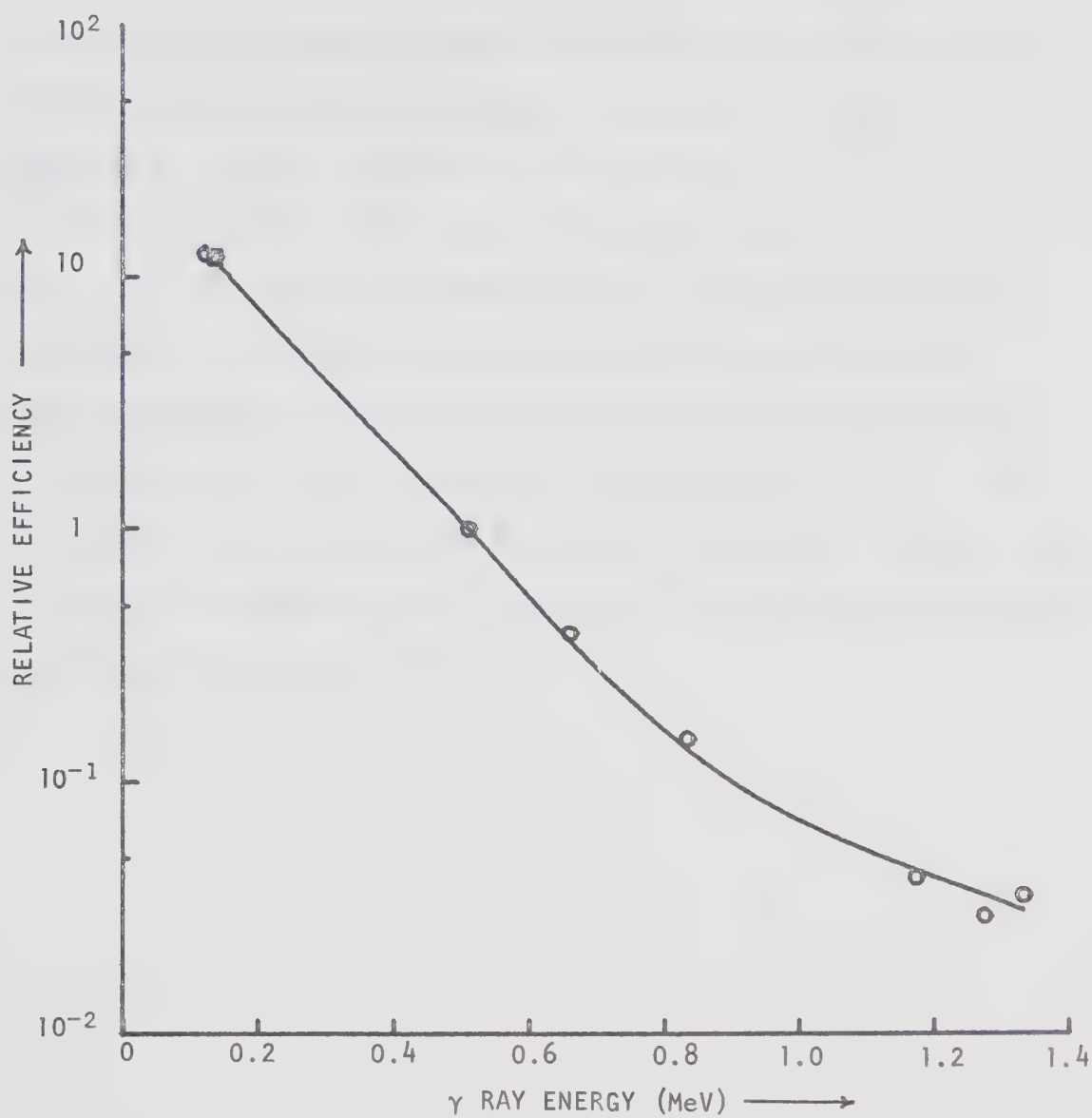


Figure 9. Efficiency curve for the 48 cc Ge(Li), measured with ^{57}Co , ^{22}Na , ^{137}Cs , ^{54}Mn and ^{60}Co sources.

linear polarization coefficients as well as angular distribution coefficients. The transmission coefficients required as input to this program were calculated by the computer program ABACUS (Au 64), using the optical model parameters of Bjorkland and Fernbach (Bj 58) for both proton and neutron channels. Partial waves up to and including $\ell = 4$ were considered in all channels.

For many of the transitions in ^{64}Cu , both angular distribution and $\gamma - \gamma$ triple correlation measurements in two geometries were performed. For these transitions, all three sets of data were used to minimize a total χ^2 to find acceptable values for the spin and mixing ratio, using the computer code SUPERCHI (Gr 73). Since only three linear polarization measurements were made, they were not included in the computation of the total χ^2 for the respective decays, and they were analyzed separately.

CHAPTER 4

EXPERIMENTAL RESULTS

A typical Ge(Li) singles spectrum, taken at a proton bombarding energy of 3.75 MeV, is shown in Figure 2. γ -ray transitions between levels in ^{64}Cu are identified by the energies of the initial and final states in the decay. The energies determined in this work agree well with the more accurate results of Shera and Bolotin (Sh 68), and since the emphasis in this work was not on precise energy determination, the values of this reference have been adopted throughout.

Figure 10 summarizes the decay scheme of the levels below 1 MeV excitation in ^{64}Cu , as well as the branching ratios and spin-parity assignments determined in this work. This decay scheme differs from that of Shera and Bolotin (Sh 68) in the following respects:

- i) A weak 362 keV γ ray is observed, which is assigned to the ground state decay of the 362 keV level.
- ii) A 719 keV γ ray is observed, which is attributed to the $878 \rightarrow 159$ transition.
- iii) The 534 keV transition, which Shera and Bolotin (Sh 68) assign to the $895 \rightarrow 362$ decay, is re-assigned as the $878 \rightarrow 344$ transition, on the basis of coincidence with the 344 keV γ ray.
- iv) A 736 keV transition is observed, which is attributed to the $895 \rightarrow 159$ decay.

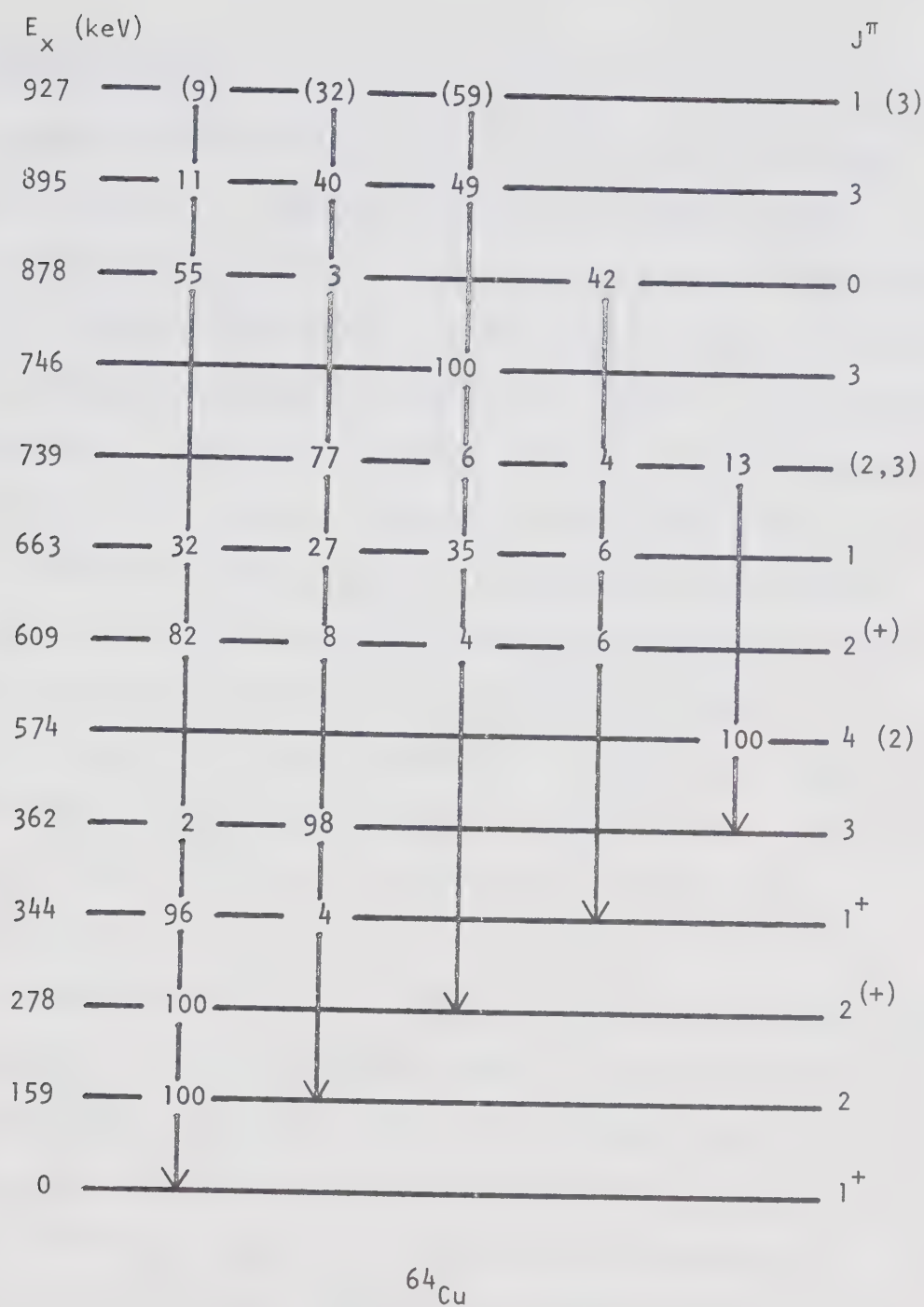


Figure 10. Level scheme for ^{64}Cu , showing spin-parity assignments and γ -decay branching ratios determined in this experiment.

4.1 Branching Ratios

A summary of the branching ratios measured in this experiment is given in Table II. Although several γ -ray studies of ^{64}Cu have appeared in the literature, only Shera and Bolotin (Sh 68) give results for the branching ratios. Their results, as well as those of Drum (Dr 70) who studied only the levels up to 663 keV, are also shown for comparison. The results of Shera and Bolotin (Sh 68) have been corrected for their improper placement of the 534 keV decay.

For some of the weaker decays in ^{64}Cu , angular distribution measurements could not be made, so it was not possible to use the procedure outlined in Section 3.5 to calculate the branching ratios. For these transitions, it was assumed that the yield at $\theta = 55^\circ$ gave a good estimate of the a_0 coefficient in equation (3-1). This will be the case provided that the a_4 coefficient is small, since $P_2(\theta=55^\circ) = 0.0$.

The three sets of results in Table II are in good agreement, with the exception of the 895 and 927 keV levels. For the 895 keV level, Shera and Bolotin do not observe the 736 keV transition to the first excited state, which we measure to be of comparable strength to the branch to the 278 keV level. This decay was also observed by Davidson et al (Da 70), but they give no estimate of the relative strength of this branch.

For the 927 keV level, our branching ratios are only approximate values, and it is difficult to assign reliable error estimates to the values quoted. The uncertainty regarding this level stems mainly from the presence of the strong 770 keV γ ray from the $^{64}\text{Ni}(p,\gamma\gamma)^{65}\text{Cu}$

Table II A summary of the γ -decay branching ratios for levels below 1 MeV in ^{64}Cu . The results of the present experiment are compared with those of Shera and Bolotin (Sh 68) and Drum (Dr 70).

E_i (keV)	E_f (keV)	E_γ (keV)	This Expt.	(Sh 68)	(Dr 70)
159	0	159	100	100	100
278	0	278	100	100	100
344	0	344	96 ± 1	95 ± 2	96 ± 4
	159	185	4 ± 1	5 ± 2	4 ± 4
362	0	362	2 ± 1	Not Observed	7 ± 4
	159	203	98 ± 1	100	93 ± 4
574	362	212	100	100	100
609	0	609	82 ± 2	73 ± 5	80 ± 4
	159	450	8 ± 1	9 ± 2	3 ± 4
	278	331	4 ± 1	10 ± 3	9 ± 4
	344	265	6 ± 1	8 ± 2	8 ± 4
663	0	663	32 ± 2	28 ± 5	30 ± 4
	159	504	27 ± 2	34 ± 6	24 ± 4
	278	385	35 ± 2	29 ± 5	46 ± 4
	344	319	6 ± 1	9 ± 2	Not Observed
739	159	580	77 ± 1	74 ± 5	
	278	461	6 ± 1	7 ± 2	
	344	395	4 ± 1	2 ± 1	
	362	377	13 ± 1	17 ± 4	
746	278	468	100	100	
878	0	878	55 ± 2	64 ± 7	
	159	719	3 ± 1	Not Observed	
	344	534	42 ± 2	36 ± 7	
895	0	895	11 ± 4	20 ± 9	
	159	736	40 ± 4	Not Observed	
	278	617	49 ± 4	80 ± 9	
927	0	927	(9)	11 ± 5	
	159	768	(32)	16 ± 4	
	278	649	(59)	73 ± 6	

reaction, which partially obscures the 768 keV transition from the 927 to 159 keV level. Estimates of the contribution of the 768 keV γ ray to this unresolved doublet were made by fitting two Gaussian peaks to the spectrum at $\theta = 55^\circ$ using the computer code PEAKFIT (Ea 72), but the overall fit to the peak shape was poor. A similar procedure was followed for the 927 keV to ground state transition. In Figure 2, the peak labelled $927 \rightarrow 0$ is about twice the width of the other ^{64}Cu peaks, and it is likely composed of two γ rays. The source of the other transition has not been identified. Because of the above uncertainties, the branching ratios of Shera and Bolotin (Sh 68) for this level are considered more reliable.

4.2 The Levels of ^{64}Cu

Table III gives the experimental a_2 and a_4 coefficients for the measured angular distributions of transitions between low-lying states in ^{64}Cu . Table IV lists the measured a_2 and a_4 coefficients for both geometries of the $\gamma - \gamma$ triple correlations. The triple correlation results were obtained at a bombarding energy of 3.75 MeV.

A summary of the spins and mixing ratios determined in the present work is given in Table V. Table VI compares these spin assignments with those obtained in previous works, and Table VII compares the mixing ratios measured in this work with those of Davidson et al (Da 70).

It was mentioned earlier that, in many cases, more than one measurement was made at each angle. Although these measurements were treated as independent data points in the χ^2 analysis, the

Table III Experimental a_2 and a_4 coefficients for the γ ray angular distributions.

E_p	E_γ	a_2	a_4
2.75	159	-0.29 ± 0.01	0.0 ± 0.01
3.00	278	-0.35 ± 0.01	0.02 ± 0.01
	344	0.01 ± 0.03	0.02 ± 0.03
	185	-0.02 ± 0.02	-0.01 ± 0.02
	203	-0.42 ± 0.01	0.02 ± 0.01
3.30	212	-0.28 ± 0.02	0.02 ± 0.02
	609	-0.34 ± 0.01	0.01 ± 0.01
	450	0.15 ± 0.01	-0.01 ± 0.02
	265	-0.27 ± 0.03	-0.04 ± 0.04
	663	0.00 ± 0.02	0.03 ± 0.03
	385	0.02 ± 0.02	0.03 ± 0.03
	319	-0.02 ± 0.02	0.00 ± 0.02
3.75	580	0.28 ± 0.01	0.02 ± 0.02
	461	0.28 ± 0.06	0.14 ± 0.07
	377	-0.11 ± 0.02	0.04 ± 0.03
	468	-0.39 ± 0.02	0.03 ± 0.02
	878	-0.05 ± 0.04	0.05 ± 0.04
	719	-0.16 ± 0.15	0.22 ± 0.18
	534	0.00 ± 0.01	-0.02 ± 0.02
	736	-0.75 ± 0.03	0.00 ± 0.03
	617	-0.85 ± 0.14	0.18 ± 0.16
	649	-0.06 ± 0.08	0.16 ± 0.10

Table IV Experimental a_2 and a_4 coefficients for the A1 and C1 geometries of the $\gamma - \gamma$ triple correlations.

$E_{\gamma_1} - E_{\gamma_2}$	A1		C1	
	a_2	a_4	a_2	a_4
185 - 159	-0.17 ± 0.06	0.10 ± 0.07	-0.15 ± 0.08	0.07 ± 0.09
212 - 203	-0.39 ± 0.04	0.04 ± 0.04	-0.14 ± 0.10	-0.26 ± 0.11
450 - 159	0.44 ± 0.13	0.14 ± 0.15	0.11 ± 0.11	0.05 ± 0.13
385 - 278	-0.18 ± 0.03	0.04 ± 0.03	-0.03 ± 0.03	0.03 ± 0.03
580 - 159	0.50 ± 0.12	-0.07 ± 0.15	0.03 ± 0.04	0.04 ± 0.05
461 - 278	0.46 ± 0.17	0.00 ± 0.16	0.30 ± 0.16	-0.10 ± 0.19
468 - 278	-0.46 ± 0.07	-0.02 ± 0.07	-0.33 ± 0.05	-0.03 ± 0.05
534 - 344	0.27 ± 0.06	-0.02 ± 0.06	0.23 ± 0.09	-0.12 ± 0.11
649 - 278	-0.18 ± 0.05	0.00 ± 0.05	-0.17 ± 0.06	0.06 ± 0.07

weighted average of all measurements at one angle is plotted in the diagrams.

Both the angular distribution and angular correlation measurements are independent of the parity of the radiation, since they are not sensitive to the direction of the electric vector of the radiation. These experiments may be sensitive to the parity of the initial state in the decay, however, if the degree of alignment (specified by the $B_k(J_1)$ coefficients) is parity dependent. This is the case if the Statistical Compound Nuclear model is used, since the population parameters are determined, in part, by the optical model transmission coefficients $T_{\ell j}$ which depend on the orbital angular momentum of the incoming and outgoing particles.

Figure 11 shows this dependence on parity for the angular distribution of the 278 keV transition. The effect is most marked for low spins ($J = 1$ in this case, since $J = 0$ always gives an isotropic angular distribution). For all of the transitions studied in this work, calculations were done for both parity assignments, and in no case was it possible to exclude one parity assignment on this basis. Since the differences are usually small, all results shown in this section (except for the linear polarization measurements) are for positive parity assignments. The measurements of Park and Daehnick (Pa 69) indicate that there are no negative parity levels in ^{64}Cu below 1.4 MeV excitation.

4.2.1 The 159 and 278 keV Levels

Both of these levels decay 100% to the ground state, which has spin-parity $J^\pi = 1^+$ (Le 54, Do 66, Wa 67). The measured angular

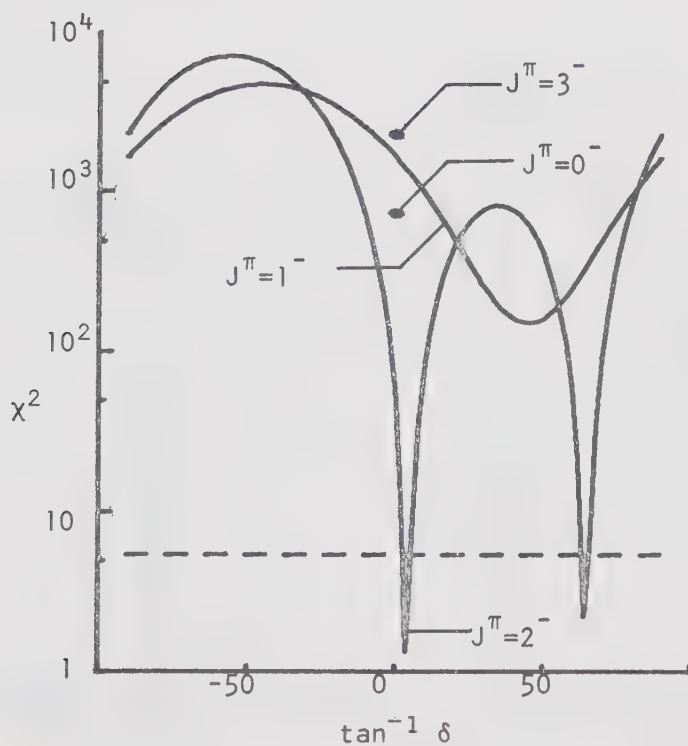
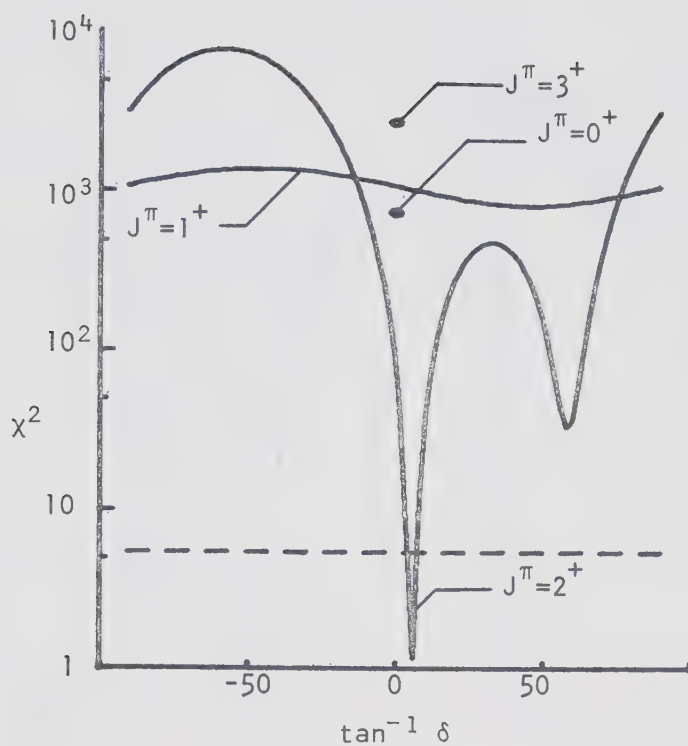


Figure 11. χ^2 curves for the $278 \rightarrow 0$ angular distribution, showing the dependence of the angular distribution on the parity of the initial state in the decay.

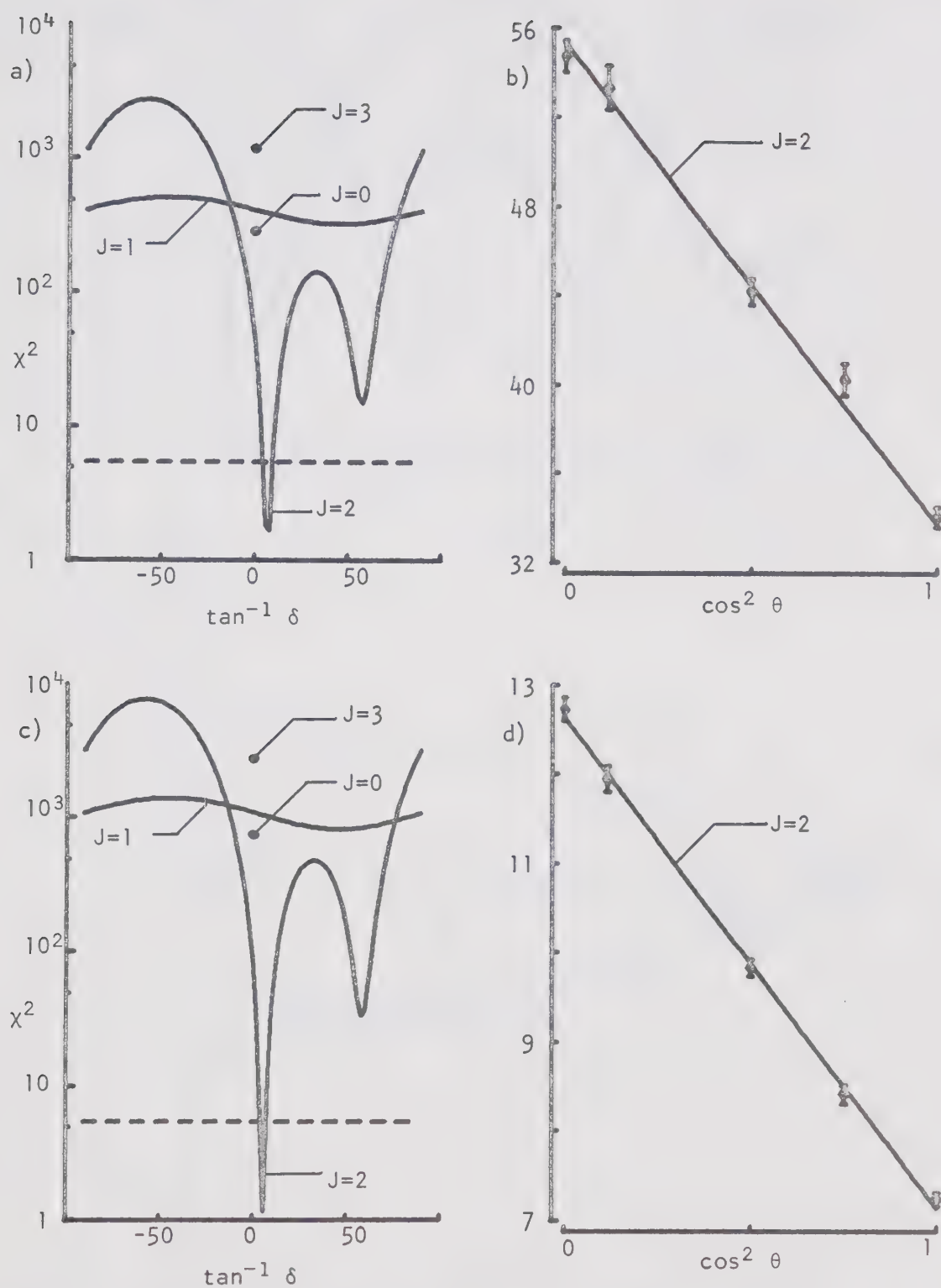


Figure 12. The 159 keV level: a) χ^2 curves and b) angular distribution for the 159 \rightarrow 0 transition. The 278 keV level: c) χ^2 curves and d) angular distribution for the 278 \rightarrow 0 transition.

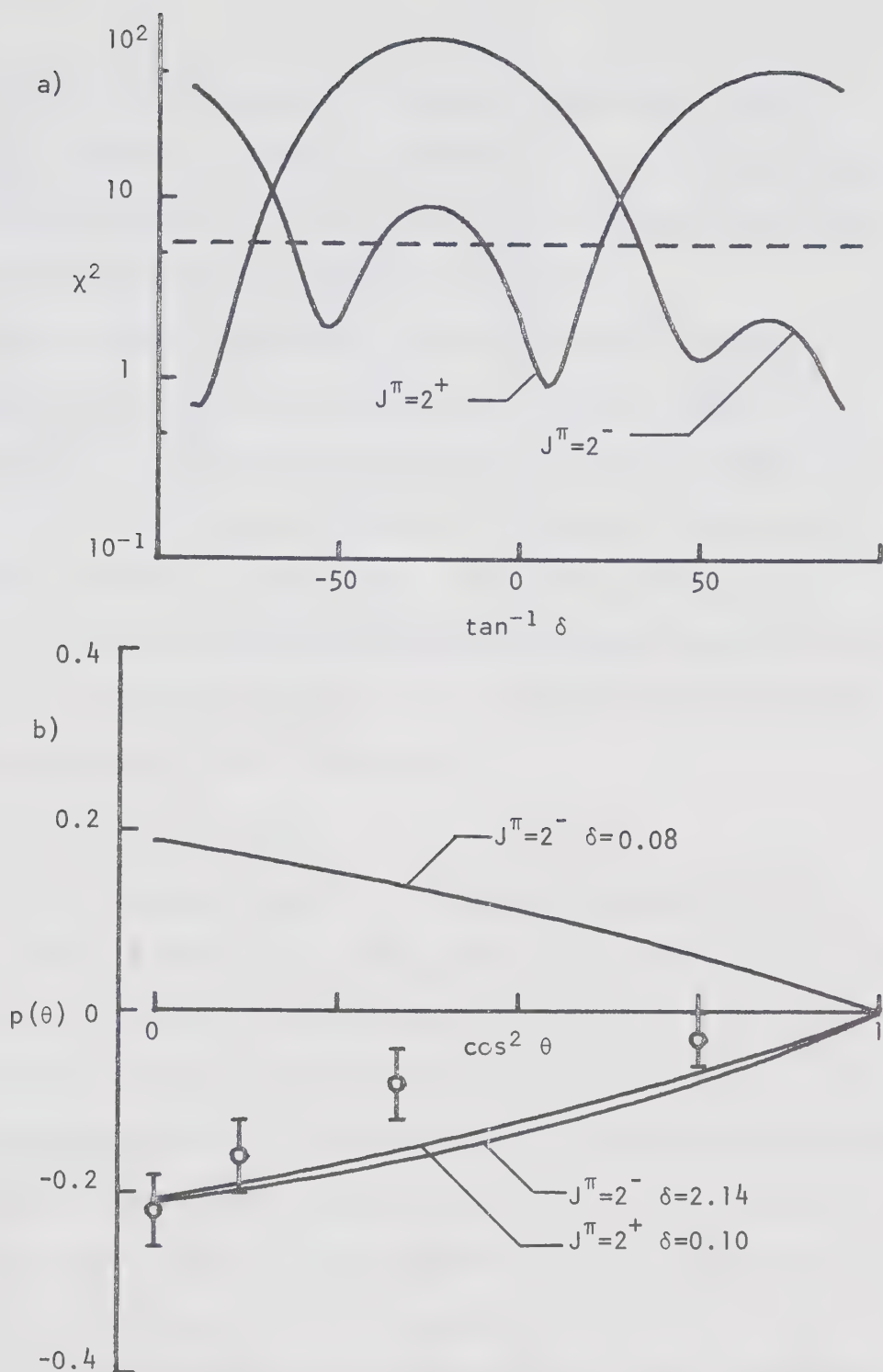


Figure 13. The 278 keV level: a) χ^2 curves and b) linear polarization distribution for the 278 keV γ ray. The solid lines in b) show the expected linear polarization distributions for values of J^π and δ which gave good fits to the angular distribution.

distributions and χ^2 curves for these two transitions, shown in Figure 12, indicate a unique spin assignment of $J = 2$ in both cases, with a mixing ratio of $\delta = 0.12 \pm 0.04$ for the 159 keV transition, and $\delta = 0.10 \pm 0.02$ for the 278 keV transition.

Figure 13 shows the results of the linear polarization measurement for the 278 keV transition. The solid lines in the lower half of this diagram are the expected linear polarization distributions for the various spin and mixing ratio combinations which give a good fit to the angular distribution data. The $J^\pi = 2^-$, $\delta = 2.14$ assignment is considered unlikely because of the large M2/E1 enhancement required to fit the data, and we therefore assign positive parity for this level.

4.2.2 The 344 keV Level

This level decays primarily to the ground state, with a 4% branch to the 159 keV level. The angular distribution of the ground state decay is isotropic within experimental limits ($a_2 = 0.01 \pm 0.03$) and acceptable fits were obtained for $J = 0, 1$ and 2 (Figure 15).

The measured angular distribution of the 185 keV transition was also isotropic, but the A1 geometry of the $344 \rightarrow 159 \rightarrow 0$ angular correlation had an appreciable anisotropy of $a_2 = -0.17 \pm 0.06$. The curves shown in Figure 14 indicate acceptable fits for $J = 1, 2$ or 3 , but $J = 3$ is not allowed from the ground state angular distribution.

The $J = 0$ assignment can also be eliminated from the $609 \rightarrow 344$ angular distribution (Figure 19). The spin of the 609 keV level is known to be 2 from analysis of the ground state angular distribution

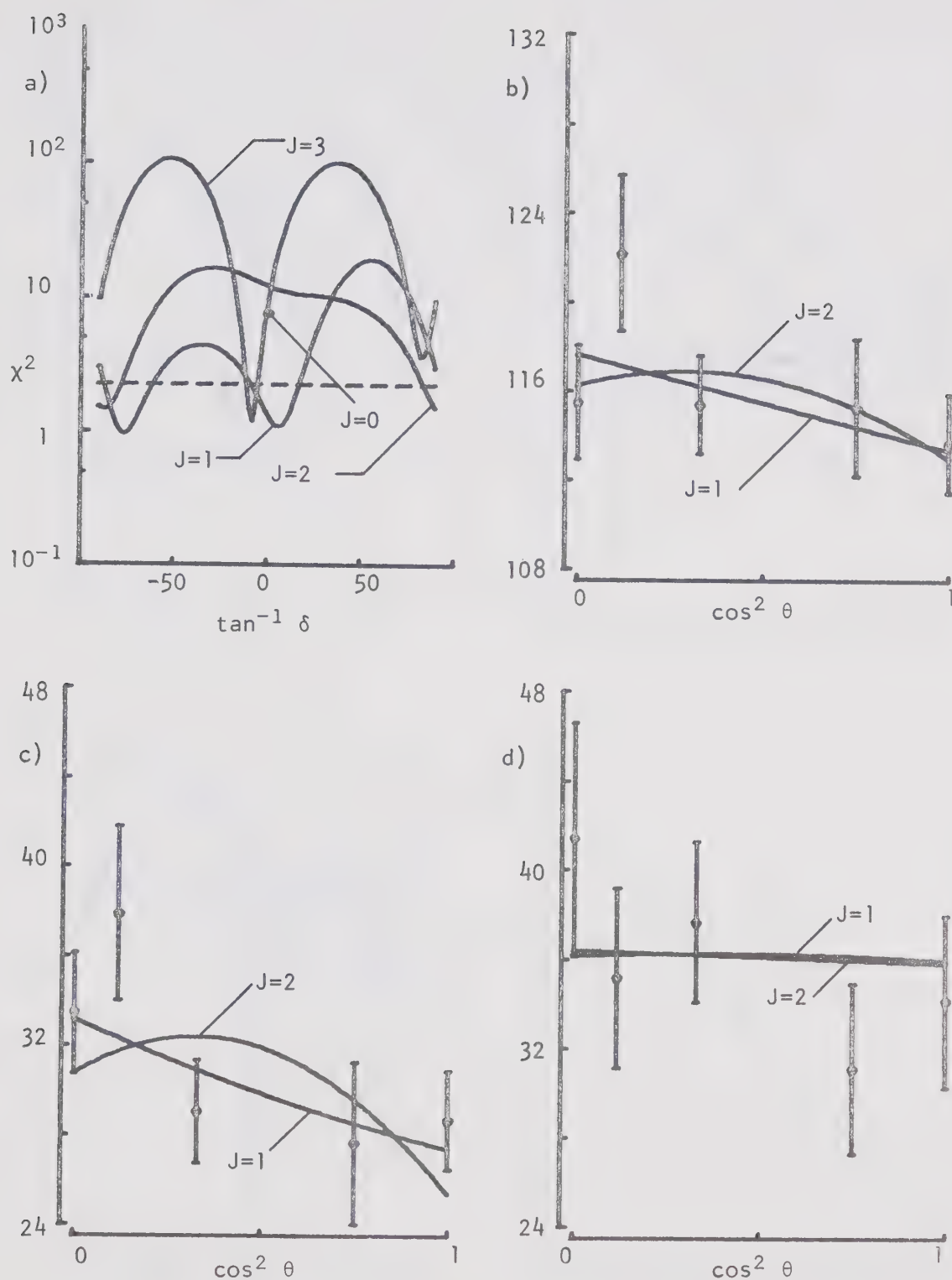


Figure 14. The 344 keV level: a) χ^2 curves, b) angular distribution for the 185 keV γ ray, c) A1 geometry and d) C1 geometry of the $344 \rightarrow 159 \rightarrow 0$ angular correlation.

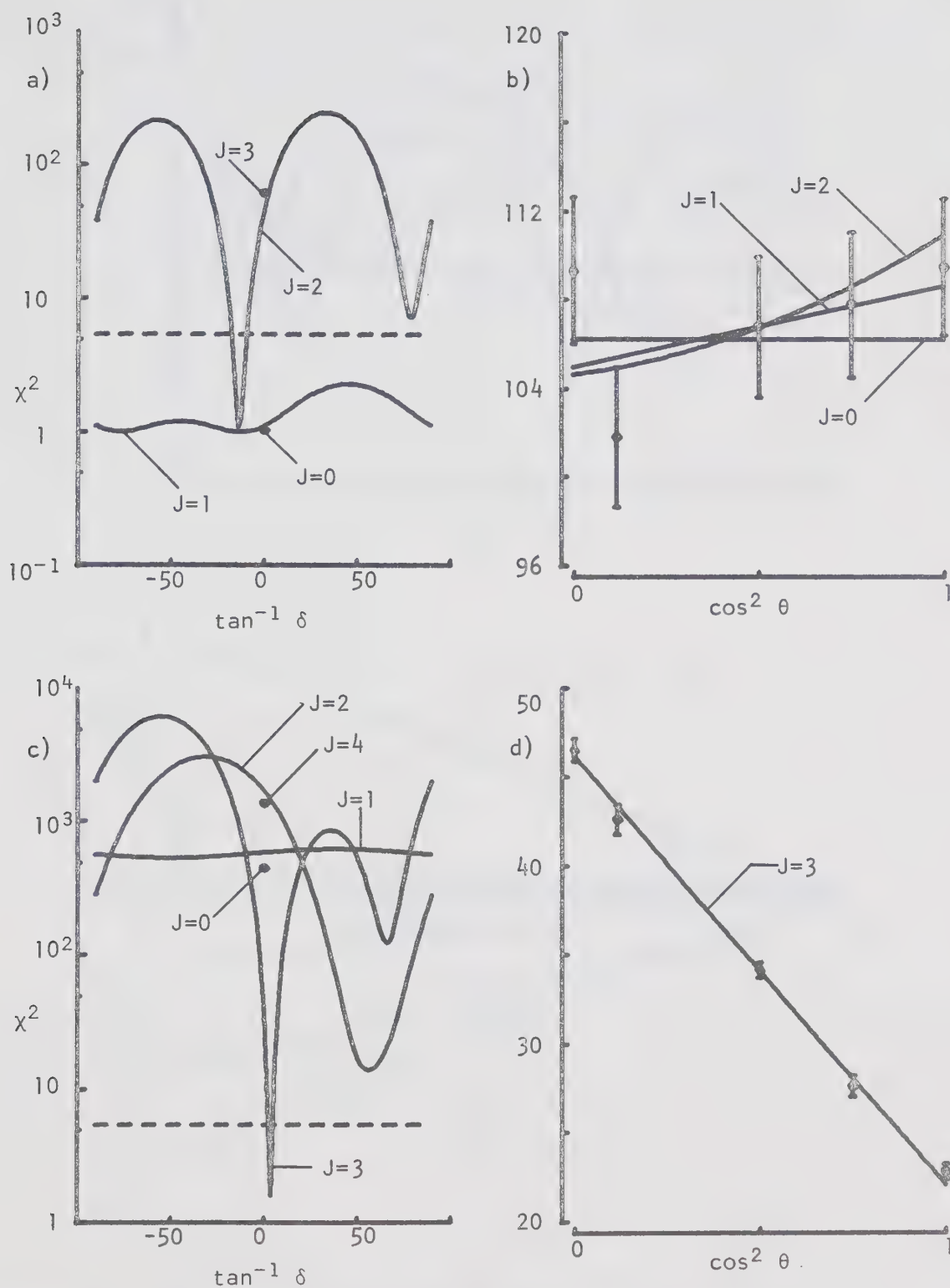


Figure 15. The 344 keV level: a) χ^2 curves and b) angular distribution for the $344 \rightarrow 0$ transition. The 362 keV level: c) χ^2 curves and d) angular distribution for the $362 \rightarrow 159$ transition.

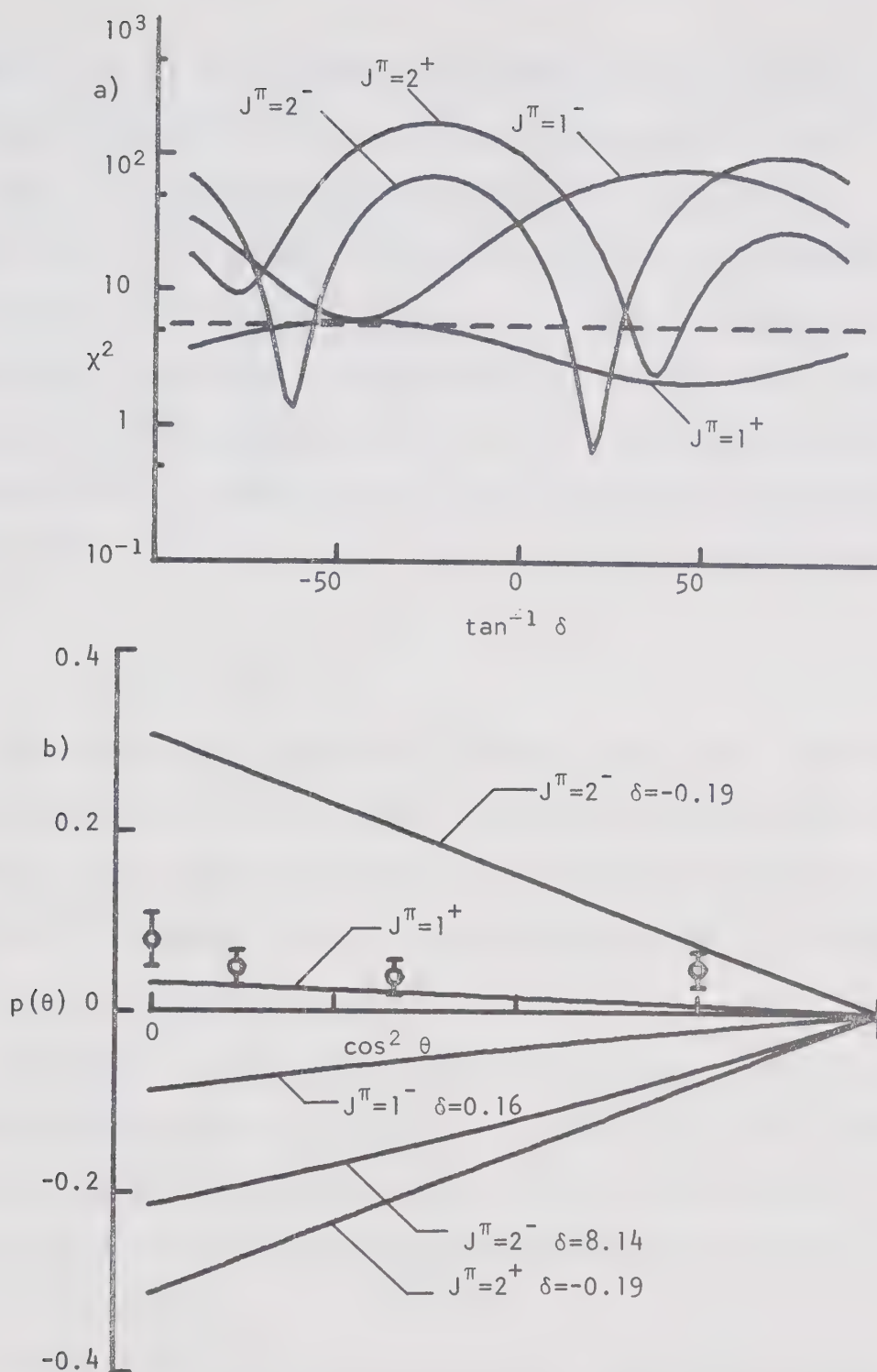


Figure 16. The 344 keV level: a) χ^2 curves and b) linear polarization distribution for the 344 keV γ ray.

(Section 4.2.5), and the angular distribution of the 265 keV transition is inconsistent with a $J = 0$ assignment for the 344 keV level.

The $J = 2$ assignment can be ruled out on the basis of a combination of the angular distribution and linear polarization distribution of the 344 keV γ ray. For $J = 2$, an isotropic angular distribution occurs for a mixing ratio of $\delta = -0.19$, which gives rise to a polarization of about 30% at $\theta = 90^\circ$. The near isotropy of both the angular distribution and the linear polarization distribution (Figure 16) is consistent only with a spin-parity combination of $J^\pi = 1^+$.

4.2.3 The 362 keV Level

This level decays 98% to the 159 keV state, with a weak ground state branch also being observed. The angular distribution of the 203 keV γ ray, shown in the lower half of Figure 15, results in a unique spin assignment of $J = 3$, with a mixing ratio of $\delta = 0.06 \pm 0.03$.

4.2.4 The 574 keV Level

This level is only weakly excited in the $(p, n\gamma)$ reaction, and was observed to decay only to the $J = 3$ state at 362 keV. Although the presence of this state has been reported by many authors, no previous angular distribution measurements have been reported for the 212 keV γ ray.

In the present study, both the angular distribution and the $574 \rightarrow 362 \rightarrow 159$ angular correlation were measured. The results of these measurements are presented in Figure 17, showing possible fits for $J = 4$ ($\delta = 0.01 \pm 0.03$) and $J = 2$ ($-4.7 \leq \delta \leq -2.6$).

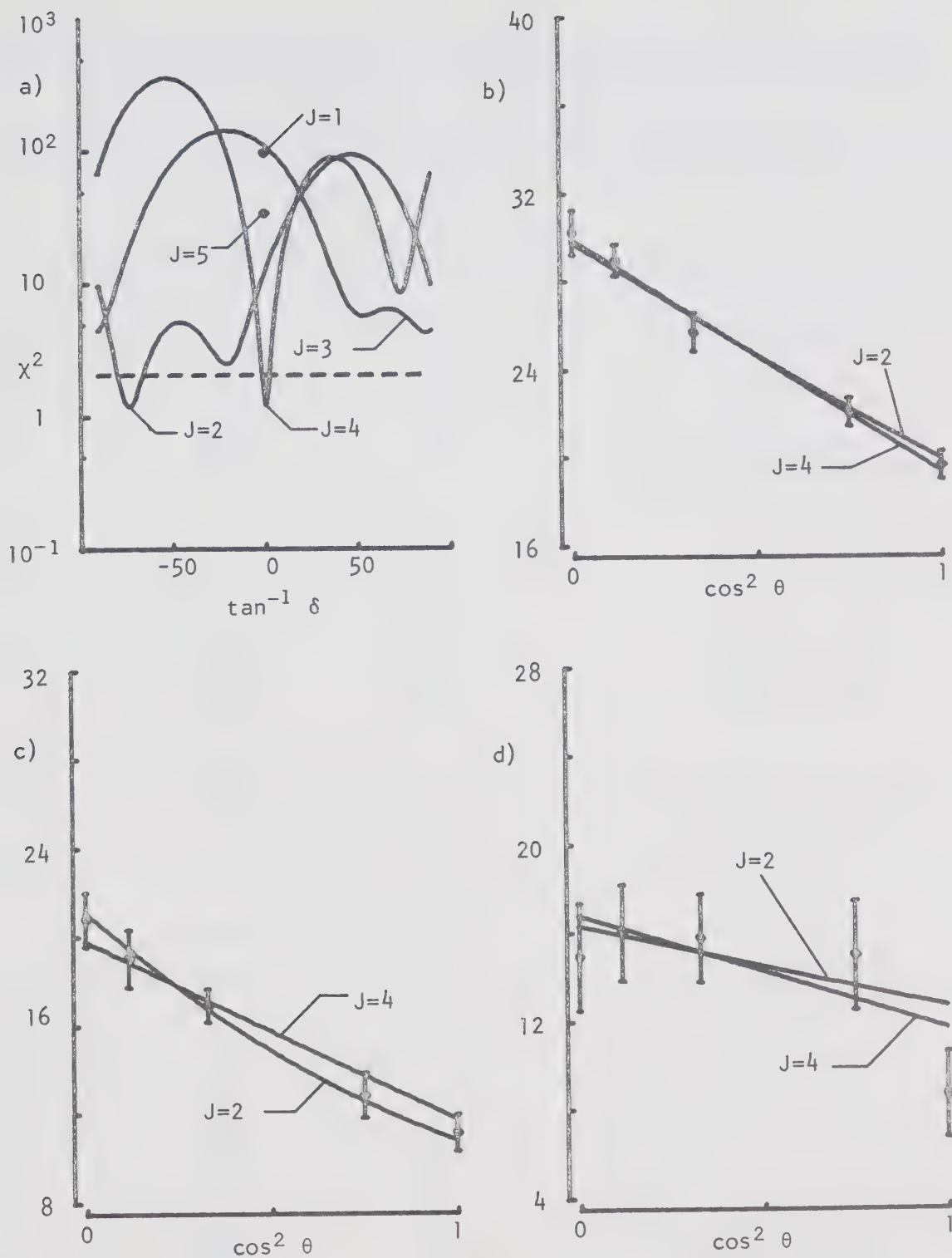


Figure 17. The 574 keV level: a) χ^2 curves, b) angular distribution for the 212 keV γ ray, c) A1 geometry and d) C1 geometry of the 574 \rightarrow 362 \rightarrow 159 angular correlation.

Table V A summary of the spin assignments and multipole mixing ratios determined in this work.

E_x	E_γ	$J(\pi)$	δ
159	159	2	0.12 ± 0.04
278	278	$2^{(+)}$	0.10 ± 0.02
344	344 185	1^+ 1^+	All values $0.10 \pm 0.10 \quad -7.1 \leq \delta \leq -3.0$
362	203	3	0.06 ± 0.03
574	212	4 2	0.01 ± 0.03 $-4.7 \leq \delta \leq -2.6$
609	609 450 265	$2^{(+)}$ $2^{(+)}$ $2^{(+)}$	0.30 ± 0.08 0.02 ± 0.07 0.24 ± 0.17
663	663 385 319	1 1 1	All values $0.07 \pm 0.05 \quad -4.7 \leq \delta \leq -2.9$ $0.2 \leq \delta \leq 5.7$
739	580 461 377	2 3 2 3 2 3	-0.18 ± 0.11 -0.38 ± 0.04 -0.29 ± 0.25 -0.43 ± 0.10 -0.11 ± 0.18 0.57 ± 0.18
746	468	3	0.08 ± 0.03
878	878 719 534	0 0 0	- - -
895	736 617	3 3	0.40 ± 0.13 $0.07 \leq \delta \leq 2.5$
927	649	1 3	$-5.7 \leq \delta \leq -2.5 \quad 0.04 \pm 0.11$ -0.11 ± 0.05

Table VI A comparison between the spin assignments determined in the present experiment and those of previous works.

E_x	$J(\pi)$						
	Present Work	Da 70	Pa 69	We 71	Ba 70	Dr 70	Sh 68
159	2	2	2^+	2	2(1,0)	2	(2)
278	$2^{(+)}$	2	2^+	(1,2)	2(1,0)	2	2
344	1^+	(0,1,2)	2^+	1(2)	2(0)	(1,2)	(1,2)
362	3	(2,3)	3^+	3	3	3	(3)
574	4(2)	-	4^+		4	-	(4)
609	$2^{(+)}$	2	$2^+(1^+)$		0(2)	2	(1,2)
663	1	(0,1,2)	3^+	1(2)	1(2)	(0,1,2)	(1,2)
739	(2,3)	2(3)	$(2^+, 3^+)$				(2,3)
746	3	(2,3)	$(1^+, 2^+, 3^+)$		(3,2)		(1,2,3)
878	0	(1,2)	$0^+(1^+, 2^+)$		0(3)		(0,1,2)
895	3	(2,3)	3^+		3		(2)
927	1(3)	(0,1,2)	1^+		2(0,1)		(1,2)

The $J = 4$ assignment seems more likely, for the following reasons. The level is very weakly populated in this reaction, suggesting that the spin is high, and that particles of high angular momentum (and hence smaller transmission coefficients) are required to form this state. The fact that the only observed γ decay is to a $J = 3$ state also tends to favour the assignment of $J = 4$. The $^{66}\text{Zn}(d,\alpha)$ measurements of Park and Daehnick (Pa 69) indicate $L = 4$ for this level, limiting the spin to 3^+ , 4^+ or 5^+ .

4.2.5 The 609 keV Level

The primary mode of decay for the 609 keV level is the ground state decay (82%) with weaker branches of 8%, 4%, and 6% respectively to the first three excited states. The angular distribution of the ground state branch was highly anisotropic ($a_2 = -0.34 \pm 0.01$), and the χ^2 analysis resulted in a unique assignment of $J = 2$ (Figure 19), with possible values for the mixing ratio of $\delta = 0.30 \pm 0.08$ and $\delta = 1.15 \pm 0.25$.

The linear polarization distribution for this decay is shown in Figure 20. Of the four possible solutions for the fit to the angular distribution (two possible mixing ratios for each parity), the 2^+ , $\delta = 1.15$ and 2^- , $\delta = 0.25$ solutions can be eliminated on the basis of the polarization measurement. The $J^\pi = 2^-$, $\delta = 1.30$ assignment is considered unlikely because of the large $M2/E1$ enhancement required to fit the data, and positive parity is the preferred assignment.

The measured angular distribution and $\gamma - \gamma$ angular correlation of the 450 keV transition are shown in Figure 18. Here again, the

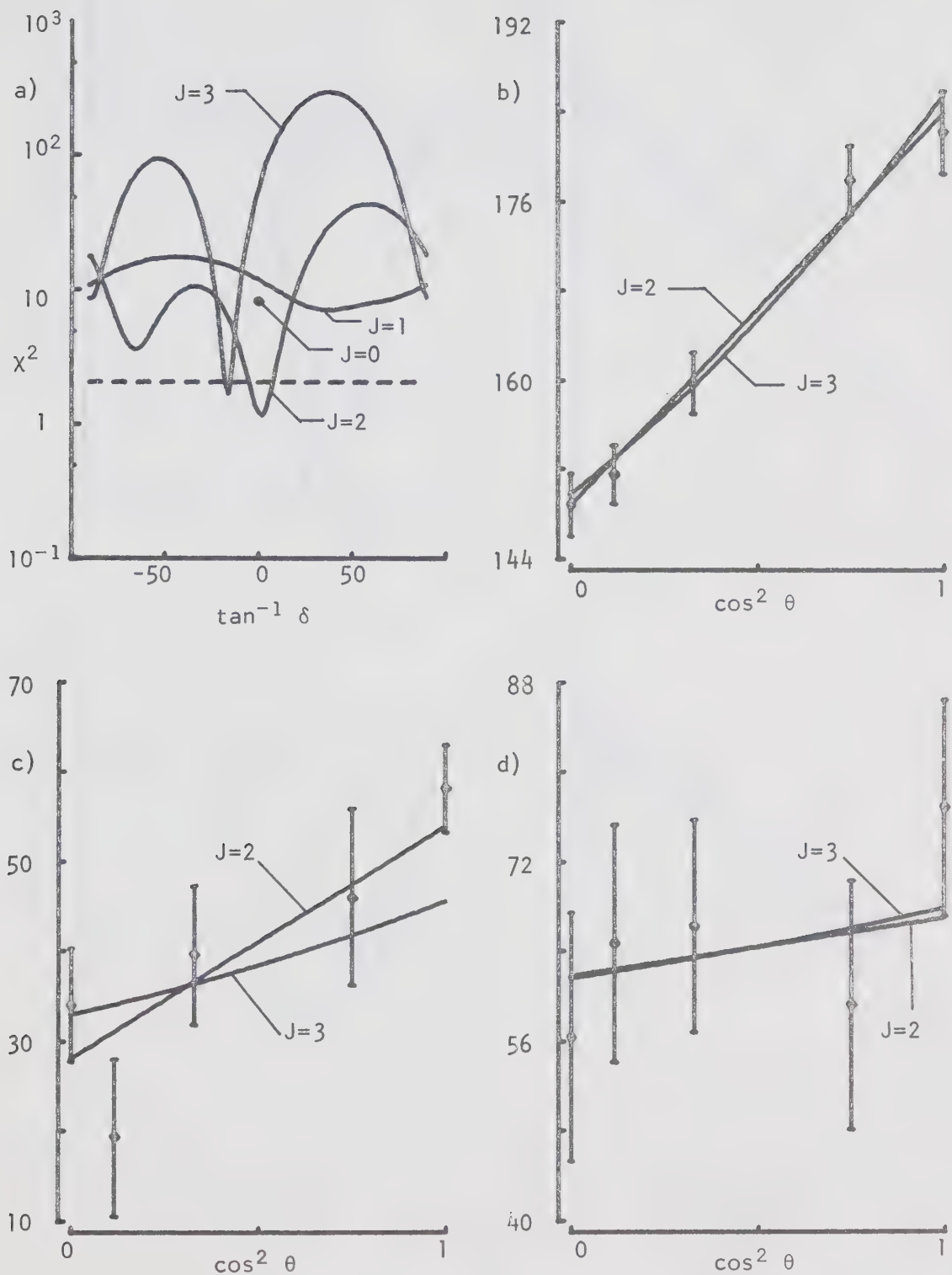


Figure 18. The 609 keV level: a) χ^2 curves, b) angular distribution for the 450 keV transition, c) A1 geometry and d) C1 geometry of the 609→159→0 angular correlation.

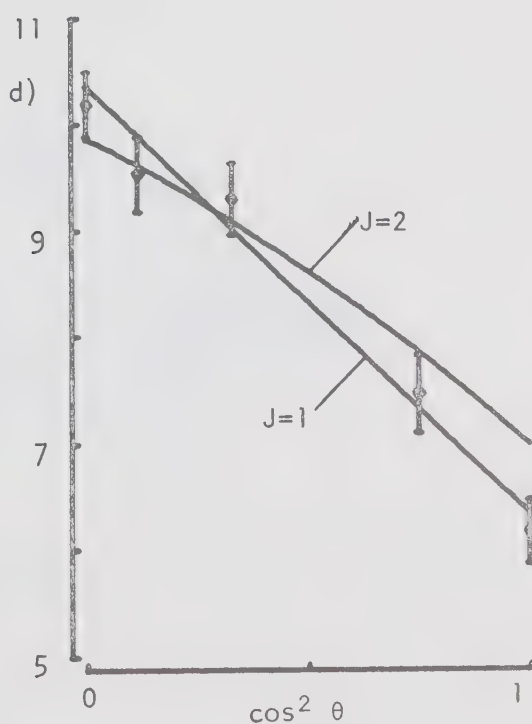
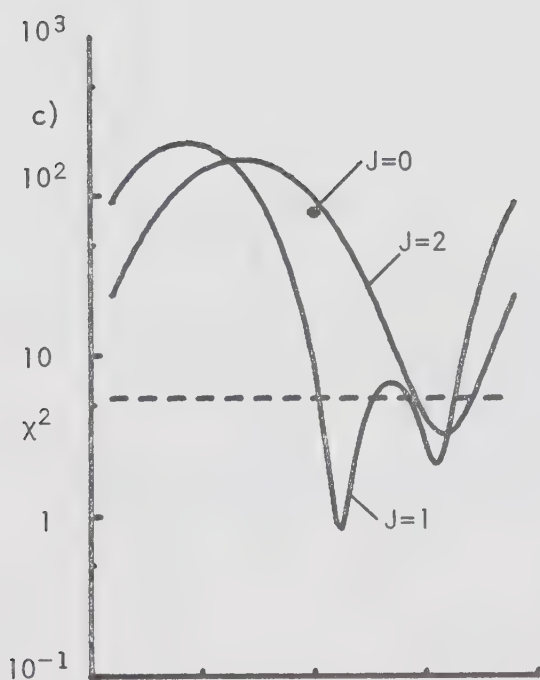
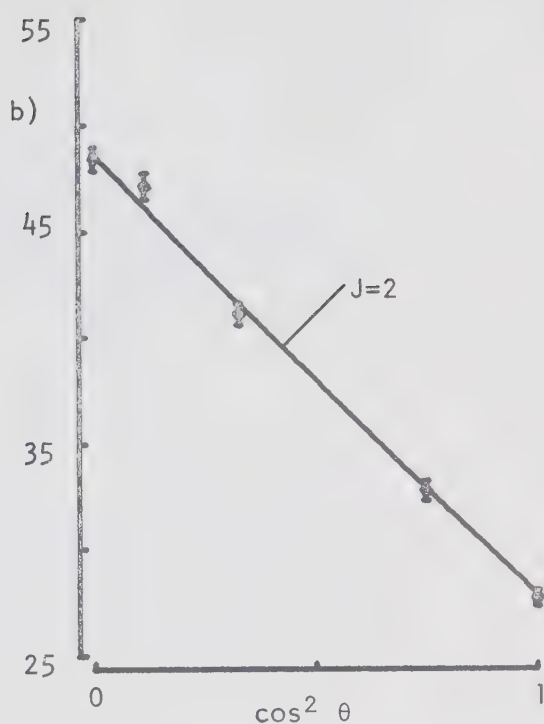
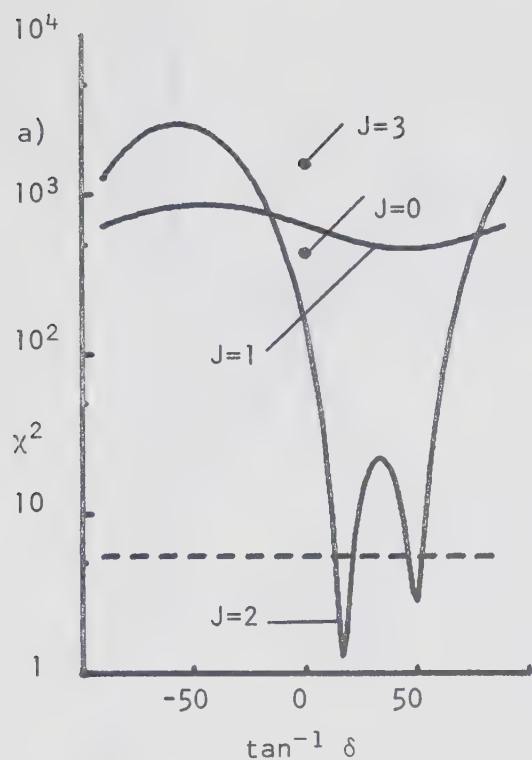


Figure 19. The 609 keV level: a) χ^2 curves and b) angular distribution for the 609 keV γ ray. c) χ^2 curves and d) angular distribution for the 609→344 transition. For c) and d), J refers to the spin of the 344 keV level.

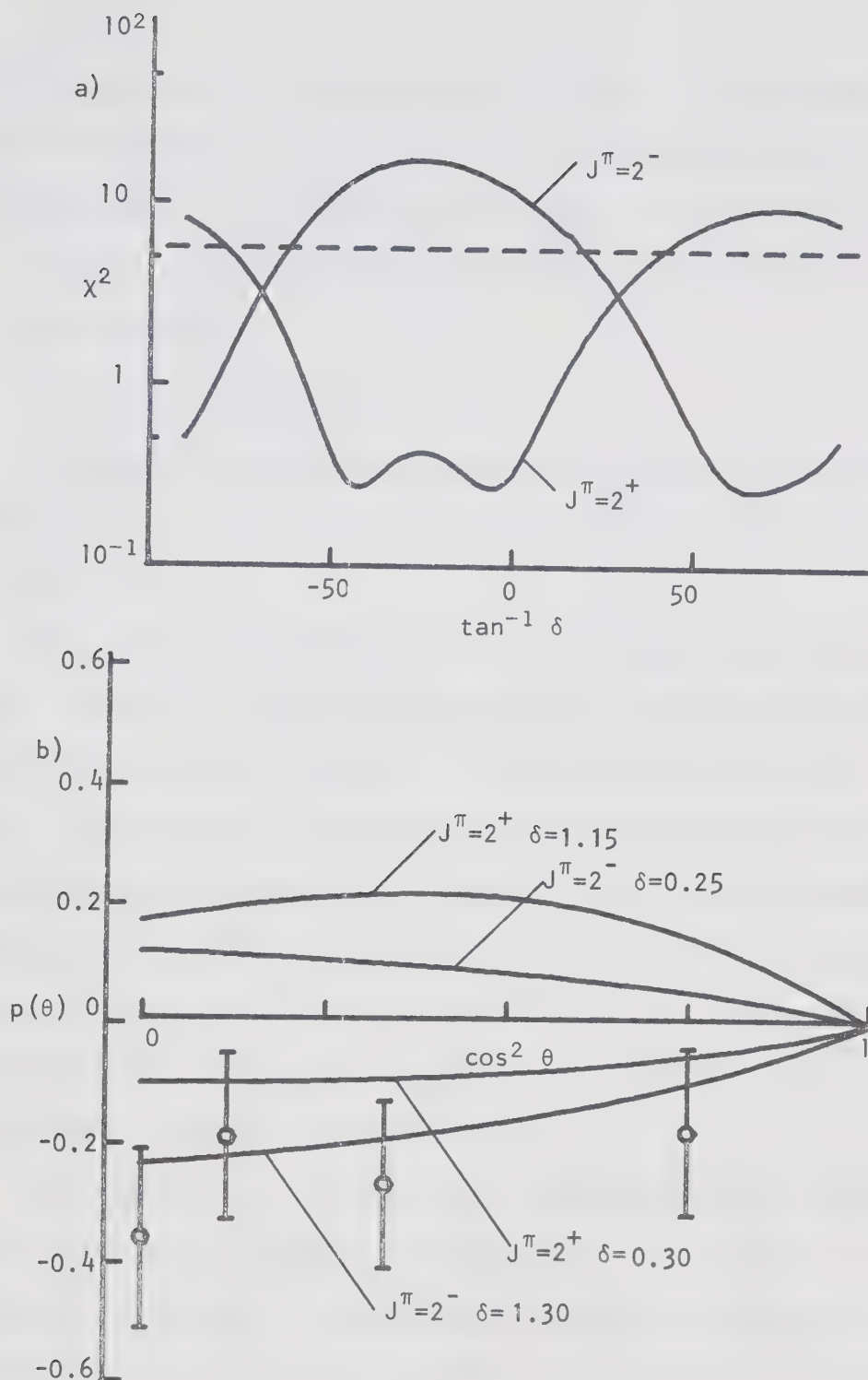


Figure 20. The 609 keV level: a) χ^2 curves and b) linear polarization distribution for the 609 keV γ ray.

$J = 2$ assignment fits the data best, with the $J = 3$ assignment being almost eliminated on the basis of the 0.1% confidence limit. The mixing ratio of the 450 keV γ ray is found to be 0.02 ± 0.07 .

Angular distribution measurements were not possible for the 331 keV transition.

4.2.6 The 663 keV Level

This level was observed to decay almost equally to the ground state and first two excited states, with a weaker branch (6%) to the 344 keV level.

The angular distribution of the ground state branch was isotropic ($a_2 = 0.00 \pm 0.02$), and as was the case for the 344 keV transition, acceptable fits were found for $J = 0, 1$ and 2 (see Figure 22). For the $J = 2$ assignment, the values of the mixing ratio which resulted in isotropy were quite limited. Figure 22 also shows the measured angular distribution of the 319 keV γ ray ($a_2 = -0.02 \pm 0.02$), which likewise gave possible fits for $J = 0, 1$ and 2 . Measurements on the 504 keV transition were not possible, due to the proximity of the large annihilation radiation peak at 511 keV.

The angular distribution and two geometries of the angular correlation for the 385 keV γ ray are shown in Figure 21. Both the distribution and the C1 geometry are isotropic, indicating that the initial state is not strongly aligned, while the A1 geometry has $a_2 = -0.18 \pm 0.03$. Simultaneous analysis of these measurements yields a unique assignment of $J = 1$ for this level, with $\delta = 0.07 \pm 0.05$ or $-4.7 \leq \delta \leq -2.9$. This assignment is in disagreement with Park and Daehnick (Pa 69), who favour a 3^+ assignment on the basis of an $L = 4$

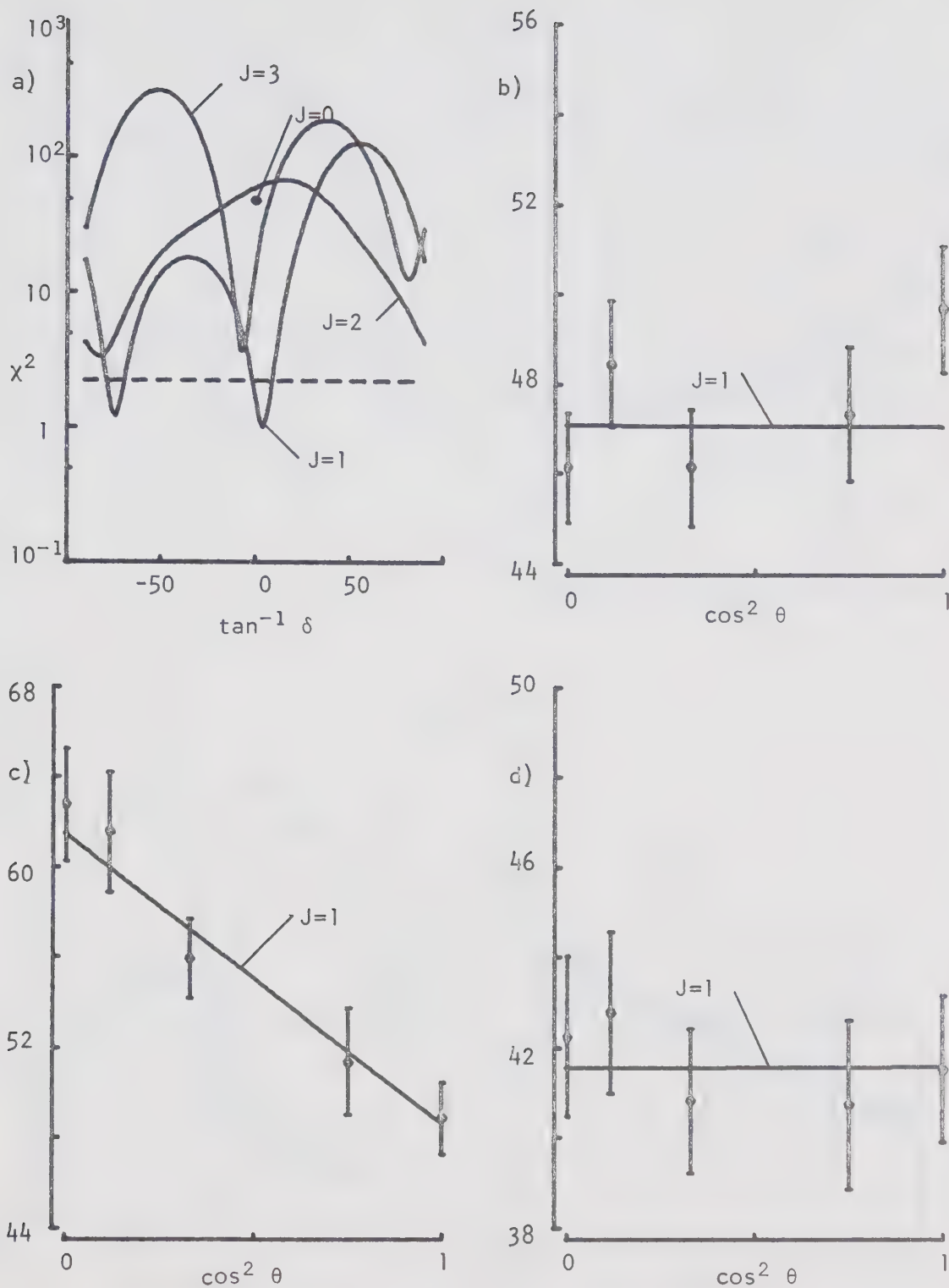


Figure 21. The 663 keV level: a) χ^2 curves, b) angular distribution for the 385 keV transition, c) A1 geometry and d) C1 geometry for the $663 \rightarrow 278 \rightarrow 0$ angular correlation.

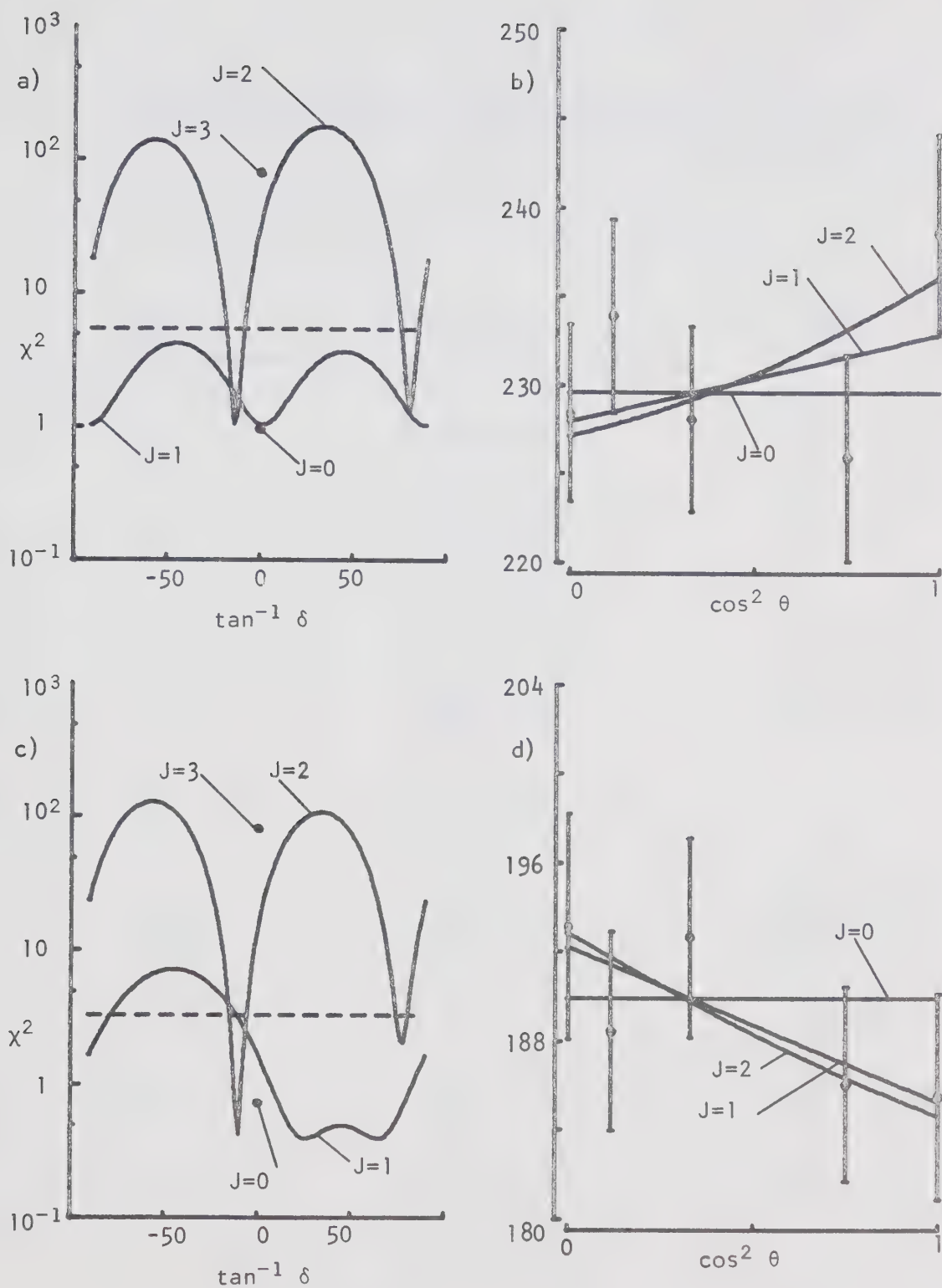


Figure 22. The 663 keV level: a) χ^2 curves and b) angular distribution for the 663 keV transition. c) χ^2 curves and d) angular distribution for the 663→344 transition.

Table VII A comparison between the mixing ratios determined in the present experiment and those of Davidson et al (Da 70).

E	Spins	δ	
		Present Work	Da 70
159	$2 \rightarrow 1$	0.12 ± 0.04	-0.01 ± 0.02
278	$2 \rightarrow 1$	0.10 ± 0.02	0.025 ± 0.025
344	$1 \rightarrow 1$	All Values	$(\delta > 0)$
185	$1 \rightarrow 2$	$0.10 \pm 0.10 \quad -7.1 \leq \delta \leq -3.0$	-
203	$3 \rightarrow 2$	0.06 ± 0.03	0.04 ± 0.035
609	$2 \rightarrow 1$	0.30 ± 0.08	0.03 ± 0.03
450	$2 \rightarrow 2$	0.02 ± 0.07	-0.05 ± 0.10
265	$2 \rightarrow 1$	0.24 ± 0.17	
663	$1 \rightarrow 1$	All values	-
385	$1 \rightarrow 2$	$0.07 \pm 0.05 \quad -4.7 \leq \delta \leq -2.9$	-
319	$1 \rightarrow 1$	$0.2 \leq \delta \leq 5.7$	-
580	$2 \rightarrow 2$	-0.18 ± 0.11	0.05 ± 0.04
	$3 \rightarrow 2$	-0.38 ± 0.04	-0.34 ± 0.06
461	$2 \rightarrow 2$	-0.29 ± 0.25	0.4 ± 0.1
	$3 \rightarrow 2$	-0.43 ± 0.10	-0.15 ± 0.07
377	$2 \rightarrow 3$	-0.11 ± 0.18	~ 0.05
	$3 \rightarrow 3$	0.57 ± 0.18	~ 0.50
468	$3 \rightarrow 2$	0.08 ± 0.03	-0.04 ± 0.035
736		0.40 ± 0.13	
617	$3 \rightarrow 2$	$0.07 \leq \delta \leq 2.5$	0.0 ± 0.1
649	$1 \rightarrow 2$	$0.04 \pm 0.11 \quad -5.7 \leq \delta \leq -2.5$ -0.11 ± 0.05	-

transfer from their $^{66}\text{Zn}(d,\alpha)$ measurement. Wellborn et al (We 71) studied the $663 \rightarrow 278 \rightarrow 0$ cascade, and found acceptable fits for either $J = 1$ or $J = 2$ for this state, with the $J = 1$ assignment more probable. Bass and Stelson (Ba 70) also found $J = 1$ (2) for this level.

4.2.7 The 739 and 746 keV Levels

The 739 keV level decays 77% to the first excited state, 6% to the 278 keV level, 4% to the 344 keV level and 13% to the 362 keV level. No ground state branch was seen.

The results for the 580 keV decay are shown in Figure 23, and indicate either $J = 2$, $\delta = -0.18 \pm 0.11$, or $J = 3$, $\delta = -0.38 \pm 0.04$. Similarly, the analysis of the results for the 461 keV γ ray yield possible solutions for either $J = 2$ or $J = 3$ (Figure 24), as does the angular distribution of the 377 keV transition, shown in Figure 25.

For the 746 keV level, only a single branch to the 278 keV state was observed. The results of the measurements on the 468 keV transition are shown in Figure 26, and the χ^2 analysis results in a unique assignment of $J = 3$, with a mixing ratio of $\delta = 0.08 \pm 0.03$.

4.2.8 The 878 keV Level

This state was observed to decay 55% to the ground state and 42% to the 344 keV state, with a very weak (3%) branch to the 159 keV level. The absence of strong decays to the two low-lying $J = 2$ levels suggests $J = 0$ for this level.

The angular distributions of the 878 keV and 719 keV γ rays are shown in Figure 27. Both of these decays were almost isotropic within experimental error ($a_2 = -0.05 \pm 0.04$ and $a_2 = -0.16 \pm 0.15$).

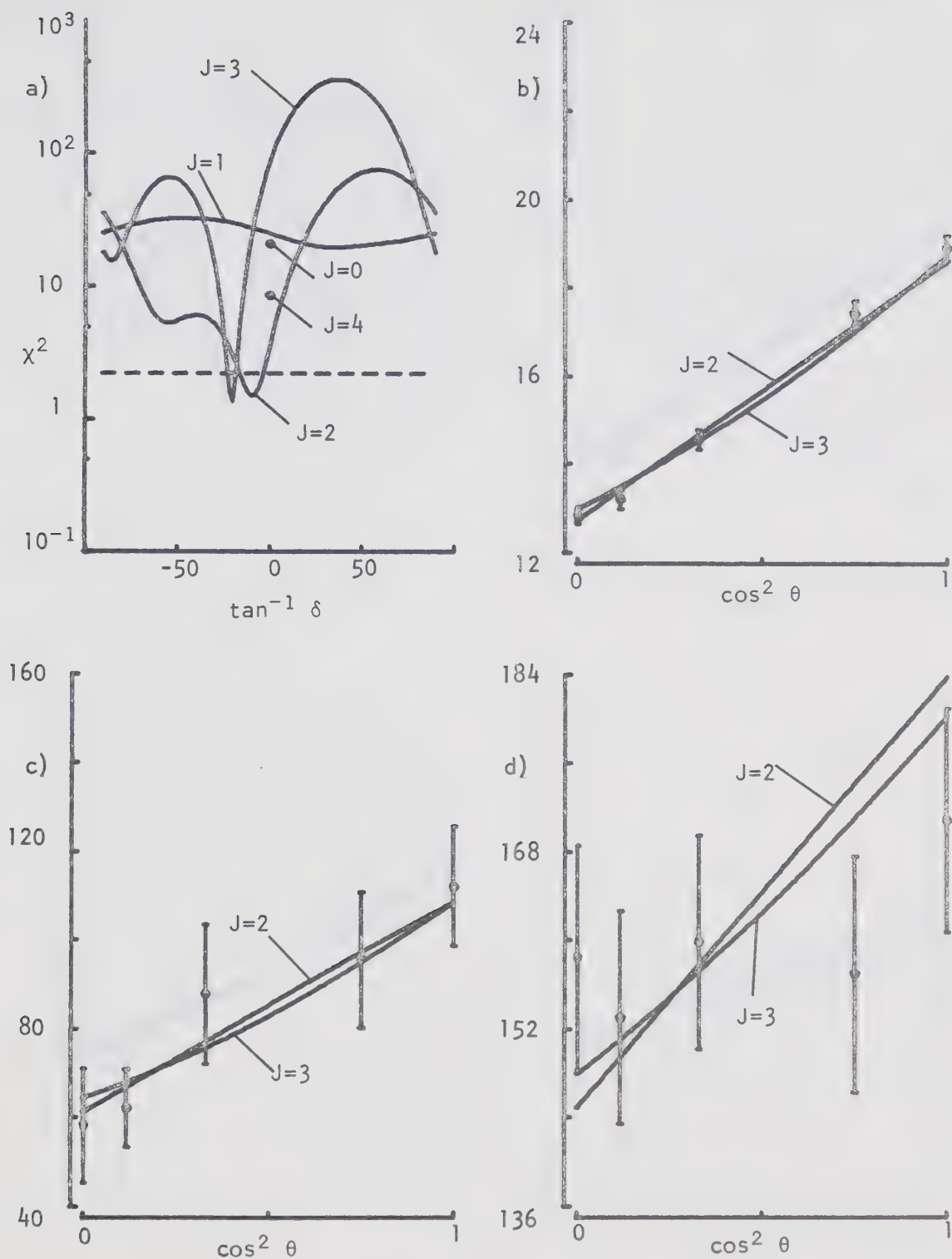


Figure 23. The 739 keV level: a) χ^2 curves, b) angular distribution for the 580 keV γ ray, c) A1 geometry and d) C1 geometry of the $739 \rightarrow 159 \rightarrow 0$ angular correlation.

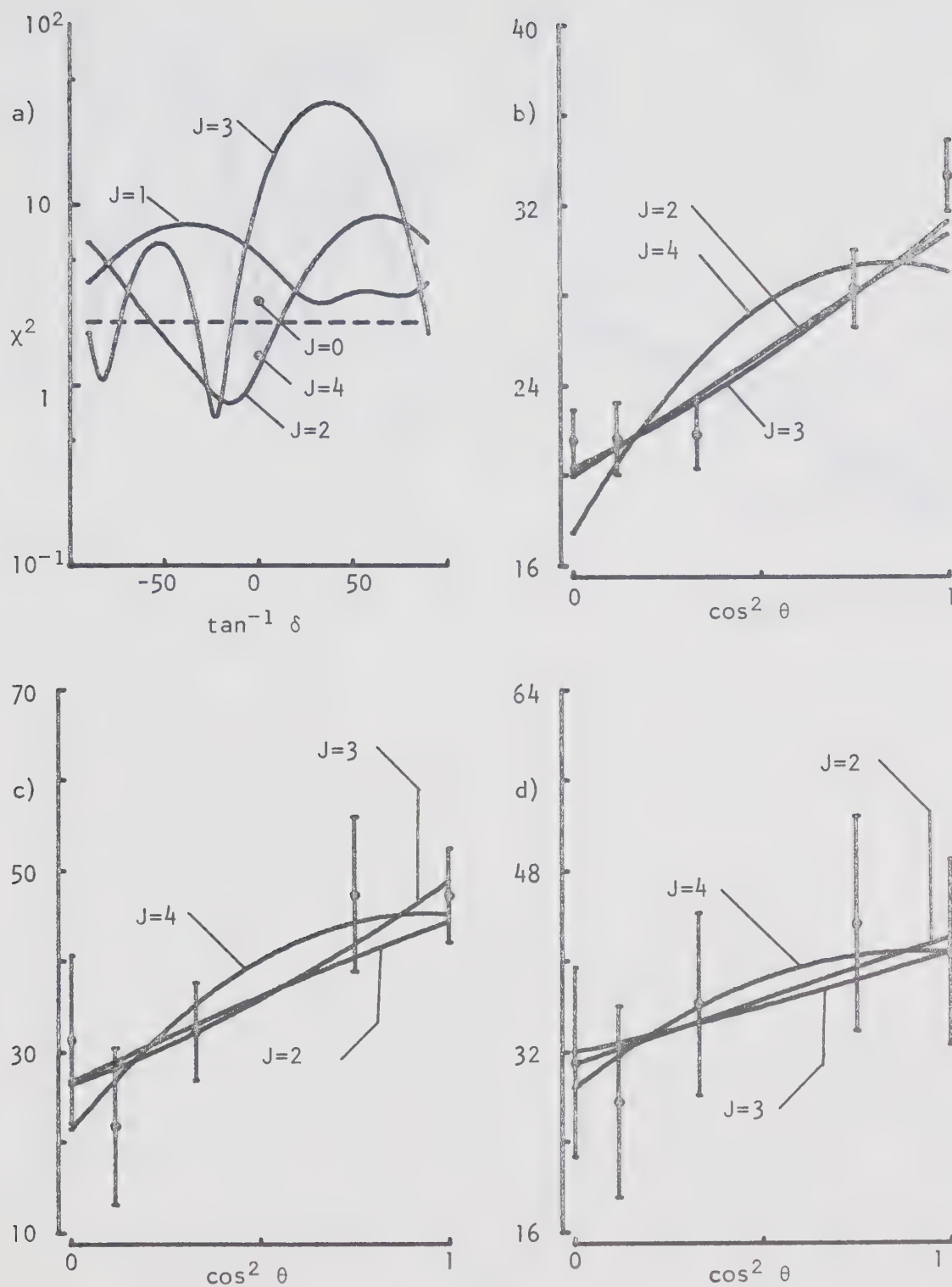


Figure 24. The 739 keV level: a) χ^2 curves, b) angular distribution for the 461 keV γ ray, c) A1 geometry and d) C1 geometry of the $739 \rightarrow 278 \rightarrow 0$ angular correlation.

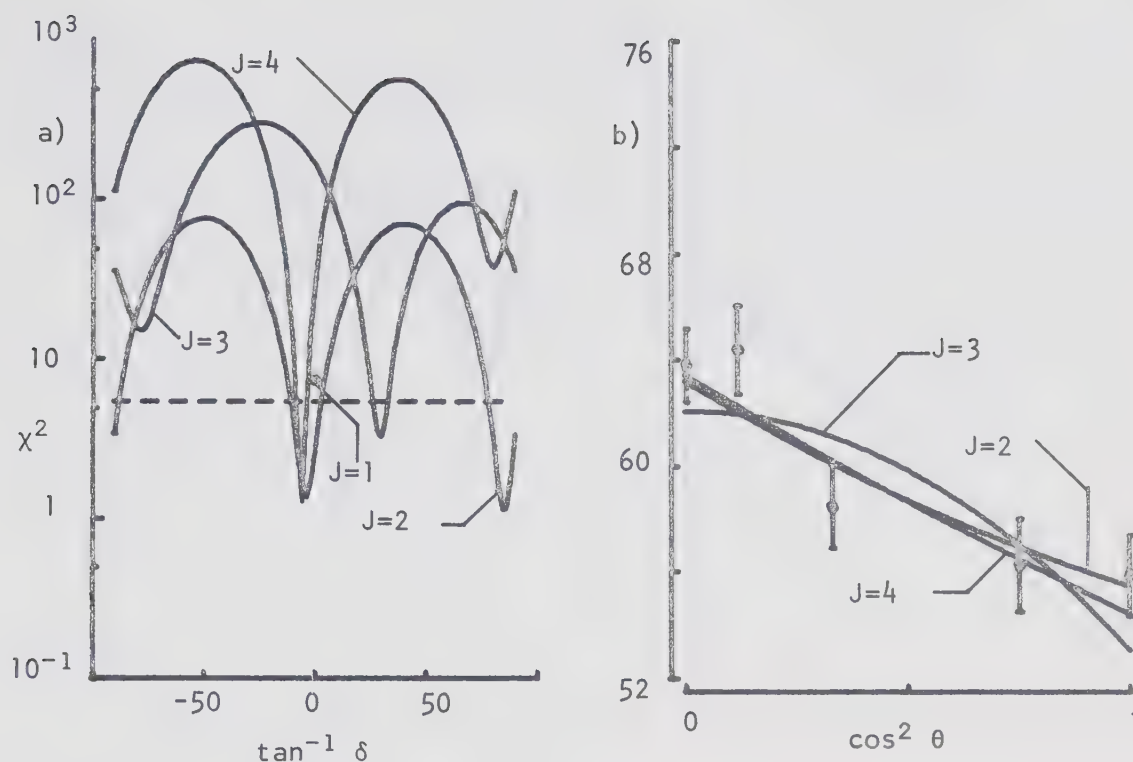


Figure 25. The 739 keV level: a) χ^2 curves and b) angular distribution for the 739→362 transition.

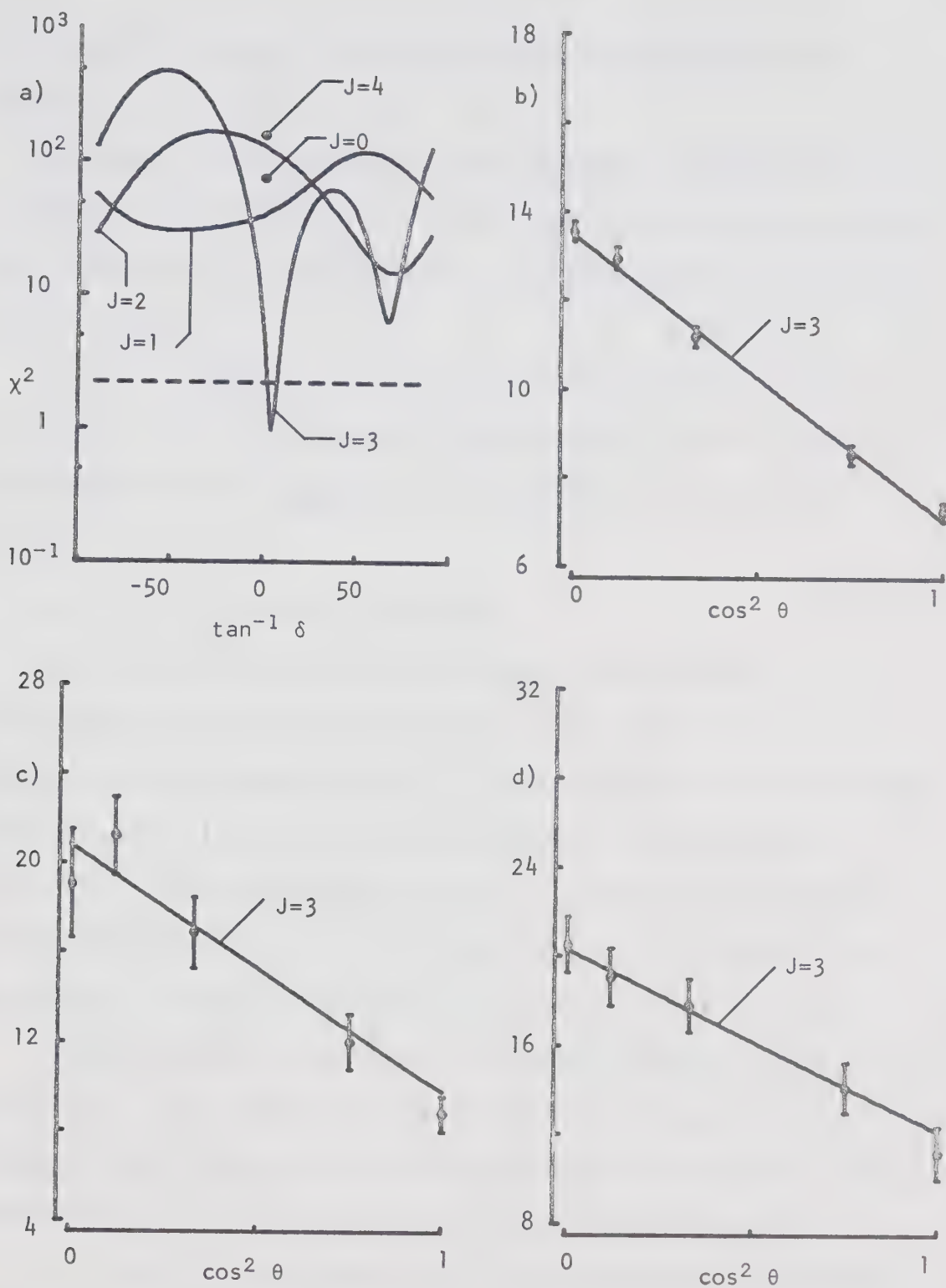


Figure 26. The 746 keV level: a) χ^2 curves, b) angular distribution for the 468 keV γ ray, c) A1 geometry and d) C1 geometry of the $746 \rightarrow 278 \rightarrow 0$ angular correlation.

respectively), and the χ^2 analysis shows acceptable fits for both distributions for $J = 0, 1$ or 2 .

The results for the 534 keV γ ray are shown in Figure 28. The Al geometry of the angular correlation showed appreciable anisotropy ($a_2 = 0.27 \pm 0.06$), and the data result in a unique assignment of $J = 0$ for this state.

The $J = 0$ assignment is in agreement with the most likely assignments of Park and Daehnick (Pa 69) and Bass and Stelson (Ba 70), but not with Davidson et al (Da 70), who find $J = 1$ or 2 , with $J = 1$ favoured.

4.2.9 The 895 and 927 keV Levels

The level at 895 keV was found to decay almost equally to the 159 keV and 278 keV states (40% and 49% respectively), with an 11% branch to the ground state as well. Angular distribution measurements were performed for the two strongest branches, and are shown in Figure 29. Both measurements resulted in a unique spin assignment of 3 for the 895 keV state, with mixing ratios of $\delta = 0.40 \pm 0.13$ for the 736 keV transition, and $0.07 \leq \delta \leq 2.5$ for the 617 keV γ ray.

As was mentioned in Section 4.1, accurate branching ratios for the 927 keV level could not be determined from our experiment. The strongest branch was to the 278 keV level, with weaker decays to the ground state and first excited state also being observed.

The results of the angular distribution and angular correlation measurements for the 649 keV transition are shown in Figure 30. Possible fits were obtained for $J = 1$, $\delta = 0.04 \pm 0.11$ or $-5.7 \leq \delta \leq -2.5$, and $J = 3$, $\delta = -0.11 \pm 0.05$. Park and Daehnick (Pa 69) assigned $J^\pi = 1^+$

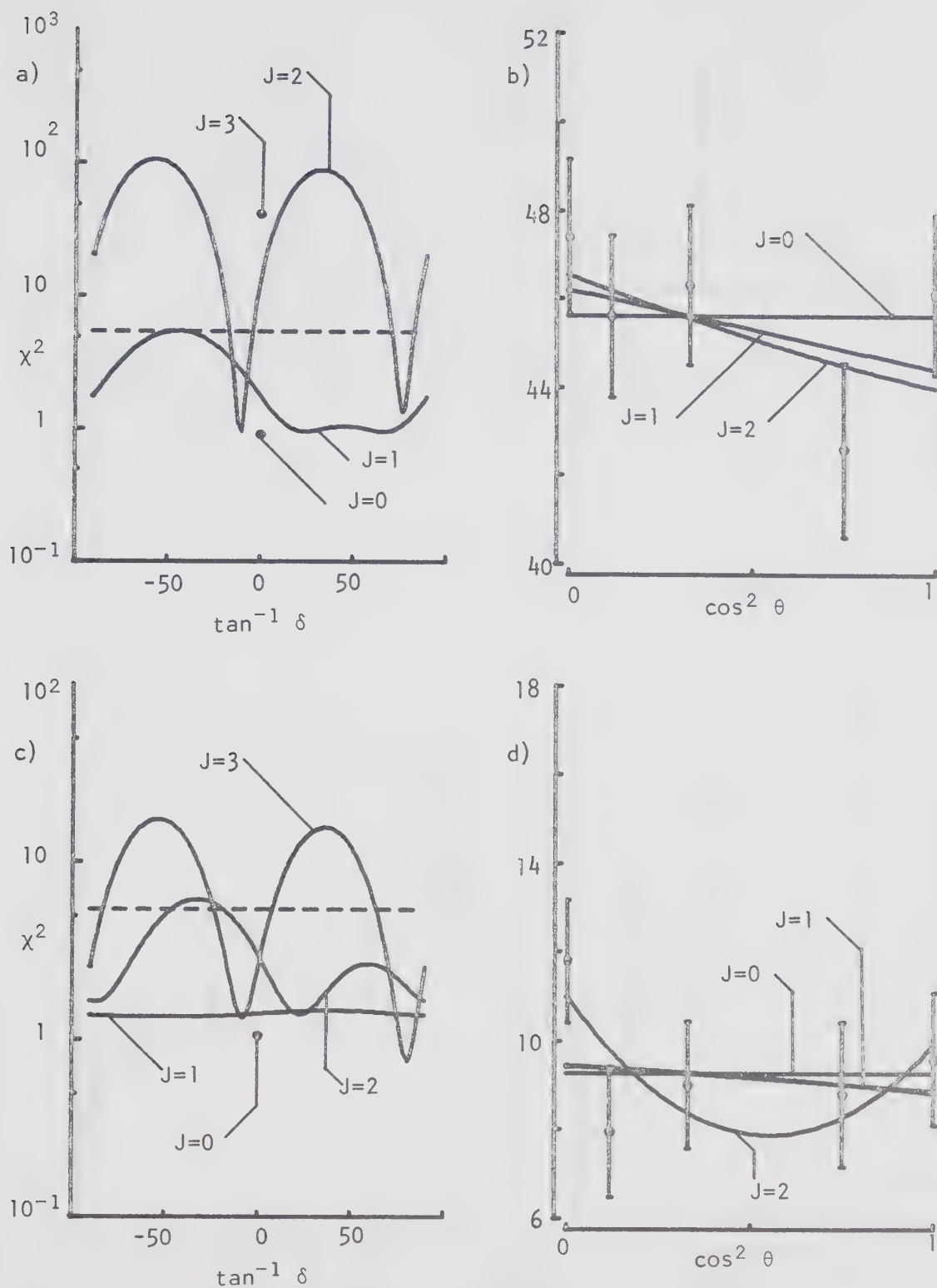


Figure 27. The 878 keV level: a) χ^2 curves, b) angular distribution for the $878 \rightarrow 0$ transition. c) χ^2 curves and d) angular distribution for the $878 \rightarrow 159$ transition.

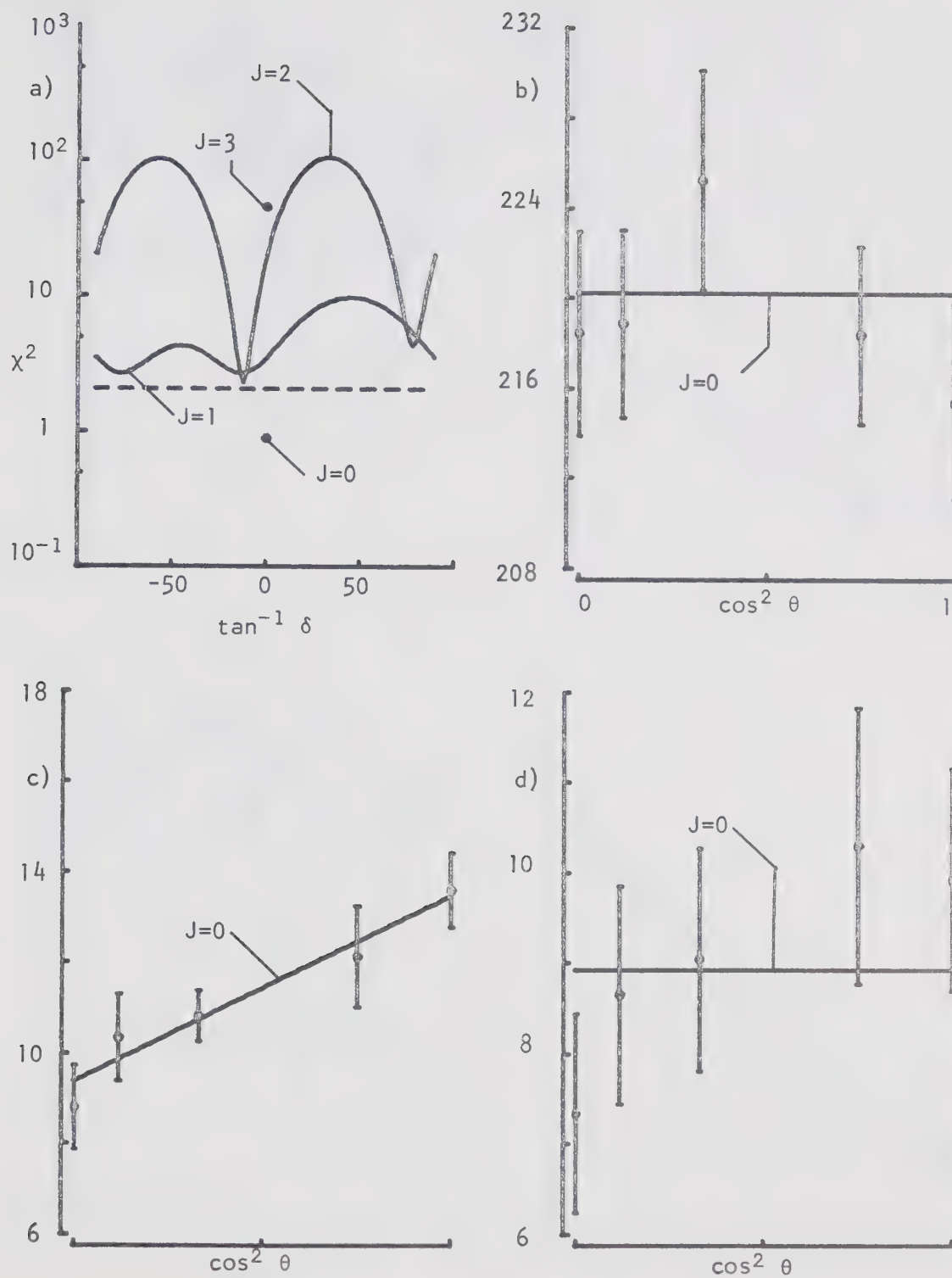


Figure 28. The 878 keV level: a) χ^2 curves, b) angular distribution for the 534 keV γ ray, c) A1 geometry and d) C1 geometry of the $878 \rightarrow 344 \rightarrow 0$ angular correlation.

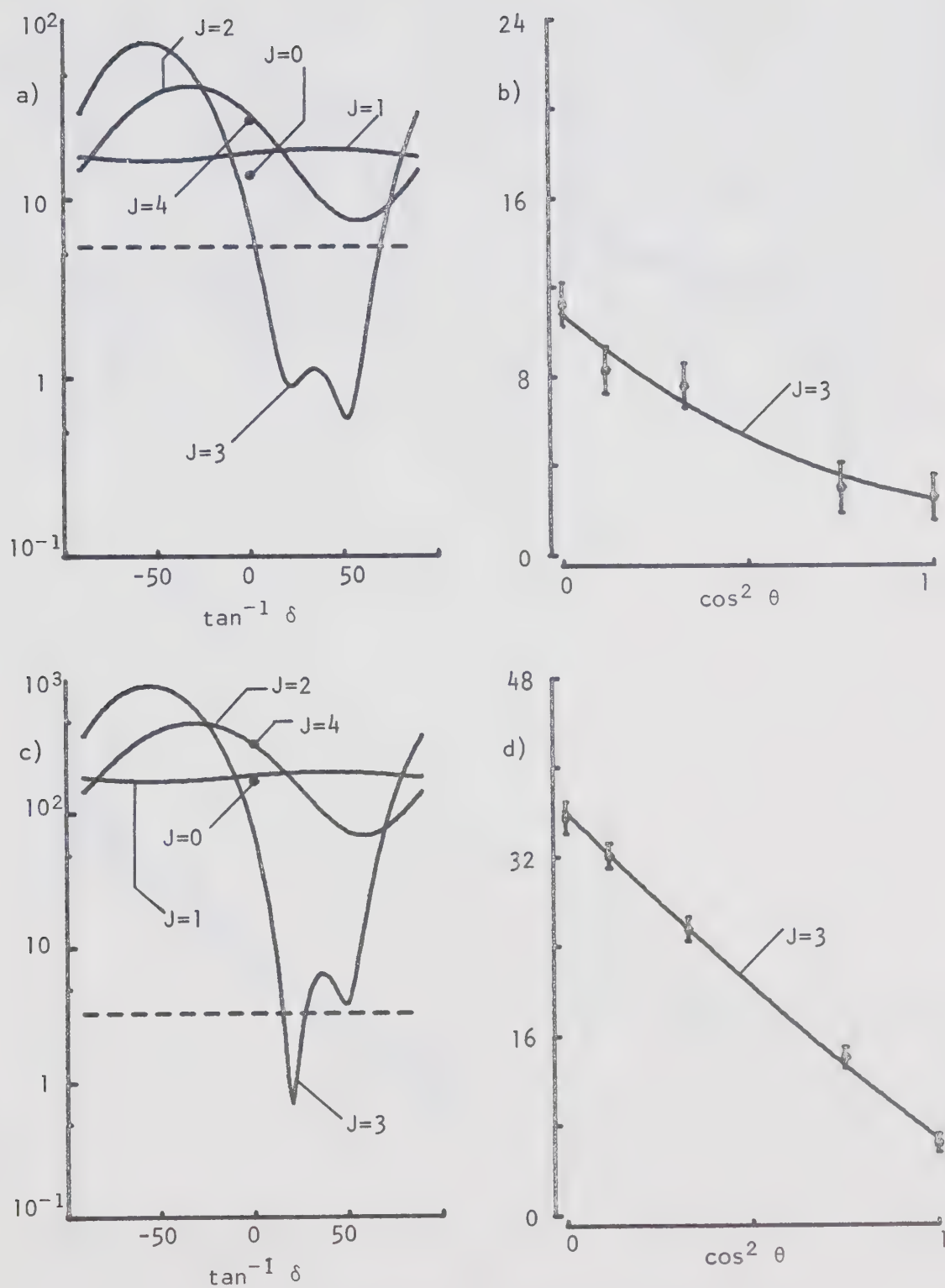


Figure 29. The 895 keV level: a) χ^2 curves and b) angular distribution for the 895→278 transition. c) χ^2 curves and d) angular distribution for the 895→159 transition.

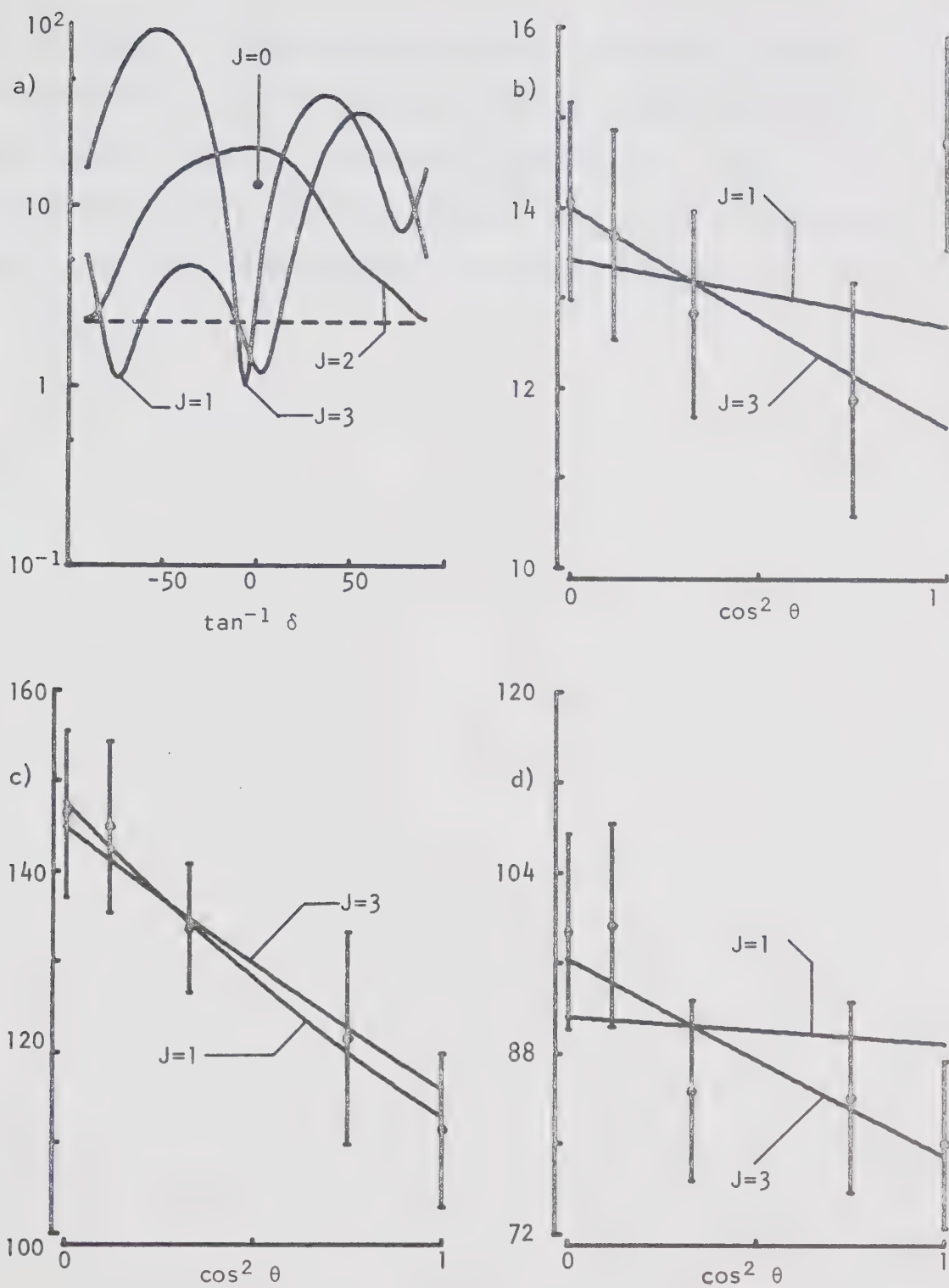


Figure 30. The 927 keV level: a) χ^2 curves, b) angular distribution for the 649 keV γ ray, c) A1 geometry and d) C1 geometry of the 927 \rightarrow 278+0 angular correlation.

for this level, on the basis of a strong $L = 0$ transfer in the $^{66}\text{Zn}(d,\alpha)^{64}\text{Cu}$ reaction while Bass and Stelson (Ba 70) find $J = 2$ most likely, with 0 or 1 assignments also possible. The $J = 1$ assignment therefore seems more probable, although our data cannot convincingly distinguish between the two possibilities.

CHAPTER 5

THE INTERMEDIATE COUPLING MODEL

5.1 Motivation

There is evidence, from the (d,p) stripping measurements of Park and Daehnick (Pa 69), for considerable fragmentation of the neutron single particle orbitals in ^{64}Cu . Although most of the $f_{5/2}$ strength has been assigned to the two levels at 362 keV and 574 keV excitation, considerable $l_n = 3$ admixtures are also observed for the ground state, first two excited states, and the level at 895 keV excitation. Much smaller fragments are observed for several states between 1.5 MeV and 3 MeV.

The $l_n = 1$ strength is concentrated mainly in the states below 1.5 MeV, but is split among about ten energy levels in this region. As in the case of the $f_{5/2}$ orbital, smaller fragments are observed up to 3 MeV.

As mentioned in Chapter 1, the low-lying energy levels of the even-even nucleus ^{62}Ni exhibit a characteristic vibrational spectrum, with a 2^+ first excited state lying midway between the 0^+ ground state and a triplet of states with $J^\pi = 0^+, 2^+$ and 4^+ . Such nuclei can be described by the collective vibrational model. The measured $B(E2)$ for the $2^+ \rightarrow 0^+$ transition in ^{62}Ni of 154 ± 17 e^2fm^4 (Du 66) is about 11 times larger than a single particle estimate

would give, again indicating that some sort of collective motion is taking place. Recently, Gomez (Go 71) and Markham (Ma 71) have presented calculations in which the odd-A nucleus ^{64}Cu is described as a single proton coupled to the surface vibrations of ^{62}Ni . Both of these calculations are able to reproduce the energy spectrum of ^{63}Cu extremely well, as well as the single particle spectroscopic factors and $B(E2)$ values for the γ decays. In view of the success of these calculations, it is tempting to apply a similar model to ^{64}Cu .

Calculations based on the Intermediate Coupling model have been carried out by several authors, mostly for odd-A nuclei (Ra 63, Ch 67, Ca 71, Go 71, Ma 71). Of the calculations which have been performed for even-A nuclei, the majority have been concerned with describing the properties of even-even nuclei in terms of two identical particles coupled to the vibrating core (Ma 63, He 67, Pa 71), and only the calculation of Heyde and Brussaard (He 68) for ^{140}La attempts to apply the model to odd-odd nuclei. This calculation gave fair agreement with the experimental energy spectrum of ^{140}La .

Section 2 of this chapter gives a brief discussion of two possible approaches to calculations of this type, the "Thakkar and True" model, and the Intermediate Coupling model, and a discussion of the relative merits of each. Section 3 contains a detailed discussion of the Intermediate Coupling model for odd-A and odd-odd nuclei, and Section 4 gives the results of the calculations for ^{64}Cu . A discussion of the results is presented in Section 5.

5.2 Basis for the Model

There are two general methods of approaching calculations in the Unified model. The first considers a single nucleon coupled to some sort of core state, but makes no assumptions about either the nature of these core states or the details of the interaction between the core and the extra particle. This type of approach was suggested by Lawson and Uretsky (La 57) and de Shalit (Sh 61), who assumed only that the particle-core interaction energy could be expressed as a sum of scalar products of two tensors, one of which acts only on the co-ordinates of the particle and one of which acts only on the co-ordinates of the core

$$H_{INT} = \sum_k T_k(p) \cdot T_k(c) \quad (5-1)$$

This model was later developed by Thankappen and True (Th 65, Th 66), who used an interaction of the form

$$H_{INT} = -\xi(\vec{J}(c) \cdot \vec{J}(p)) - \eta(Q(c) \cdot Q(p)) \quad (5-2)$$

where \vec{J} is the total angular momentum operator and Q the quadrupole moment operator. Using this model, they calculated the properties of the low-lying states of ^{63}Cu and obtained good agreement with the experimental energy spectrum and $B(E2)$ values for this nucleus.

In the Thankappen and True model, the matrix elements of the total Hamiltonian depend on the interaction strengths η and ξ , and reduced matrix elements of the form $\langle j' || Q(p) || j \rangle$ and $\langle J' || Q(c) || J \rangle$. The particle reduced matrix elements $\langle j' || Q(p) || j \rangle$ are calculated

using harmonic oscillator wave functions. Since the model does not assume a detailed knowledge of the core states, it is not possible to calculate the core reduced matrix elements, and they must be treated as adjustable parameters. One obvious disadvantage of this type of approach is that it is usually necessary to restrict the number of core states in the calculation rather severely, in order to keep the number of free parameters reasonably small.

The second approach to calculations of this type is to assume that the core is capable of performing collective oscillations, of the type described by Bohr and Mottelson (Bo 60). Usually, it is assumed that the core is described by a quadrupole surface oscillation, and that the form of the interaction between the extra particle and the core is known. The only adjustable parameter in this type of calculation is the strength of this interaction. Calculations of this type have been used by several authors (Go 71, Ma 71) to describe odd-mass nuclei in the vicinity of the Cu isotopes.

We will follow the second approach in studying the odd-odd nucleus ^{64}Cu . Besides the obvious computational advantage of having fewer adjustable parameters in the model, it is felt that the added generality of treating the ^{62}Ni core states as unknown is unnecessary. The spectrum of ^{62}Ni , along with the success of the calculations for ^{63}Cu , seems to indicate that the ^{62}Ni core is adequately described in terms of the vibrational model.

5.3 Formulation of the Model

This section contains a brief description of the mathematical formulation of the Intermediate Coupling model. A more detailed discussion of the model, including the derivation of most of the formulae presented here, is given in Appendix B.

For simplicity, we first consider the case of a single particle coupled to a core. It is assumed that the core is capable of performing collective oscillations, and that the nuclear radius can be expanded in the form

$$R(\theta, \phi) = R_0 [1 + \sum_{\lambda \mu} \alpha_{\lambda}^{\mu} Y_{\lambda}^{\mu}(\theta, \phi)] \quad (5-3)$$

The term with $\lambda = 0$ corresponds to changes in the density of the nucleus. Such "breathing modes" of excitation require a great deal of energy, and are not expected to be important in the description of low-energy properties of the nucleus. The $\lambda = 1$ term corresponds to oscillations of the centre-of-mass of the nucleus. The first term which is expected to be important for the low energy properties of nuclei is that for $\lambda = 2$, and we will assume that all higher order terms in (5-3) are negligible. The extra particle is assumed to have several single particle orbits available to it.

The total Hamiltonian for this system can be written as a sum of three terms

$$H = H_c + H_p + H_{INT} \quad (5-4)$$

The Hamiltonian for the core (H_c) can be written as

$$H_c = \sum_{\mu} (b_{\mu}^{\dagger} b_{\mu} + 1/2) \hbar \omega \quad (5-5)$$

where b_{μ}^{\dagger} and b_{μ} are respectively the creation and annihilation operators for (spin 2) phonons of energy $\hbar \omega$. The explicit form of the Hamiltonian for the extra particle (H_p) is not important for this discussion, and it is sufficient to note that when it acts on a single particle wavefunction, it has the single particle energy ϵ_j for that particular orbital as its eigenvalue. The interaction Hamiltonian is given by

$$H_{INT} = -(\frac{\pi}{5})^{\frac{1}{2}} \hbar \omega \xi [(-)^{\mu} b_{-\mu}^{\dagger} + b_{\mu}] Y_2^{\mu}(\theta, \phi) \quad (5-6)$$

where (θ, ϕ) are the polar angles of the extra particle. The strength of this interaction is given by the dimensionless coupling constant ξ .

The basis states are chosen as those of the uncoupled system, and are specified by the number of phonons in the core state N , which are coupled to total angular momentum R , the single particle angular momentum j and the total angular momentum $I = |\vec{R} + \vec{j}|$. Neglecting the zero-point energy, the diagonal elements of the total Hamiltonian are

$$\langle NRj; IM | H_c + H_p | NRj; IM \rangle = N \hbar \omega + \epsilon_j \quad (5-7)$$

The off-diagonal elements in the Hamiltonian matrix are due entirely to H_{INT} , and including this term results in mixing between the basis

states. The selection rules for non-vanishing matrix elements of H_{INT} are $\Delta N = \pm 1$, $\Delta R \leq 2$, $\Delta j \leq 2$ and $\Delta l = 0, 2$ only. The eigenvectors of the complete system are given as linear combinations of the basis states

$$|E; IM\rangle = \sum_{NRj} B^E(NRjI) |NRj; IM\rangle \quad (5-8)$$

and the expansion coefficients $B^E(NRjI)$ are found by diagonalizing the Hamiltonian matrix.

For a system composed of two particles outside a collective core, the Hamiltonian is

$$H = H_c + H_p(1) + H_{INT}(1) + H_p(2) + H_{INT}(2) + H_{12} \quad (5-9)$$

where the indices 1 and 2 refer to particles 1 and 2 respectively, and H_{12} is the residual interaction between the two extra particles. As explained in Appendix B, it is convenient to choose as a basis set for this system, states in which particle 2 is coupled to eigenstates of the core plus the first particle

$$|\alpha_1 J_1 j_2; IM\rangle = \sum_{m_2} (J_1 j_2; M-m_2 \ m_2 | IM) |\alpha_1 J_1 M-m_2\rangle |j_2 m_2\rangle \quad (5-10)$$

The states $|\alpha_1 J_1 M-m_2\rangle$ are given by equation (5-8), and are found by diagonalizing the first three terms in the Hamiltonian (5-9). The first four terms in (5-9) are diagonal in this representation

$$\begin{aligned} \langle \alpha_1 J_1 j_2; IM | H_c + H_p(1) + H_{INT}(1) + H_p(2) | \alpha_1 J_1 j_2; IM \rangle \\ = (E_{J_1}^{\alpha_1} + \epsilon_{j_2}) \end{aligned} \quad (5-11)$$

where ϵ_{j_2} is the single particle energy of particle 2, and $E_{J_1}^{\alpha_1}$ is the energy of the core plus first particle eigenstate. $H_{INT}(2)$ and H_{12} have both diagonal and off-diagonal matrix elements in this representation. Explicit formulae are given in Appendix B.

5.4 Application of the Model to ^{64}Cu

5.4.1 Energy Levels of ^{63}Cu

The first step in this calculation is to consider the nucleus ^{63}Cu as a single proton coupled to the ^{62}Ni core. This problem has been treated by Gomez (Go 71) and Markham (Ma 71). The odd proton is assumed to have the $2p_{3/2}$, $1f_{5/2}$ and $2p_{1/2}$ orbitals available. The single particle energy spacings were taken as $\epsilon_{5/2} - \epsilon_{3/2} = 1.500$ MeV and $\epsilon_{1/2} - \epsilon_{3/2} = 2.200$ MeV in agreement with the best-fit values found by Gomez. These values are not very different from those found by Blair (Bl 65) from the $^{62}\text{Ni}(^3\text{He},d)$ reaction. The phonon energy $\hbar\omega = 1.172$ MeV was obtained from the excitation energy of the first 2^+ level in the ^{62}Ni core. In order to keep the number of components in the ^{63}Cu eigenstates small enough so that the two particle calculations remain reasonably simple, only core states with $N \leq 2$ were considered in this calculation.

Using the above values for the parameters, the Hamiltonian matrices for total spin values $I = 1/2, 3/2, 5/2, 7/2$ and $9/2$ were diagonalized using the computer code CUPPLE-1 (Gr 73a). Figure 31 shows how the energy levels for the different spin values vary as a function of the coupling parameter ξ . The best fit was found for a value of $\xi = 2.12$ which is indicated by a vertical dashed line in

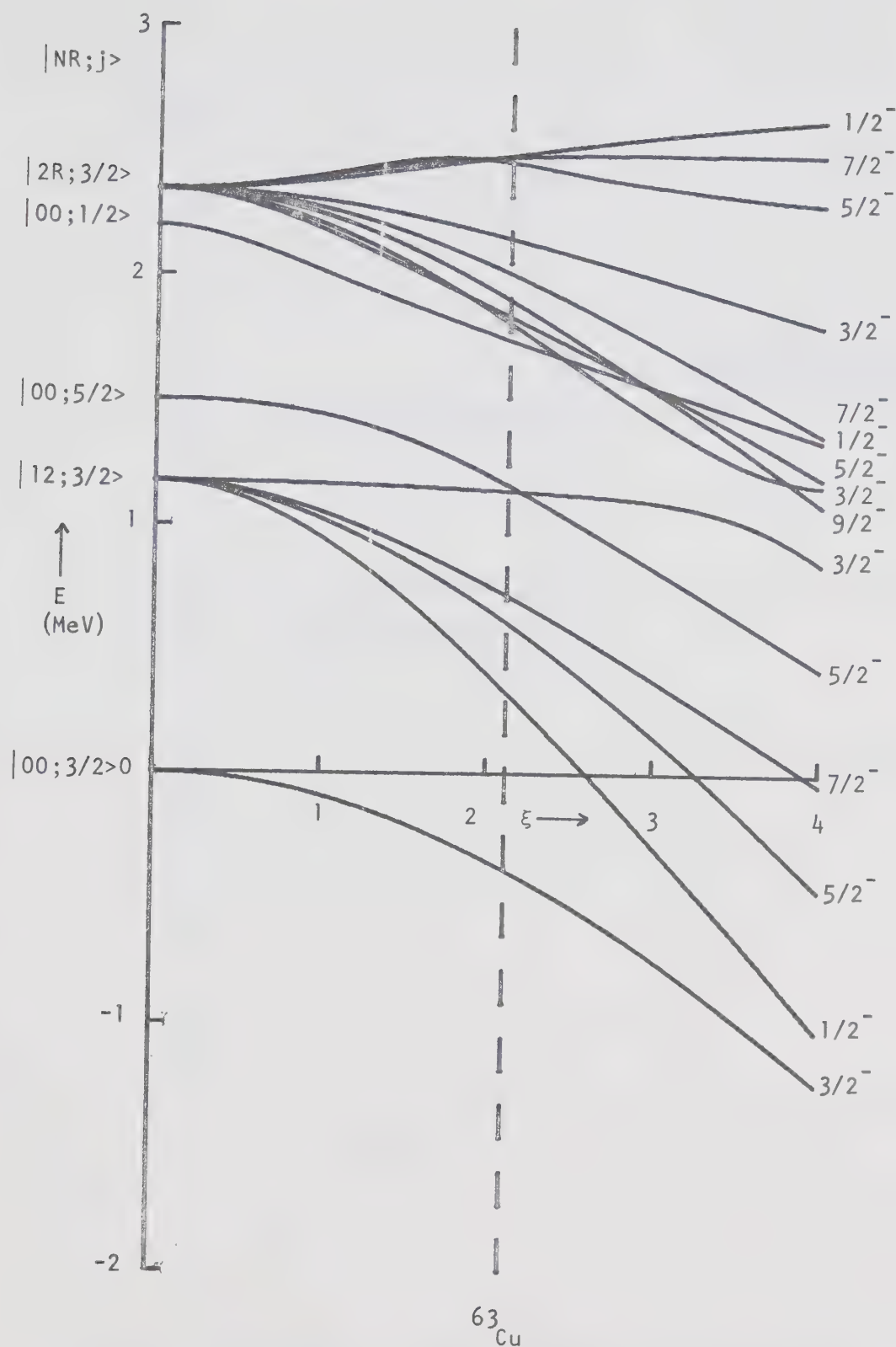


Figure 31. The Intermediate Coupling Model: Energy levels of the $^{62}\text{Ni}+p$ system as a function of the coupling strength ξ . The best fit to the levels of ^{63}Cu occurs for $\xi=2.12$.

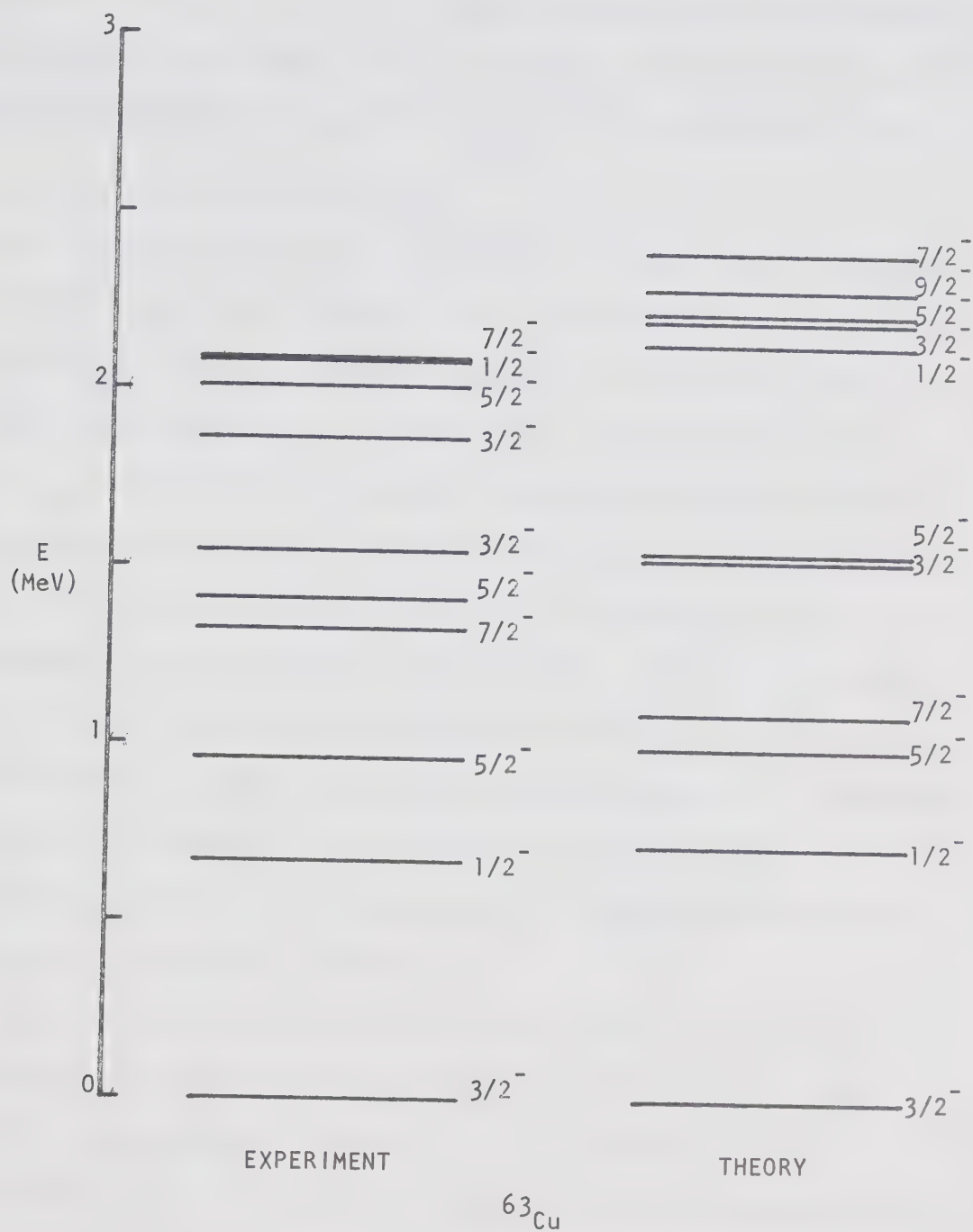


Figure 32. A comparison between the experimental energy spectrum of ^{63}Cu and the level scheme calculated from the Intermediate Coupling model.

Figure 31. Figure 32 shows the comparison between the calculated and experimental energy levels for ^{63}Cu , and Table VIII lists the expansion coefficients $B^E(\text{NRj}l)$ of equation (5-8) for the lowest energy levels.

5.4.2 Energy Levels of ^{64}Cu

For the ^{64}Cu calculations, the lowest 11 eigenstates of the ^{63}Cu system were used as basis states, and the odd neutron was assumed to have the $1f_{5/2}$ and $2p_{1/2}$ orbitals available. The energy separation for these two single particle orbitals was chosen originally as $\epsilon_{1/2} - \epsilon_{5/2} = 0.500$ MeV in agreement with the value deduced from the (d,p) measurements of Fulmer and McCarthy (Fu 63). This value was later reduced to 0.400 MeV to obtain better agreement with the experimental energy spectrum. The value of ξ_p (for the proton) was fixed at 2.12, the value which gave the best fit to the ^{63}Cu spectrum. The two-particle residual interaction H_{12} was chosen as a δ -function. The calculation then has three parameters, these being the neutron interaction strength ξ_n , the single particle energy spacing and the two particle interaction strength.

Figure 33 shows the calculated energy levels of ^{64}Cu , as a function of the neutron coupling strength ξ_n , for $\eta = 0.0$. The best fit corresponds to a value of $\xi_n = 1.5$. No significant improvement in the fit was obtained when the two particle interaction strength η was varied from zero. The left-hand side of Figure 34 shows the calculated energy levels of ^{64}Cu using this model, compared to the experimental spectrum shown in the centre. Only positive parity levels are shown, and spin assignments for the levels above 1 MeV are taken from the work of Park and Daehnick (Pa 69). Table IX

Table VIII Expansion coefficients for the states $|E(\text{keV}); I^\pi\rangle$ in ^{63}Cu .

$ NRJ\rangle$	$ 0; 3/2^- \rangle$	$ 714; 1/2^- \rangle$	$ 993; 5/2^- \rangle$	$ 1092; 7/2^- \rangle$
$ 00\ 3/2\rangle$	0.8941			
$ 12\ 3/2\rangle$	-0.3773	0.7647	0.7456	0.9070
$ 00\ 5/2\rangle$			-0.4884	
$ 00\ 1/2\rangle$		0.4701		
$ 20\ 3/2\rangle$	0.0801			
$ 22\ 3/2\rangle$	0.0258	-0.2823	0.1483	-0.1050
$ 24\ 3/2\rangle$			-0.3034	-0.3503
$ 12\ 5/2\rangle$	0.1228	0.2908	0.1816	-0.0028
$ 12\ 1/2\rangle$	-0.1644		-0.1934	
$ 20\ 5/2\rangle$			-0.0853	
$ 22\ 5/2\rangle$	0.0029	-0.1121	-0.0578	0.0696
$ 24\ 5/2\rangle$	-0.0736		0.0258	0.0870
$ 20\ 1/2\rangle$		0.1321		
$ 22\ 1/2\rangle$	0.0610		-0.0989	
$ 24\ 1/2\rangle$				-0.1767

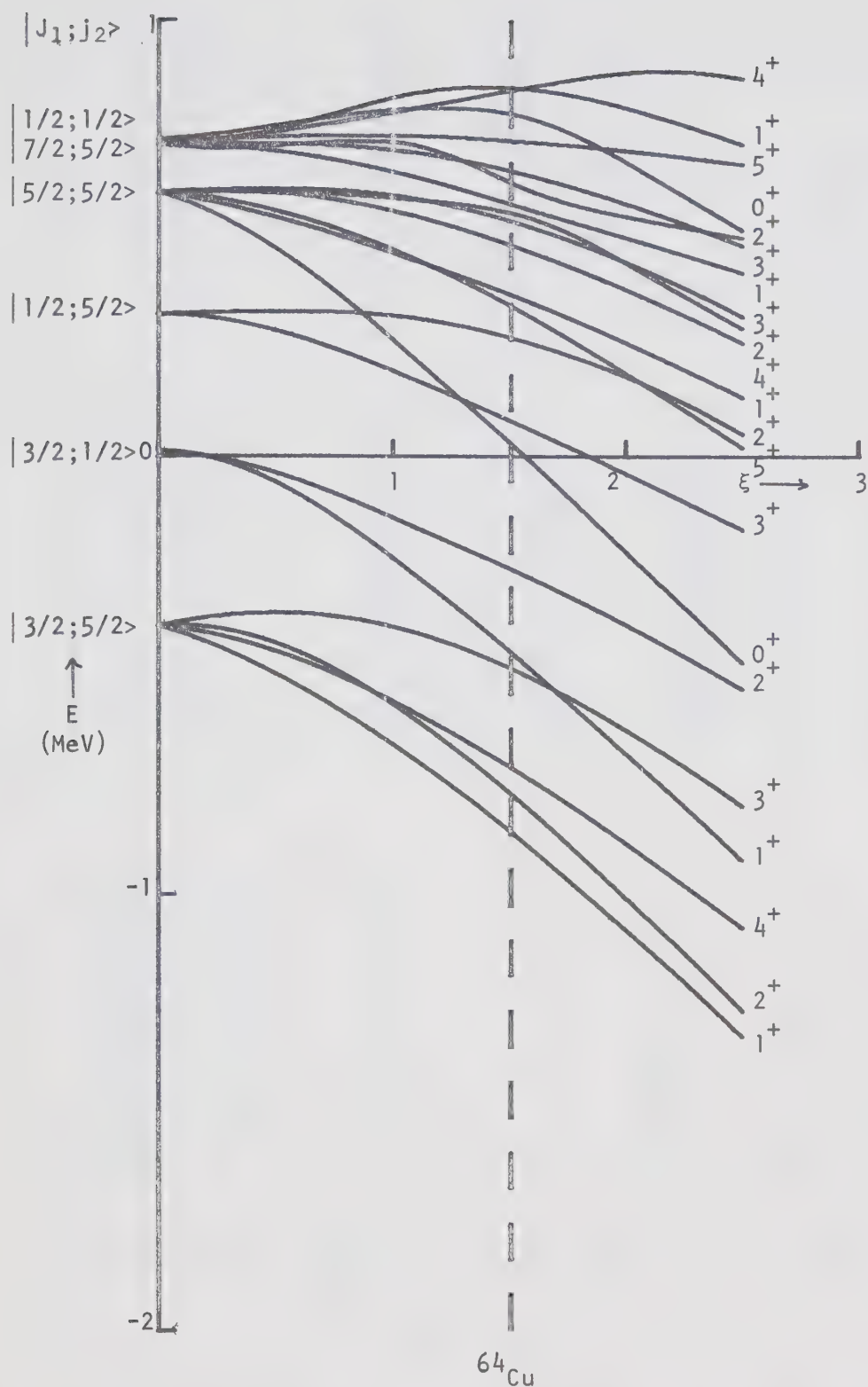


Figure 33. The Intermediate Coupling model: Energy levels of the $^{63}\text{Cu}+n$ system as a function of the coupling strength ξ . The best fit to the levels of ^{64}Cu occurs for $\xi=1.5$.

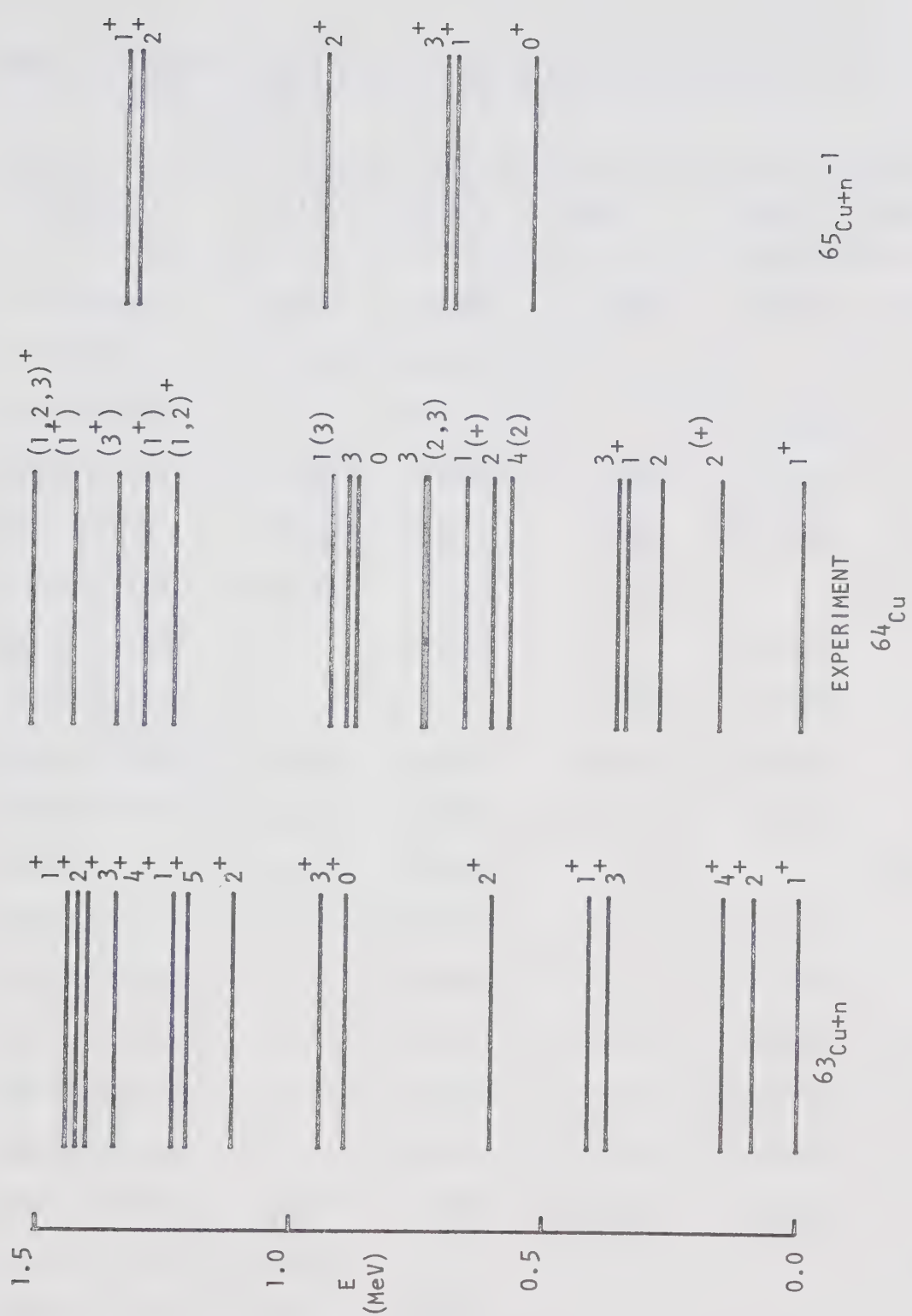


Figure 34. A comparison between the experimental level scheme of ^{64}Cu and the energy levels predicted by the Intermediate Coupling model.

Table IX Expansion coefficients for the states $|E(\text{keV}); I^\pi\rangle$ in ^{64}Cu .

$ EJ_1; j_2\rangle$	$ 0; 1^+\rangle$	$ 86; 2^+\rangle$	$ 146; 4^+\rangle$	$ 375; 3^+\rangle$	$ 413; 1^+\rangle$
$ 0\ 3/2^-; 5/2\rangle$	0.9117	0.7360	0.9285	0.8716	0.1408
$ 0\ 3/2^-; 1/2\rangle$	-0.1827	-0.5119			0.8053
$ 714\ 1/2^-; 5/2\rangle$		-0.3346		0.2888	
$ 993\ 5/2^-; 5/2\rangle$	0.1682	-0.0089	-0.1594	0.1442	0.3127
$ 1092\ 7/2^-; 5/2\rangle$	-0.1356	-0.2465	-0.2330	-0.2269	0.4598
$ 714\ 1/2^-; 1/2\rangle$	-0.2553				-0.1159
$ 993\ 5/2^-; 1/2\rangle$		-0.0440		-0.2494	
$ 1092\ 7/2^-; 1/2\rangle$			0.2259	0.0800	
$ 1525\ 3/2^-; 5/2\rangle$	-0.1237	-0.0597	-0.0563	0.0856	0.0323
$ 1546\ 5/2^-; 5/2\rangle$	0.0265	0.0313	-0.0508	0.0008	0.0436
$ 1525\ 3/2^-; 1/2\rangle$	0.0455	0.0943			-0.0138
$ 1546\ 5/2^-; 1/2\rangle$		-0.0125		-0.0337	
$ 2134\ 1/2^-; 5/2\rangle$		0.0481		-0.0186	
$ 2199\ 3/2^-; 5/2\rangle$	0.0318	0.0405	0.0126	0.0098	-0.0043
$ 2221\ 5/2^-; 5/2\rangle$	-0.0470	0.0391	0.0095	-0.0413	-0.0470
$ 2290\ 9/2^-; 5/2\rangle$		-0.0181	0.0228	-0.0507	
$ 2397\ 7/2^-; 5/2\rangle$	-0.0060	0.0077	0.0031	0.0221	-0.0589
$ 2134\ 1/2^-; 1/2\rangle$	0.0434				0.0057
$ 2199\ 3/2^-; 1/2\rangle$	-0.0191	-0.0457			0.0118
$ 2221\ 5/2^-; 1/2\rangle$		0.0035		-0.0492	
$ 2290\ 9/2^-; 1/2\rangle$			-0.0010		
$ 2397\ 7/2^-; 1/2\rangle$			-0.0259	-0.0041	

gives the expansion coefficients for the first few levels of ^{64}Cu . Table X lists the best fit values for the parameters used in this calculation.

An inspection of Figure 34 shows that not all of the levels of ^{64}Cu are reproduced by this calculation. In particular, there are no levels in the theoretical spectrum which correspond to the 2^+ state at 278 keV, the $J = 1$ level at 663 keV or the $J = 3$ level at 746 keV excitation. It was thought that these levels might be due to the excitation of a $p_{3/2}$ neutron into the $f_{5/2}$ orbital, and could therefore be explained as a $p_{3/2}$ neutron hole coupled to the levels of ^{65}Cu .

The outline of this calculation follows that of the previous one. The parameters for ^{65}Cu are identical to those used by Gomez (Go 71). Figure 35 shows the energy levels of ^{65}Cu as a function of ξ_p , with the best fit value of $\xi_p = 2.10$ shown as a dashed line. Figure 36 shows a comparison of the experimental and calculated energy levels of ^{65}Cu .

The predicted energy levels of ^{64}Cu arising from this configuration are shown on the right hand side of Figure 34. It was not possible to obtain a good fit for any value of the coupling strength ξ_n ; the levels shown in this diagram are those for $\xi_n = 1.5$. The agreement between the experimental levels and the theoretical predictions is not good. The parameters used for this calculation are given in Table X.

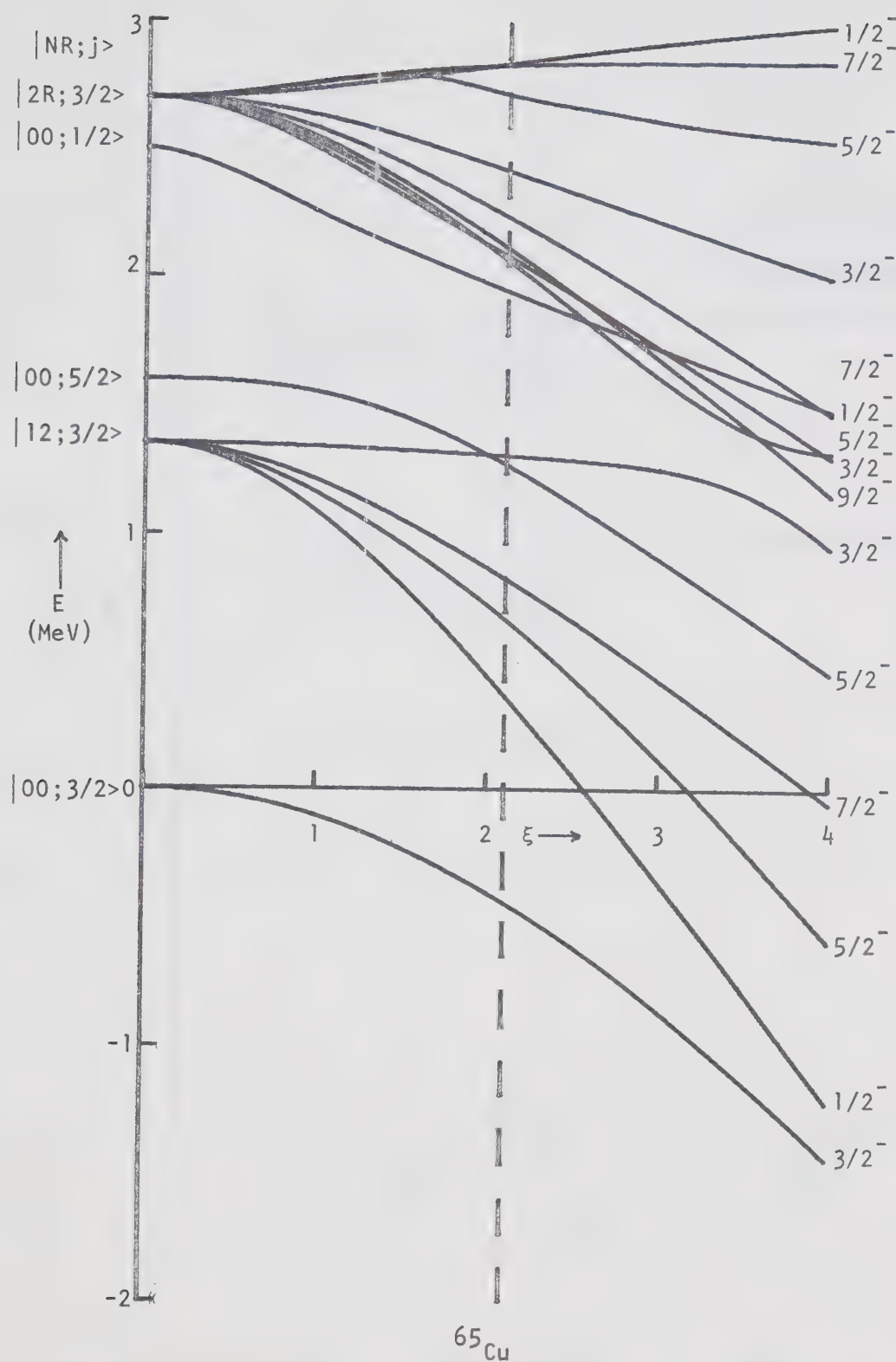


Figure 35. The Intermediate Coupling model: Energy levels of the $^{64}\text{Ni}+p$ system as a function of the coupling strength ξ . The best fit to the levels of ^{65}Cu occurs for $\xi=2.10$.

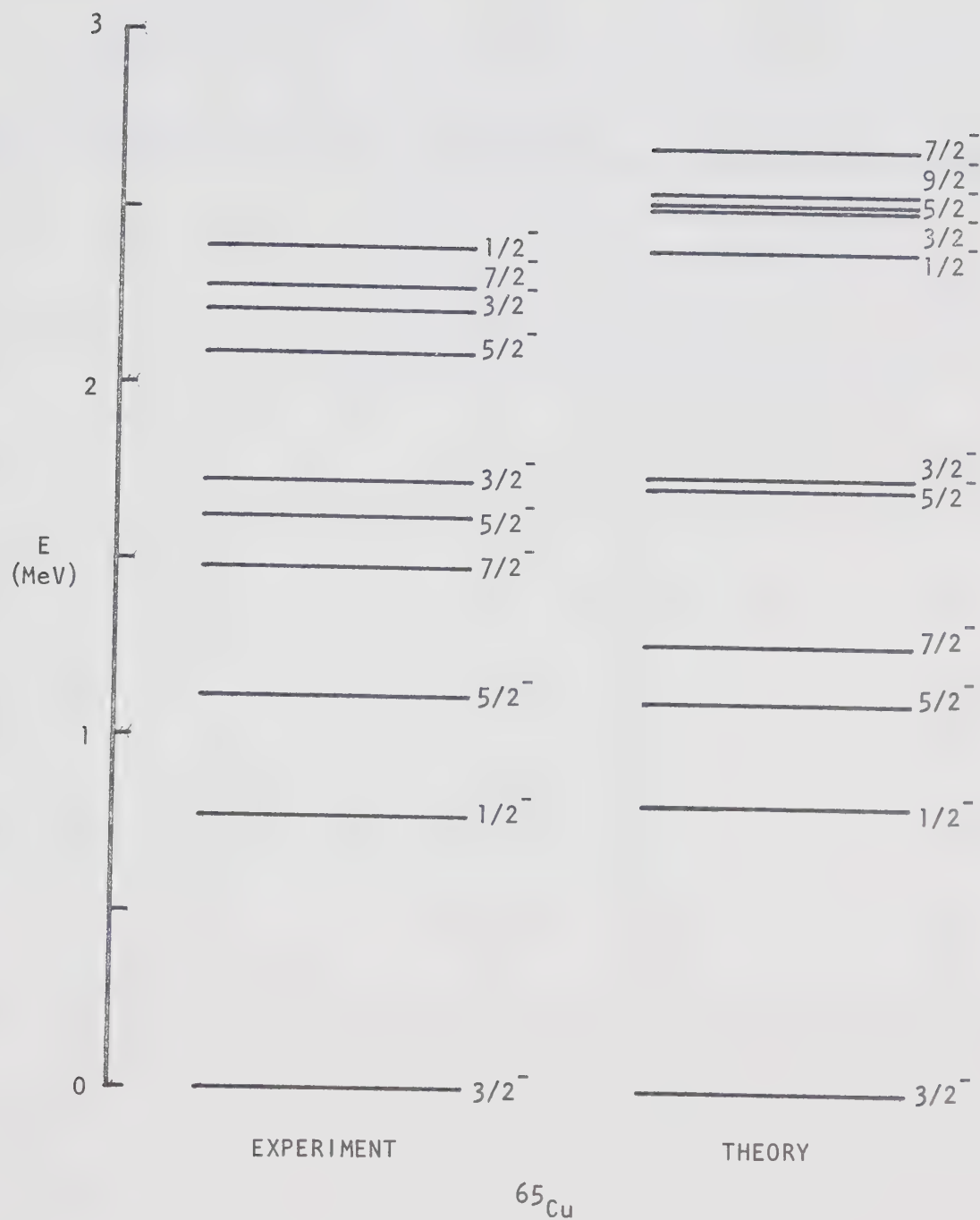


Figure 36. A comparison between the experimental energy spectrum of ^{65}Cu and the level scheme calculated from the Intermediate Coupling model.

Table X Parameters used in the Intermediate Coupling model calculations.

	^{63}Cu	^{65}Cu
$\hbar\omega$ (MeV)	1.172	1.348
N_{MAX}	2	2
$\epsilon_{5/2} - \epsilon_{3/2}$ (MeV)	1.500	1.600
$\epsilon_{1/2} - \epsilon_{3/2}$ (MeV)	2.200	2.500
ξ_p	2.12	2.10
	^{64}Cu	^{64}Cu
$\epsilon_{1/2} - \epsilon_{5/2}$ (MeV)	0.400	-
η	0.0	0.0
ξ_n	1.5	(1.5)

5.4.3 Spectroscopic Factors

Spectroscopic factors for the $^{63}\text{Cu}(d,p)^{64}\text{Cu}$ reaction are given by the expression

$$S_{\ell_2 j_2} = U_{j_2}^2 |A^0(3/2^- j_2; 1)|^2 \quad (5-12)$$

where $A^0(3/2^- j_2; 1)$ is the expansion coefficient for the ^{64}Cu eigenstate in terms of a neutron in the (ℓ_2, j_2) orbit coupled to the $J^\pi = 3/2^-$ ground state of ^{63}Cu . $U_{j_2}^2$ is the "emptiness" of the orbit (ℓ_2, j_2) for ^{63}Cu , and is equal to 1 for the $p_{1/2}$ orbital and 0.67 for the $f_{5/2}$ orbital.

A comparison between the measured spectroscopic factors of Park and Daehnick (Pa 69) and the results predicted by the Intermediate Coupling model is shown in Table XI. The calculated values are in fair agreement with the experimental results, with the exception of the 278 keV and 609 keV levels. The values of Park and Daehnick have an estimated error of about 25%.

5.5 Discussion of the Results

Figure 34 shows a comparison between the experimental level scheme of ^{64}Cu and the level scheme predicted by the Intermediate Coupling model. The overall agreement for the levels below 1 MeV excitation is fairly good. The ground state and first excited state are well reproduced, although the excitation energy of the 2^+ level is about a factor of two too low, and the 3^+ level at 362 keV excitation is predicted very well by the model. The 1^+ level at 344 keV is predicted to lie above the 3^+ , but the energy

Table XI Spectroscopic factors $(2J + 1)S$ for the $^{63}\text{Cu}(d,p)^{64}\text{Cu}$ reaction, calculated from the Intermediate Coupling model. The calculated values are compared with the experimental results of Park and Daehnick (Pa 69).

E_x (keV)	J (Present Work)	ℓ_n	$(2J + 1)S$	
			Exp (Pa 69)	THEORY
0	1	1	0.17	0.11
		3	0.73	1.65
159	2	1	0.84	1.30
		3	1.09	1.82
278	2	1	0.85	-
		3	0.92	-
344	1	1	1.18	1.92
		3	-	0.04
362	3	1	0.14	-
		3	3.29	3.52
574	4	1	-	-
		3	3.64	5.18
609	2	1	0.74	1.86
		3	-	1.00
663	1	1	0.16	-
		3	-	-
739 } *	(2,3)	1	1.73	0.62 [†]
746 }	3	3	-	0.00
878	0	1	0.17	-
		3	-	-
895	3	1	0.20	-
		3	0.89	0.48
927	1	1	0.40	0.31
		3	-	0.03

* These two levels were not resolved in the work of Park and Daehnick (Pa 69)

† Assuming $J = 2$ for the 739 keV level, and that this level corresponds to the $J = 2$ state predicted at 1134 keV.

discrepancy is only about 70 keV. The 2^+ at 609 keV and the 0^+ and 3^+ at about 880 keV are also well reproduced by this calculation.

This model fails to predict the second excited state, the $J = 1$ state at 663 keV, the doublet around 740 keV and the 927 keV level. Attempts to reproduce these levels by considering a $p_{3/2}$ neutron hole coupled to ^{65}Cu did not meet with success. These calculations do predict a closely spaced doublet with $J^\pi = 1^+, 3^+$ which might correspond to the 663 and 746 keV levels, but the 2^+ member of this configuration lies about 250 keV above this doublet rather than 400 keV below it, which would be the case if this state corresponded to the 278 keV level. These calculations also predicted another low-lying 0^+ state for which there is no candidate.

The calculations could probably be improved by considering mixing between the particle and hole configurations. The level at 663 keV, which we have identified as being primarily due to a neutron hole configuration, decays with almost equal branches to the 159 and 278 keV levels, indicating that the configurations of these two low-lying 2^+ states are not radically different. The (d,p) stripping measurements of Park and Daehnick (Pa 69) give almost equal spectroscopic factors for these two levels, supporting the conclusion that these two states have a similar structure. The 895 keV level also decays to these two levels with comparable strengths. This is clearly not the complete picture, however, since it is then difficult to explain why the 746 keV level decays only to the 278 keV level and not to the lower 159 keV state or the ground state. This situation seems to suggest that this level is a relatively pure hole state, and has a small overlap

with the two low-lying particle configurations.

There is no reason why the addition of a neutron to ^{63}Cu should not affect the coupling between the proton and the ^{62}Ni core. While this model assumes that the presence of the extra nucleons does not significantly perturb the core (and hence we can use the excitation energy of the first 2^+ core state for the phonon energy $\hbar\omega$), this is only approximately true, since the addition of two neutrons changes the phonon energy from 1.172 MeV in ^{62}Ni to 1.348 MeV in ^{64}Ni . It therefore seems reasonable to allow the proton coupling strength ξ_p to vary somewhat from the value which gives the best fit to the levels of ^{63}Cu . However, Heyde and Brussaard (He 68) found in their calculations for ^{140}La that the energy spectrum was relatively insensitive to the individual values of ξ_p and ξ_n , provided that the sum $\xi_p + \xi_n$ was a constant. It is doubtful therefore that allowing ξ_p to vary would produce a much better fit.

It is also considered unlikely that including $N = 3$ phonon states in the calculation would significantly alter the low-energy spectrum of ^{64}Cu . Table IX shows that the lowest energy levels of ^{64}Cu are built mainly on the lowest six states of ^{63}Cu , which are composed predominantly of 0 and 1 phonon states. The contributions from two phonon states are in many cases not negligible, but those from three phonon states almost certainly will be.

CHAPTER 6

CONCLUSIONS

The $(p,n\gamma)$ reaction has been shown to be an extremely powerful tool for studying nuclei in the nuclear p-f shell. Because of the fact that the reaction mechanism is well described by the Statistical Compound Nuclear model, angular distribution measurements alone are often sufficient to uniquely determine the spin of the decaying level in the residual nucleus, as well as the multipole mixing ratio of the γ ray.

In certain instances, the angular distribution measurement does determine the level spin uniquely, but cannot distinguish between two possible values of the mixing ratio. Linear polarization measurements can often be helpful in resolving this ambiguity. Such measurements also provide information on the parity of the radiation, and hence on the relative parities of the initial and final nuclear states in the decay.

When the angular distribution of the decay is nearly isotropic, little information can be deduced concerning the spins and mixing ratios. For the $(p,n\gamma)$ reaction near threshold, this situation is expected to occur whenever the spin of the decaying level is less than or equal to $I_T + 1$, where I_T is the spin of the target nucleus. In such cases, the measurement of a γ -ray triple correlation can often

eliminate one or more of the possible spin assignments.

In the present experiment, we have used all of the above techniques to obtain unique spin assignments for almost all of the levels in ^{64}Cu below 1 MeV excitation, and multipole mixing ratios for most of the γ rays. The spin assignments deduced in the present work are generally in good agreement with other available results. Values for the multipole mixing ratios determined in this experiment are also in fairly good agreement with previous works, although our values tend to show somewhat higher E2 contributions for many of the decays.

From a theoretical standpoint, the Intermediate Coupling model given a fairly good description of many of the low-lying energy levels of ^{64}Cu , but there are still some aspects of this nucleus which are not clearly understood. The failure to predict the second 2^+ state at 278 keV excitation must be regarded as one of the most serious failings of the model. It is possible that including mixing between particle and hole states in ^{64}Cu would yield a better overall agreement with the experimental energy spectrum. Calculation of properties which are more sensitive to the details of the nuclear wavefunctions, such as electromagnetic decay properties, would undoubtedly give further insight into the validity of this model for ^{64}Cu .

REFERENCES

- Au 64 E.H. Auerbach, Brookhaven National Laboratory Report BNL-6562 (1964) unpublished.
- Ba 70 W.T. Bass and P.H. Stelson, Phys. Rev. C2 (1970) 2154.
- Bi 53 L.C. Biedenharn and M.E. Rose, Revs. Mod. Phys. 25 (1953) 729.
- Bi 60 L.C. Biedenharn in Nuclear Spectroscopy, Part B, F. Ajzenberg-Selove, Ed. (Academic Press, New York, 1960) p 732.
- Bj 58 F. Bjorkland and S. Fernbach, Phys. Rev. 109 (1958) 1296.
- Bl 65 A.G. Blair, Phys. Rev. 140 (1965) B648.
- Bo 60 A. Bohr and B.R. Mottelson in Nuclear Spectroscopy, Part B, F. Ajzenberg-Selove, Ed. (Academic Press, New York, 1960) p 1009.
- Ca 71 T.P.G. Carola and H. Ohnuma, Nucl. Phys. A165 (1971) 259.
- Ch 54 D.C. Choudhury, Mat. Fys. Medd. Dan. Vid. Selsk. 28, no. 4 (1954).
- Ch 67 D.C. Choudhury and T.F. O'Dwyer, Nucl. Phys. A93 (1967) 300.
- Cl 70 D. Cline and P.M.S. Lesser, Nucl. Instr. and Meth. 82 (1970) 291.
- Co 56 C.F. Coleman, Phys. Rev. 103 (1956) 647.
- Da 70 W.F. Davidson et al, Nucl. Phys. A142 (1970) 167.
- De 57 S. Devons and L.J.B. Goldfarb in Handbuch der Physik, S. Flügge, Ed. (Springer Verlag, Berlin, 1957) Vol. 42, p 362.
- Do 66 B.M. Dodsworth and H.A. Shugart, Phys. Rev. 142 (1966) 638.
- Dr 70 M.M. Drum, MSc. Thesis, University of Alberta, (1970) unpublished.
- Du 66 M.A. Duguay et al, Phys. Rev. Lett. 17 (1966) 28.
- Dw 67 T.F. O'Dwyer, PhD Thesis, Polytechnic Institute of Brooklyn (1967) unpublished.

- Ea 72 J.F. Easton and W.K. Dawson, University of Alberta Internal Report UAE-NPL-38 (1972) unpublished.
- Fa 59 L.W. Fagg and S.S. Hanna, Revs. Mod. Phys. 31 (1959) 711
- Fe 65 A.J. Ferguson, Angular Correlation Methods in Gamma-Ray Spectroscopy (North Holland Publ. Co., Amsterdam, 1965).
- Fu 63 R.H. Fulmer and A.L. McCarthy, Phys. Rev. 131 (1963) 2133.
- Go 71 J.M.G. Gomez, Nucl. Phys. A173 (1971) 537.
- Gr 71 P.W. Green et al, Nucl. Instr. and Meth. 92 (1971) 329.
- Gr 71a P.W. Green, University of Alberta Internal Report UAE-NPL-33 (1971) unpublished.
- Gr 71b P.W. Green, University of Alberta Internal Report UAE-NPL-27 (1971) unpublished.
- Gr 72 P.W. Green, University of Alberta Internal Report UAE-NPL-46 (1972) unpublished.
- Gr 72a P.W. Green et al, Nucl. Instr. and Meth. 98 (1972) 45.
- Gr 73 P.W. Green, University of Alberta Internal Report UAE-NPL-61 (1973) unpublished.
- Gr 73a P.W. Green, University of Alberta Internal Report UAE-NPL-62 (1973) unpublished.
- He 67 K. Heyde and P.J. Brussaard, Nucl. Phys. A104 (1967) 81.
- He 68 K. Heyde and P.J. Brussaard, Nucl. Phys. A112 (1968) 494.
- Ho 58 A.M. Hoogenboom, PhD Thesis, Utrecht (1958) unpublished.
- Ko 65 J. Kopecky et al, Nucl. Phys. 68 (1965) 449
- Ko 69 J. Kopecky and E. Warming, Nucl. Phys. A127 (1969) 385.
- La 57 R.D. Lawson and J.L. Uretsky, Phys. Rev. 108 (1957) 1300.
- Le 54 A. Lemonick and F.M. Pippin, Phys. Rev. 95 (1954) 1356.
- Li 64 A.E. Litherland, Radiative Transitions Following Nuclear Reactions, Scottish Universities Summer School in Physics (1964).
- Ma 63 N. Macdonald, Nucl. Phys. 48 (1963) 500.

- Ma 71 R. Markham and H.W. Fulbright, University of Rochester Report UR-NSRL-41 (1971).
- Mc 70 M.T. McEllistrem et al, Phys. Rev. C1 (1970) 1409.
- Mi 62 R. Michalec and T. Ruskov, Czech. J. Phys. T12 (1962) 325.
- Mi 72 V.M. Mischenko et al, Sov. J. Nucl. Phys. 14 (1972) 512.
- Pa 69 Y.S. Park and W.W. Daehnick, Phys. Rev. 180 (1969) 1082.
- Pa 71 Th. Paradellis et al, Nucl. Phys. A168 (1971) 539.
- Pi 70 A.A. Pilt et al, Nucl. Phys. A150 (1970) 439.
- Po 65 A.R. Poletti and E.K. Warburton, Phys. Rev. 137 (1965) B595.
- Ra 63 K. Ramavataram, Phys. Rev. 132 (1963) 2255.
- Ro 53 M.E. Rose, Phys. Rev. 91 (1953) 610.
- Ro 67 H.J. Rose and D.M. Brink, Revs. Mod. Phys. 39 (1967) 306.
- Ro 71 B.C. Robertson et al, Nucl. Phys. A160 (1971) 137.
- Sh 61 A. de Shalit, Phys. Rev. 122 (1961) 1530.
- Sh 63 E. Sheldon, Revs. Mod. Phys. 35 (1963) 795.
- Sh 65 E. Sheldon and D.M. Van Patter, Revs. Mod. Phys. 38 (1966) 143.
- Sh 68 E.B. Shera and H.H. Bolotin, Phys. Rev. 169 (1968) 940.
- Sh 69 E. Sheldon and R.M. Strang, Comp. Phys. Comm. 1 (1969) 35.
- Su 59 M. Suffert et al, Physica 25 (1959) 659.
- Ta 68 P. Taras and J. Matas, Nucl. Instr. and Meth. 61 (1968) 317.
- Th 65 V.K. Thankappen and W.W. True, Phys. Rev. 137 (1965) B793.
- Th 66 V.K. Thankappen, Phys. Rev. 141 (1966) 957.
- Tw 70 P.J. Twin et al, Nucl. Phys. A143 (1970) 481.
- Ve 61 J. Vervier, Nucl. Phys. 26 (1961) 10.
- Vo 68 E. Vogt in Advances in Nuclear Physics, M. Baranger and E. Vogt, Ed. (Plenum Press, New York, 1968) Vol. 1, p 261.

- Wa 67 Nuclear Data Sheets B, K. Way, Ed. (Academic Press, New York, 1967) Vol. 2, no. 3.
- We 71 C.C. Wellborn et al, Phys. Rev. C3 (1971) 153.

A P P E N D I X A

A PHASE CONSISTENT DEVELOPMENT OF γ -RAY POLARIZATION TRIPLE CORRELATIONS

I. INTRODUCTION

The study of the electromagnetic decay of an excited nucleus is a widely used technique for the determination of the properties of nuclear states. The radiation pattern (i.e., angular distribution or double correlation) of the γ rays emitted by these states is intimately related to the multipole character of the radiation, and its measurement can provide useful information on the angular momenta of the nuclear states involved in the decay. Measurement of the double correlation can also provide information on the values of the multipole mixing ratios, which are proportional to the relative amplitudes of the different multipoles contributing to the decay.

The information obtained from the measurement of a mixing ratio is, in principle, twofold, since both a sign and an absolute magnitude are required to fit the experimental data. Until quite recently, the sign of the mixing ratio has been of little importance in the comparison of experimental data with the predictions of nuclear models, since it was impossible to relate the phase conventions of different authors back to a common starting point. However, with the recent development of a phase consistent theory for γ decay by Rose and Brink (1967) (hereafter referred to as RB), this problem has been largely overcome, and the measured sign of the mixing ratio has now become a useful parameter to be compared with model predictions.

The amount of information obtainable from the analysis of a double correlation measurement is severely limited by the fact that the number

of unknowns in the problem often exceeds the number of experimentally measurable parameters. This restriction can be overcome to a certain extent by measuring the circular and linear polarization distributions of the γ decay. Since the linear polarization double correlation depends on the parity of the radiation (the polarization insensitive double correlation does not), one additional parameter is introduced.

Further information about the decay can be obtained from the measurement of the angular triple correlation (two radiations in coincidence). The number of experimentally measurable quantities is greatly increased in this case, and (although more unknown parameters are again introduced) the problem is, in general, overdetermined. Linear polarization triple correlations can also provide information on the parities of the radiations.

Since the measurement of triple correlations represents such a powerful tool in nuclear spectroscopy, it is clearly desirable to extend the phase consistent theory of RB to cover the more general case. The formula, which is derived in detail in RB, for the transition amplitude for the γ decay of an initial state $|J_1 M_1\rangle$ to a final state $|J_2 M_2\rangle$ is used as a starting point in this derivation. From this expression, formulae for the double correlation and polarization double correlations of a single γ decay will be derived. Only cases where the initial nuclear state possesses axial symmetry with respect to a space fixed z -axis will be considered, and the initial state J_1 can then be completely specified by the relative populations of its magnetic substates (the population parameters $P(M_1)$).

Time-dependent perturbation theory allows one to relate this amplitude to the transition amplitude for the emission of two successive γ rays, and the angular triple correlation and polarization triple correlation formulae are then derived in a phase-consistent manner. The formalism can be extended to include an arbitrary number of successive γ decays, and a recipe is provided for writing down the correlation in such cases.

II. γ -RAY DOUBLE CORRELATIONS

Consider the transition from a nuclear state $|J_1 M_1\rangle$ to a state $|J_2 M_2\rangle$ by the emission of a γ ray in the direction \vec{k} with a given polarization $\vec{\epsilon}$. Since the electromagnetic field is a transverse field, it is clear that (at most) two linearly independent vectors orthogonal to \vec{k} are required to describe the polarization (which is conventionally taken to be parallel to the electric vector of the radiation).

It is advantageous to choose as a basis set, unit vectors which have convenient properties under rotations. A suitable set of basis vectors for describing the polarization is

$$\begin{aligned}\hat{e}_q &= -\frac{q}{\sqrt{2}} (\hat{e}_x \pm i\hat{e}_y) & q &= \pm 1 \\ \hat{e}_0 &= \hat{e}_z\end{aligned}\tag{1}$$

where \hat{e}_z has been chosen parallel to the direction of propagation \vec{k} . The vector with $q = +1$ represents a state of right circular

polarization, and that with $q = -1$ a state of left circular polarization.

The amplitude for the emission of a γ ray with circular polarization $\hat{\epsilon} = \hat{e}_q$ is given in RB

$$A_{M_1 M_2}^q(\vec{k}) = - \left(\frac{k}{2\pi\hbar} \right)^{\frac{1}{2}} \sum_{L\pi} q^\pi \langle J_1 M_1 | T_L^{<\pi>} | J_2 M_2 \rangle D_{M_1 - M_2 q}^L(R) \quad (2)$$

where $R = (\phi, \theta, 0)$ is the rotation which takes the z -axis from the initial (space-fixed) direction to the direction of propagation \vec{k} of the γ ray (see Fig.37). The definition of the rotation matrices used here is that of RB.

The $T_{LM}^{<\pi>}$ of (2) are the phase-defined electromagnetic transition operators of order L (explicit definitions are given in RB). They are defined such that they transform under time reversal according to

$$\theta T_{LM}^{<\pi>} \theta^{-1} = (-)^{L-M} T_{L-M}^{<\pi>} \quad (3)$$

where θ is the time reversal operator. This, together with the requirement that the nuclear wavefunctions transform according to

$$\theta |JM\rangle = (-)^{J-M} |J-M\rangle \quad (4)$$

is sufficient to ensure that the matrix elements $\langle J_1 M_1 | T_{LM}^{<\pi>} | J_2 M_2 \rangle$ are real.

The index π specifies the electric or magnetic nature of the radiation ($\pi = 0$ for electric multipoles and $\pi = 1$ for magnetic multipoles). The parity of the radiation is then $(-)^{L+\pi}$.

In general, the orientation (i.e. the projection M_2) of the final nuclear state is not observed with the result that the transition probability is summed over all M_2 . Moreover, the initial state generally exists in several magnetic substates M_1 with relative populations $P(M_1)$. The total transition probability is then given by

$$\begin{aligned}
 P^q(\vec{k}) &= \sum_{M_1} P(M_1) \sum_{M_2} |A_{M_1 M_2}^q(\vec{k})|^2 \\
 &= \frac{k}{2\pi\hbar} \sum_{M_1} P(M_1) \sum_{M_2} \sum_{\substack{L\pi \\ L'\pi'}} q^{\pi+\pi'} \langle J_1 M_1 | T_{L M_1-M_2}^{<\pi>} | J_2 M_2 \rangle \\
 &\quad \times \langle J_1 M_1 | T_{L' M_1-M_2}^{<\pi'>} | J_2 M_2 \rangle^* D_{M_1-M_2, q}^L(R) D_{M_1-M_2, q}^{L'}{}^*(R) \quad (5)
 \end{aligned}$$

Since the matrix elements of $T_{LM}^{<\pi>}$ are real, the complex conjugation on the matrix element can be dropped.

The Wigner-Eckart theorem separates the dependence of the matrix elements on magnetic quantum numbers

$$\langle J_1 M_1 | T_{L M_1-M_2}^{<\pi>} | J_2 M_2 \rangle = (-)^{2L} (J_2 L; M_2 M_1-M_2 | J_1 M_1) \langle J_1 || T_L^{<\pi>} || J_2 \rangle \quad (6)$$

and the two rotation matrices can be combined.

$$D_{M_1-M_2, q}^L(R) D_{M_1-M_2, q}^{L'}{}^*(R) = (-)^{M_1-M_2-q} D_{M_1-M_2, q}^L(R) D_{M_2-M_1-q}^{L'}(R)$$

$$\begin{aligned}
&= \sum_k (-)^{M_1-M_2-q} (LL'; M_1-M_2 \ M_2-M_1 | k0) \\
&\times (LL'; q - q | k0) D_{00}^k(R)
\end{aligned} \tag{7}$$

Since $D_{00}^k(\phi, \theta, 0) = P_k(\cos\theta)$, Eq. (5) becomes

$$\begin{aligned}
P^q(\vec{k}) &= \frac{k}{2\pi\hbar} \sum_{M_1} P(M_1) \sum_k P_k(\cos\theta) \sum_{\substack{L\pi \\ L'\pi'}} q^{\pi+\pi'} \langle J_1 || T_L^{<\pi>} || J_2 \rangle \\
&\times \langle J_1 || T_{L'}^{<\pi'>} || J_2 \rangle \sum_{M_2} (-)^{M_1-M_2-q} (J_2 L; M_2 M_1-M_2 | J_1 M_1) \\
&\times (J_2 L'; M_2 M_1-M_2 | J_1 M_1) (LL'; M_1-M_2 \ M_2-M_1 | k0)
\end{aligned} \tag{8}$$

Due to the assumed axial symmetry of the initial state $|J_1 M_1\rangle$, the transition probability is independent of the azimuthal angle ϕ . The sum over M_2 in Eq. (8) can be evaluated explicitly to give

$$(-)^{q+J_1-J_2+L-L'-k} \hat{J}_1^2 W(J_1 J_1 L L'; k J_2) (-)^{J_1-M_1} (J_1 J_1; M_1-M_1 | k0) \tag{9}$$

where $\hat{J} \equiv \sqrt{2J+1}$. The sum over M_1 defines the "alignment coefficients"

$$\begin{aligned}
B_k(J_1) &= \hat{J}_1 \sum_{M_1} (-)^{J_1-M_1} P(M_1) (J_1 J_1; M_1-M_1 | k0) \\
B_0(J_1) &= 1
\end{aligned} \tag{10}$$

which contain all of the information about the initial state in the γ decay. Defining (RB)

$$R_k^q(LL'J_1J_2) = (-)^{q+J_1-J_2+L-L'-k} \hat{J}_1 \hat{L} \hat{L}' (LL'; q-q|k0) W(J_1J_1LL'; kJ_2)$$

$$R_k(LL'J_1J_2) = R_k^{q=1}(LL'J_1J_2) = (-)^{L+L'-k} R_k^{q=-1}(LL'J_1J_2)$$

$$R_0(LL'J_1J_2) = \delta(L, L') \quad (11)$$

Equation (8) becomes

$$\begin{aligned} P^q(\vec{k}) &= \frac{k}{2\pi\hbar} \sum_k B_k(J_1) P_k(\cos\theta) \sum_{\substack{L\pi \\ L'\pi'}} q^{\pi+\pi'} R_k^q(LL'J_1J_2) \\ &\times \frac{1}{\hat{L}\hat{L}'} \langle J_1 || T_L^{<\pi>} || J_2 \rangle \langle J_1 || T_{L'}^{<\pi'>} || J_2 \rangle \end{aligned} \quad (12)$$

In the angular distribution and polarization distribution experiments, the relative yield only is determined as a function of angle, and it is clear that only the ratios of the reduced matrix elements can be determined. For this purpose, multipole mixing ratios, $\delta_L^{<\pi>}$, are defined

$$\delta_L^{<\pi>} = \frac{\langle J_1 || T_L^{<\pi>} || J_2 \rangle / \hat{L}}{\langle J_1 || T_{\bar{L}}^{<\bar{\pi}>} || J_2 \rangle / \hat{\bar{L}}} \quad (13)$$

where $(\bar{L}, \bar{\pi})$ is the lowest allowed multipole in the decay $J_1 \rightarrow J_2$.

Since the reduced matrix elements are real, the mixing ratios are also real numbers. Normalizing Eq. (12) by dividing by the factor

$2 \sum_{L\pi} (\delta_L^{<\pi>})^2$, and neglecting constants, the circular polarization double correlation is given by

$$W^q(\theta) = \sum_k B_k(J_1) P_k(\cos\theta) \sum_{\substack{L\pi \\ L'\pi'}} q^{\pi+\pi'} R_k^q(LL'J_1J_2) \Delta(L,L') \quad (14)$$

where

$$\Delta(L,L') = \frac{\delta_L^{<\pi>} \delta_{L'}^{<\pi'>}}{2 \sum_{L\pi} (\delta_L^{<\pi>})^2} \quad (15)$$

If the circular polarization of the γ ray is not measured, Eq. (14) must be summed incoherently over the circular polarization quantum number q , to arrive at the formula for the polarization-insensitive double correlation.

$$\begin{aligned} W(\theta) &\equiv W^{q=1}(\theta) + W^{q=-1}(\theta) \\ &= \sum_k B_k(J_1) P_k(\cos\theta) \sum_{\substack{L\pi \\ L'\pi'}} R_k(LL'J_1J_2) \{1 + (-)^{L+L'+\pi+\pi'-k}\} \Delta(L,L') \\ &= \sum_k a_k P_k(\cos\theta) \end{aligned} \quad (16)$$

In deriving (16), the only restriction placed on the initial and final nuclear states was that they have definite angular momentum J_1 and J_2 respectively and that the initial state be formed in axial symmetry. If these states also have definite parity (and parity is conserved in the γ decay) then $(-)^{L+\pi+L'+\pi'} = 1$. The sum over k is then restricted to even values only. The normalization of (16) is such that $a_0 \equiv 1$.

III. THE $B_k(J_1)$ COEFFICIENTS

The $B_k(J_1)$ coefficients contain all of the information about the initial state of the system, through the population parameters $P(M_1)$. There are three classes of population parameters which are often encountered in practical applications.

Isotropy. $P(M_1) = 1/\hat{J}_1^2$ for all M_1 . Since the populations are equal only $B_0(J_1)$ is non-zero, and the angular distribution is isotropic. This is to be expected, since the isotropy of the substate populations has effectively removed the axis of symmetry from the initial state.

Alignment. $P(M_1) = P(-M_1)$. In this case,

$$B_k(J_1) = \delta_{M_1,0} \hat{J}_1 (-)^{J_1} (J_1 J_1; 00 | k 0) P(0) \quad (17)$$

$$+ \hat{J}_1 \{1 + (-)^k\} \sum_{M_1 > 0} P(M_1) (-)^{J_1 - M_1} (J_1 J_1; M_1 - M_1 | k 0)$$

and $B_k(J_1) = 0$ if k is odd.

Polarization. $P(M_1) \neq P(-M_1)$. The $B_k(J_1)$ coefficients are, in general, non-zero for both even and odd values of k .

IV. CIRCULAR POLARIZATION DOUBLE CORRELATION

Equation (14) gives the distribution of γ rays with a given circular polarization, specified by the quantum number q . Following

the usual definition for the degree of circular polarization,

$$\begin{aligned}
 P_c(\theta) &\equiv \frac{W^{q=1}(\theta) - W^{q=-1}(\theta)}{W^{q=1}(\theta) + W^{q=-1}(\theta)} \\
 &= \frac{1}{W(\theta)} \sum_k B_k(J_1) P_k(\cos\theta) \sum_{\substack{L\pi \\ L'\pi'}} R_k(LL'J_1J_2) \\
 &\quad \times \{1 + (-)^{L+\pi+L'+\pi'-k+1}\} \Delta(L, L')
 \end{aligned} \tag{18}$$

This definition limits $P_c(\theta)$ to lie between $+1$ and -1 , with $P_c(\theta) = 0$ corresponding to an unpolarized γ ray.

If a parity conserving transition occurs between two states of definite parity, the sum over k is restricted to odd values only. Unless the initial state is polarized in some way, as in experiments using polarized targets or polarized beams, the $B_k(J_1)$ vanish for odd k and there is no measurable circular polarization.

V. LINEAR POLARIZATION DOUBLE CORRELATION

Since the two unit vectors in Eq. (1) form a complete set of polarization states for the transverse electromagnetic field, a state of arbitrary linear polarization can be expressed as a linear superposition of the two circular polarization states, and the transition amplitude for the emission of a linearly polarized photon can be expressed as the same superposition of the two circular polarization amplitudes. Specifically, the transition amplitude for the emission of a photon linearly polarized along the x direction is

$$\begin{aligned}
A_{M_1 M_2}^x(\vec{k}) &= \frac{-1}{\sqrt{2}} (A_{M_1 M_2}^{q=1}(\vec{k}) - A_{M_1 M_2}^{q=-1}(\vec{k})) \\
&= \frac{-1}{\sqrt{2}} \sum_q q A_{M_1 M_2}^q(\vec{k}) \\
&= \frac{-1}{\sqrt{2}} \sum_q \sum_{L\pi} q^{\pi+1} \langle J_1 M_1 | T_{LM_1-M_2}^{<\pi>} | J_2 M_2 \rangle D_{M_1-M_2 q}^L(R) \quad (19)
\end{aligned}$$

Notice that the coordinate system is chosen such that the original z-axis and the direction of the γ ray (which are connected by the rotation $R \equiv (\phi, \theta, 0)$) define the x-z plane, and Eq. (19) then gives the amplitude for the emission of a photon linearly polarized parallel to the reaction plane. The amplitude for the emission of a γ ray linearly polarized at angle ξ to the reaction plane is found by rotating the coordinate system through angle ξ about the final γ ray direction, and is then given by Eq. (19) with $R = (\phi, \theta, \xi)$. The transition probability is

$$\begin{aligned}
P^\xi(\vec{k}) &= \frac{k}{4\pi\hbar} \sum_{M_1} P(M_1) \sum_{M_2} \sum_{\substack{L\pi \\ q q' L' \pi'}} q^{\pi+1} q'^{\pi'+1} \langle J_1 M_1 | T_{LM_1-M_2}^{<\pi>} | J_2 M_2 \rangle \\
&\quad \times \langle J_1 M_1 | T_{L' M_1-M_2}^{<\pi'>} | J_2 M_2 \rangle D_{M_1-M_2 q}^L(R) D_{M_1-M_2 q'}^{L'}(R) \quad (20)
\end{aligned}$$

and the linear polarization double correlation is given by

$$\begin{aligned}
W^\xi(\theta) &= \sum_{M_1 k} P(M_1) \sum_{q q'} \sum_{\substack{L\pi \\ L' \pi'}} q^{\pi+1} q'^{\pi'+1} \hat{L} \hat{L}' \frac{\Delta(L, L')}{2} \\
&\quad \times (LL'; q - q' | k \ q - q') D_{q - q'}^k(R) \sum_{M_2} (-)^{M_1 - M_2 - q'}
\end{aligned}$$

$$\times (J_2 L; M_2 M_1 - M_2 | J_1 M_1) (J_2 L'; M_2 M_1 - M_2 | J_1 M_1) (LL'; M_1 - M_2, M_2 - M_1 | k0). \quad (21)$$

After summing over M_2 and over M_1 ,

$$\begin{aligned} W^\xi(\theta) &= \sum_k B_k(J_1) \sum_{qq'} \sum_{\substack{L\pi \\ L'\pi'}} q^{\pi+1} q'^{\pi'+1} \frac{\Delta(L, L')}{2} \\ &\times R_k^{qq'}(LL' J_1 J_2) \frac{\sqrt{4\pi}}{\hat{k}} Y_k^{q-q'}(\theta, -\xi) \end{aligned} \quad (22)$$

where

$$\begin{aligned} R_k^{qq'}(LL' J_1 J_2) &= (-)^{q+L-L'+J_1-J_2-k} \hat{L} \hat{L}' \hat{J}_1 (LL'; q-q' | k, q-q') \\ &\times W(J_1 J_1 LL'; k J_2) \end{aligned} \quad (23)$$

and

$$D_{0, q-q'}^k(\phi, \theta, \xi) = (-)^{q-q'} \frac{\sqrt{4\pi}}{\hat{k}} Y_k^{q-q'}(\theta, -\xi) \quad (24)$$

By analogy with the case for circular polarization, the degree of linear polarization is defined as

$$\begin{aligned} P_L(\theta) &= \frac{W^0(\theta) - W^{\pi/2}(\theta)}{W^0(\theta) + W^{\pi/2}(\theta)} \\ &= \frac{1}{W(\theta)} \sum_k B_k(J_1) \sum_{\substack{L\pi \\ L'\pi'}} (-)^{\pi'+1} \Delta(L, L') \end{aligned}$$

$$\begin{aligned}
& \times \{1 + (-)^{L+\pi+L'+\pi'-k}\} R_k^{1-1} (LL'J_1J_2) \\
& \times \frac{\sqrt{4\pi}}{k} Y_k^2(\theta, 0)
\end{aligned} \tag{25}$$

Note that parity considerations again restrict the sum over k to even values.

VI. γ -RAY TRIPLE CORRELATIONS

Consider the process shown in Fig.38, where two γ rays are emitted sequentially. Using first-order time dependent perturbation theory, it can be shown (Appendix 1) that the amplitude for this two step process is just the product of the amplitudes for the individual decays. In general, the cascade decay $|J_1M_1\rangle \rightarrow |J_2M_2\rangle \rightarrow |J_3M_3\rangle$, can proceed through any one of the $(2J_2 + 1)$ degenerate states $|J_2M_2\rangle$, and the total amplitude is given by a sum over the intermediate states

$$A_{M_1M_3}^{q_1q_2}(\vec{k}_1, \vec{k}_2) = \sum_{M_2} A_{M_1M_2}^{q_1}(\vec{k}_1) A_{M_2M_3}^{q_2}(\vec{k}_2) \tag{26}$$

where the first γ ray is emitted in the direction \vec{k}_1 with circular polarization \hat{e}_{q_1} and the second in the direction \vec{k}_2 with circular polarization \hat{e}_{q_2} . The transition probability is given by

$$P^{q_1q_2}(\vec{k}_1, \vec{k}_2) = \sum_{M_1} P(M_1) \sum_{M_3} |A_{M_1M_3}^{q_1q_2}(\vec{k}_1, \vec{k}_2)|^2$$

$$\begin{aligned}
&= \frac{(k_1 k_2)^{\frac{1}{2}}}{2\pi\hbar} \sum_{M_1} P(M_1) \sum_{M_3} \sum_{M_2 M_2'} \sum_{\substack{L_1 \pi_2 \\ L_1' \pi_1'}} \sum_{\substack{L_2 \pi_2 \\ L_2' \pi_2'}} q_1^{\pi_1 + \pi_1'} \\
&\times \langle J_1 M_1 | T_{L_1 M_1 - M_2}^{<\pi_1>} | J_2 M_2 \rangle \langle J_1 M_1 | T_{L_1' M_1 - M_2'}^{<\pi_1'>} | J_2 M_2' \rangle D_{M_1 - M_2, q_1}^{L_1} (R_1) \\
&\times D_{M_1 - M_2', q_1}^{L_1'} (R_1) q_2^{\pi_2 + \pi_2'} \langle J_2 M_2 | T_{L_2 M_2 - M_3}^{<\pi_2>} | J_3 M_3 \rangle \\
&\times \langle J_2 M_2' | T_{L_2' M_2' - M_3}^{<\pi_2'>} | J_3 M_3 \rangle D_{M_2 - M_3, q_2}^{L_2} (R_2) D_{M_2' - M_3, q_2}^{L_2'} (R_2) \quad (27)
\end{aligned}$$

with $R_1 \equiv (\phi_1, \theta_1, 0)$ and $R_2 \equiv (\phi_2, \theta_2, 0)$. This can be rewritten to give

$$\begin{aligned}
W^{q_1 q_2}(\Omega_1, \Omega_1) &= \hat{J}_1 \sum_{k_1 M_1} (-)^{J_1 - M_1} P(M_1) (J_1 J_1; M_1 - M_1 | k_1 0) \\
&\times \sum_{\substack{L_1 \pi_1 \\ L_1' \pi_1'}} q_1^{\pi_1 + \pi_1'} \hat{L}_1 \hat{L}_1' \Delta(L_1, L_1') \sum_{\substack{L_2 \pi_2 \\ L_2' \pi_2'}} q_2^{\pi_2 + \pi_2'} \hat{L}_2 \hat{L}_2' \Delta(L_2, L_2') \\
&\times \sum_{k_2 k_3} (L_1 L_1'; q_1 - q_1 | k_2 0) (L_2 L_2'; q_2 - q_2 | k_3 0) \begin{Bmatrix} J_1 & L_1 & J_2 \\ J_1 & L_1' & J_2 \\ k_1 & k_2 & k_3 \end{Bmatrix} \\
&\times W(J_2 J_2 L_2 L_2'; k_3 J_3) (k_3 k_2; \kappa - \kappa | k_1 0) \\
&\times D_{-\kappa 0}^{k_2} (R_1) D_{\kappa 0}^{k_3} (R_2) (-)^{L_2 + L_2' - J_3 + J_2 - L_1 - k_1 - k_2 + q_1 + q_2} \\
&\times \hat{J}_1 \hat{J}_2^2 \hat{k}_2 \hat{k}_3 \quad (28)
\end{aligned}$$

The sum over κ defines angular functions

$$P_{k_1 k_2 k_3}(\Omega_1, \Omega_2) = (-)^{k_2+k_3-k_1} \frac{\hat{k}_2 \hat{k}_3}{\hat{k}_1} \times \sum_K (k_3 k_2; K - K | k_1 0) D_{-K 0}^{k_2}(R_1) D_{K 0}^{k_3}(R_2) \quad (29)$$

which reduce to ordinary Legendre polynomials if either k_2 or k_3 is equal to zero. The phase $(-)^{k_2+k_3-k_1}$ is always positive since $k_1 + k_2 + k_3$ is an even number (Appendix 2).

Defining

$$L_{k_1 k_2 k_3}^{q_1}(L_1 L_1' J_1 J_2) = (-)^{q_1-L_1} \hat{L}_1 \hat{L}_1' \hat{J}_1 \hat{J}_2 \hat{k}_1 \times (L_1 L_1'; q_1 - q_1 | k_2 0) \begin{Bmatrix} J_1 & L_1 & J_2 \\ J_1 & L_1' & J_2 \\ k_1 & k_2 & k_3 \end{Bmatrix} \quad (30)$$

the correlation can be written

$$\begin{aligned} W^{q_1 q_2}(\Omega_1, \Omega_2) &= \sum_{k_1} B_{k_1}(J_1) \sum_{\substack{L_1 \pi_1 \\ L_1' \pi_1'}} q_1^{\pi_1 + \pi_1'} \Delta(L_1, L_1') \\ &\times \sum_{\substack{L_2 \pi_2 \\ L_2' \pi_2'}} q_2^{\pi_2 + \pi_2'} \Delta(L_2, L_2') \sum_{k_2 k_3} L_{k_1 k_2 k_3}^{q_1}(L_1 L_1' J_1 J_2) \\ &\times R_{k_3}^{q_2}(L_2 L_2' J_2 J_3) P_{k_1 k_2 k_3}(\Omega_1, \Omega_2) \end{aligned} \quad (31)$$

This is the basic formula for all triple correlations.

If the circular polarization is not measured for either of the γ rays, an incoherent sum over q_1 and q_2 gives the formula for

the direction-direction triple correlation

$$\begin{aligned}
 W(\Omega_1, \Omega_2) &= \sum_{k_1} B_{k_1}(J_1) \sum_{k_2 k_3} \sum_{\substack{L_1 \pi_1 \\ L_1' \pi_1'}} \Delta(L_1, L_1') \\
 &\times \{1 + (-)^{L_1 + \pi_1 + L_1' + \pi_1' - k_2}\} \sum_{\substack{L_2 \pi_2 \\ L_2' \pi_2'}} \Delta(L_2, L_2') \{1 + (-)^{L_2 + \pi_2 + L_2' + \pi_2' - k_3}\} \\
 &\times L_{k_1 k_2 k_3}(L_1 L_1' J_1 J_2) R_{k_3}(L_2 L_2' J_2 J_3) P_{k_1 k_2 k_3}(\Omega_1, \Omega_2) \quad (32)
 \end{aligned}$$

where

$$L_{k_1 k_2 k_3}(L_1 L_1' J_1 J_2) \equiv L_{k_1 k_2 k_3}^{q_1=1}(L_1 L_1' J_1 J_2) \quad (33)$$

and

$$L_{k_1 k_2 k_3}^{q_1=-1}(L_1 L_1' J_1 J_2) = (-)^{L_1 + L_1' - k_2} L_{k_1 k_2 k_3}(L_1 L_1' J_1 J_2) \quad (34)$$

Parity conservation in the γ decay, plus the requirement that all nuclear states have definite parity, limits the sums over k_2 and k_3 (and therefore k_1 also) to even values.

VII. UNOBSERVED TRANSITIONS

From the general formula for the γ - γ triple correlation (Eq.(31)) we can consider specifically the cases where only one of the γ rays is observed. If, for example, γ_2 is not observed, we integrate

Eq. (31) over all angles Ω_2 and sum over the circular polarization quantum number q_2 . Since this process is then equivalent to a single transition $|J_1 M_1\rangle \rightarrow |J_2 M_2\rangle$ the general formula should reduce to Eq. (16).

The integral over Ω_2 gives

$$\int d\Omega_2 D_{K0}^{k_3}(\Omega_2) = \frac{4\pi}{k_3} \delta_{k_3,0} \delta_{K0} \quad (35)$$

and since

$$R_0^{q_2}(L_2 L_2' J_2 J_3) = \delta_{L_2, L_2'}$$

$$L_{k_1 k_2 0}^{q_1}(L_1 L_1' J_1 J_2) = \delta_{k_1 k_2} R_{k_1}(L_1 L_1' J_1 J_2) \quad (36)$$

Eq. (31) becomes

$$\begin{aligned} W^{q_1}(\theta) = & \sum_{k_1} B_{k_1}(J_1) \sum_{\substack{L_1 \pi_1 \\ L_1' \pi_1'}} \Delta(L_1, L_1') \sum_{q_2} \sum_{\substack{L_2 \pi_2 \\ L_2' \pi_2'}} \Delta(L_2, L_2') \\ & \times q_2^{\pi_2 + \pi_2'} \delta_{L_2 L_2'} R_{k_1}^{q_1}(L_1 L_1' J_1 J_2) 4\pi P_{k_1}(\cos\theta_1) \quad (37) \end{aligned}$$

After the sum over q_2 ($= \pm 1$), this reduces to Eq. (16) for a γ -ray direction double correlation, apart from a normalization factor of 4π .

If γ_2 is observed, but γ_1 is not, we integrate Eq. (31) over all angles Ω_1 and sum over q_1 . The L -coefficient becomes

$$\begin{aligned}
L_{k_1 0 k_3}^{q_1} (L_1 L_1' J_1 J_2) &= \delta_{k_1 k_2} \delta_{L_1 L_1'} (-)^{k_1} \frac{W(J_1 J_1 J_2 J_2; k_1 L_1)}{W(J_1 J_1 J_2 J_2; 0 L_1)} \\
&\equiv \delta_{k_1 k_3} \delta_{L_1 L_1'} U_{k_1} (L_1 J_1 J_2) \quad (38)
\end{aligned}$$

and, after the sum over q_1 , Eq. (31) becomes

$$\begin{aligned}
W^{q_2}(\theta_2) &= 4\pi \sum_{k_1} B_{k_1}(J_1) \sum_{L_1 \pi_1} 2U_{k_1}(L_1 J_1 J_2) \Delta(L_1, L_1') \\
&\times \sum_{\substack{L_2 \pi_2 \\ L_2' \pi_2'}} q_2^{\pi_2 + \pi_2'} \Delta(L_2, L_2') R_{k_1}^{q_2}(L_2 L_2' J_1 J_2) P_{k_1}(\cos \theta_2) \quad (39)
\end{aligned}$$

It can be seen that the effect of an unobserved transition preceding an observed γ ray is a modification of the $B_k(J_1)$ coefficients by the factor

$$\begin{aligned}
U_{k_1}(J_1 J_2) &\equiv \sum_{L_1 \pi_1} 2U_{k_1}(L_1 J_1 J_2) \Delta(L_1, L_1') \\
&= \sum_{L_1 \pi_1} U_{k_1}(L_1 J_1 J_2) \frac{(\delta_{L_1}^{<\pi_1>})^2}{\sum_{L_1 \pi_1} (\delta_{L_1}^{<\pi_1>})^2} \quad (40)
\end{aligned}$$

Since the $U_k(L_1 J_1 J_2)$ are less than unity in absolute value for $k_1 \neq 0$, the effect of the unobserved transition is to decrease the anisotropy of the double correlation.

VIII. TRIPLE CORRELATIONS INVOLVING CIRCULAR POLARIZATION

If the circular polarization of γ_1 is measured and that of γ_2 is not, a sum of Eq. (31) over q_2 gives

$$\begin{aligned}
W^{q_1}(\Omega_1, \Omega_2) &= \sum_{k_1} B_{k_1}(J_1) \sum_{k_2 k_3} \sum_{\substack{L_1 \pi_1 \\ L_1' \pi_1'}} q_1^{\pi_1 + \pi_1'} \Delta(L_1, L_1') \\
&\times \sum_{\substack{L_2 \pi_2 \\ L_2' \pi_2'}} \Delta(L_2, L_2') \{1 + (-)^{L_2 + \pi_2 + L_2' + \pi_2' - k_3}\} \\
&\times \int_{k_1 k_2 k_3}^{q_1} (L_1 L_1' J_1 J_2) R_{k_3}(L_2 L_2' J_2 J_3) P_{k_1 k_2 k_3}(\Omega_1, \Omega_2)
\end{aligned} \quad (41)$$

The circular-direction triple correlation is then given by

$$\begin{aligned}
P_c^{(1)}(\Omega_1, \Omega_2) &= \frac{W^1(\Omega_1, \Omega_2) - W^{-1}(\Omega_1, \Omega_2)}{W^1(\Omega_1, \Omega_2) + W^{-1}(\Omega_1, \Omega_2)} \\
&\times \frac{1}{W(\Omega_1, \Omega_2)} \sum_{k_1} B_{k_1}(J_1) \sum_{k_2 k_3} \sum_{\substack{L_1 \pi_1 \\ L_1' \pi_1'}} \Delta(L_1, L_1') \{1 + (-)^{L_1 + \pi_1 + L_1' + \pi_1' - k_2 + 1}\} \\
&\times \int_{k_1 k_2 k_3} (L_1 L_1' J_1 J_2) \sum_{\substack{L_2 \pi_2 \\ L_2' \pi_2'}} \Delta(L_2, L_2') \{1 + (-)^{L_2 + \pi_2 + L_2' + \pi_2' - k_3}\} \\
&\times R_{k_3}(L_2 L_2' J_2 J_3) P_{k_1 k_2 k_3}(\Omega_1, \Omega_2)
\end{aligned} \quad (42)$$

where the superscript (1) indicates that the polarization of γ_1 is measured. Parity restrictions require that k_2 be odd.

If it is the circular polarization of γ_2 that is observed, a sum of Eq. (31) over q_1 obtains the formula for the direction-circular triple correlation. The direction-circular triple correlation in this case is

$$\begin{aligned}
P_c^{(2)}(\Omega_1, \Omega_2) &= \frac{1}{W(\Omega_1, \Omega_2)} \sum_{k_1} B_{k_1}(J_1) \sum_{k_2 k_3} \sum_{\substack{L_1 \pi_1 \\ L_1' \pi_1'}} \Delta(L_1, L_1') \\
&\times \{1 + (-)^{L_1 + \pi_1 + L_1' + \pi_1' - k_2}\} L_{k_1 k_2 k_3}(L_1 L_1' J_1 J_2) \\
&\times \sum_{\substack{L_2 \pi_2 \\ L_2' \pi_2'}} \Delta(L_2, L_2') \{1 + (-)^{L_2 + \pi_2 + L_2' + \pi_2' - k_3 + 1}\} \\
&\times R_{k_3}(L_2 L_2' J_2 J_3) P_{k_1 k_2 k_3}(\Omega_1, \Omega_2) \quad (43)
\end{aligned}$$

For the case where the circular polarization of both γ rays is measured, the circular-circular triple correlation is

$$\begin{aligned}
P_c(\Omega_1, \Omega_2) &= \frac{W^{11}(\Omega_1, \Omega_2) + W^{-1-1}(\Omega_1, \Omega_2) - W^{1-1}(\Omega_1, \Omega_2) - W^{-11}(\Omega_1, \Omega_2)}{W^{11}(\Omega_1, \Omega_2) + W^{-1-1}(\Omega_1, \Omega_2) + W^{1-1}(\Omega_1, \Omega_2) + W^{-11}(\Omega_1, \Omega_2)} \\
&= \frac{1}{W(\Omega_1, \Omega_2)} \sum_{k_1} B_{k_1}(J_1) \sum_{k_2 k_3} \sum_{\substack{L_1 \pi_1 \\ L_1' \pi_1'}} \Delta(L_1, L_1') \{1 + (-)^{L_1 + \pi_1 + L_1' + \pi_1' - k_2 + 1}\} \\
&\times L_{k_1 k_2 k_3}(L_1 L_1' J_1 J_2) \sum_{\substack{L_2 \pi_2 \\ L_2' \pi_2'}} \Delta(L_2, L_2') \{1 + (-)^{L_2 + \pi_2 + L_2' + \pi_2' - k_3 + 1}\} \\
&\times R_{k_3}(L_2 L_2' J_2 J_3) P_{k_1 k_2 k_3}(\Omega_1, \Omega_2) \quad (44)
\end{aligned}$$

IX. CORRELATIONS INVOLVING LINEAR POLARIZATION

To derive the triple correlation where the linear polarization of one (or both) of the γ rays is measured, the corresponding transition amplitude (s) must be expressed as a linear superposition of the two

circular polarization states. For the case where the first γ ray is linearly polarized at angle ξ to the reaction plane, the transition amplitude is given by

$$\begin{aligned}
 A_{M_1 M_3}^{\xi q_2}(\vec{k}_1, \vec{k}_2) &= \sum_{M_2} A_{M_1 M_2}^{\xi}(\vec{k}_1) A_{M_2 M_3}^{q_2}(\vec{k}_2) \\
 &= \frac{(k_1 k_2)^{\frac{1}{2}}}{2\pi\hbar \sqrt{2}} \sum_{M_2} \sum_{q_1} \sum_{L_1 \pi_1} \sum_{L_2 \pi_2} q_1^{\pi_1+1} \langle J_1 M_1 | T_{L_1 M_1 - M_2}^{<\pi_1>} | J_2 M_2 \rangle \\
 &\quad \times D_{M_1 - M_2 q_1}^{L_1}(R_1) q_2^{\pi_2} \langle J_2 M_2 | T_{L_2 M_2 - M_3}^{<\pi_2>} | J_3 M_3 \rangle D_{M_2 - M_3 q_2}^{L_2}(R_2)
 \end{aligned} \quad (45)$$

with $R_1 = (\phi_1, \theta_1, \xi_1)$ and $R_2 = (\phi_2, \theta_2, 0)$.

Proceeding in the usual way

$$\begin{aligned}
 W^{\xi q_2}(\Omega_1, \Omega_2) &= \sum_{k_1} B_{k_1}(J_1) \sum_{\substack{L_1 \pi_1 \\ L_1' \pi_1'}} \frac{\Delta(L_1, L_1')}{2} \sum_{q_1 q_1'} q_1^{\pi_1+1} q_1'^{\pi_1'+1} \\
 &\quad \times \sum_{\substack{L_2 \pi_2 \\ L_2' \pi_2'}} q_2^{\pi_2+\pi_2'} \Delta(L_2, L_2') \sum_{k_2 k_3} L_{k_1 k_2 k_3}^{q_1 q_1'}(L_1 L_1' J_1 J_2) \\
 &\quad \times R_{k_3}^{q_2}(L_2 L_2' J_2 J_3) P_{k_1 k_2 k_3}^{q_1 - q_1' 0}(\Omega_1, \xi_1, \Omega_2, 0) \quad (46)
 \end{aligned}$$

where

$$\begin{aligned}
 L_{k_1 k_2 k_3}^{q_1 q_1'}(L_1 L_1' J_1 J_2) &= (-)^{q_1 - L_1} \hat{L}_1 \hat{L}_1' \hat{J}_1 \hat{J}_2 \hat{k}_1 \\
 &\quad \times (L_1 L_1'; q_1 - q_1' | k_2 q_1 - q_1') \begin{Bmatrix} J_1 & L_1 & J_2 \\ J_1 & L_1' & J_2 \\ k_1 & k_2 & k_3 \end{Bmatrix}
 \end{aligned} \quad (47)$$

and

$$P_{k_1 k_2 k_3}^{q_1 - q_1' \quad q_2 - q_2'}(\Omega_1, \Omega_2) = \frac{\hat{k}_2 \hat{k}_3}{\hat{k}_1} \sum_K (k_2 k_3; K - K | k_1 0) \\ \times D_{K q_1 - q_1'}^{k_2}(R_1) D_{-K q_2 - q_2'}^{k_3}(R_2) \quad (48)$$

If the direction only of γ_2 is observed, a sum over q_2 gives

$$W^\xi(\Omega_1, \Omega_2) = \sum_{k_1} B_{k_1}(J_1) \sum_{\substack{L_1 \pi_1 \\ L_1' \pi_1'}} \frac{\Delta(L_1, L_1')}{2} \sum_{q_1 q_1'} q_1^{\pi_1 + 1} q_1'^{\pi_1' + 1} \\ \times \sum_{\substack{L_2 \pi_2 \\ L_2' \pi_2'}} \Delta(L_2, L_2') \sum_{k_2 k_3} \{1 + (-)^{L_2 + \pi_2 + L_2' + \pi_2' - k_3}\} \\ \times L_{k_1 k_2 k_3}^{q_1 q_1'}(L_1 L_1' J_1 J_2) R_{k_3}(L_2 L_2' J_2 J_3) P_{k_1 k_2 k_3}^{q_1 - q_1' 0}(\Omega_1, \xi_1, \Omega_2, 0) \quad (49)$$

and the linear polarization-direction triple correlation is given by

$$P_L^{(1)}(\Omega_1, \Omega_2) = \frac{W^0(\Omega_1, \Omega_2) - W^{\pi/2}(\Omega_1, \Omega_2)}{W^0(\Omega_1, \Omega_2) + W^{\pi/2}(\Omega_1, \Omega_2)} \\ = \frac{1}{W(\Omega_1, \Omega_2)} \sum_{k_1} B_{k_1}(J_1) \sum_{\substack{L_1 \pi_1 \\ L_1' \pi_1'}} \Delta(L_1, L_1') (-)^{\pi_1'} \\ \times \sum_{\substack{L_2 \pi_2 \\ L_2' \pi_2'}} \Delta(L_2, L_2') \sum_{k_2 k_3} \{1 + (-)^{L_1 + \pi_1 + L_1' + \pi_1' - k_2}\} \\ \times \{1 + (-)^{L_2 + \pi_2 + L_2' + \pi_2' - k_3}\} L_{k_1 k_2 k_3}^{1-1}(L_1 L_1' J_1 J_2)$$

$$\times R_{k_3} (L_2 L_2' J_2 J_3) P_{k_1 k_2 k_3}^{20} (\Omega_1, \Omega_2) \quad (50)$$

If it is γ_2 which is linearly polarized at angle ξ to the reaction plane, the transition amplitude is a linear superposition of the amplitudes for the two circular polarization states q_2 .

Proceeding as above,

$$\begin{aligned} W^{q_1 \xi}(\Omega_1, \Omega_2) &= \sum_{k_1} B_{k_1}(J_1) \sum_{\substack{L_1 \pi_1 \\ L_1' \pi_1'}} q_1^{\pi_1 + \pi_1'} \Delta(L_1, L_1') \\ &\times \sum_{\substack{L_2 \pi_2 \\ L_2' \pi_2'}} \frac{\Delta(L_2, L_2')}{2} \sum_{q_2 q_2'} q_2^{\pi_2 + 1} q_2'^{\pi_2 + 1} \sum_{k_2 k_3} L_{k_1 k_2 k_3}^{q_1} (L_1 L_1' J_1 J_2) \\ &\times R_{k_3}^{q_2 q_2'} (L_2 L_2' J_2 J_3) P_{k_1 k_2 k_3}^{0 \ q_2 - q_2'} (\Omega_1, 0, \Omega_2, \xi) \end{aligned} \quad (51)$$

As before, a sum over q_1 is required if the polarization of γ_1 is not measured. The direction-linear-polarization correlation is

$$\begin{aligned} P_L^{(2)}(\Omega_1, \Omega_2) &= \frac{1}{W(\Omega_1, \Omega_2)} \sum_{k_1} B_{k_1}(J_1) \sum_{\substack{L_1 \pi_1 \\ L_1' \pi_1'}} \Delta(L_1, L_1') \\ &\times \sum_{\substack{L_2 \pi_2 \\ L_2' \pi_2'}} (-)^{\pi_2'} \Delta(L_2, L_2') \sum_{k_2 k_3} \{1 + (-)^{L_1 + \pi_1 + L_1' + \pi_1' - k_2}\} \\ &\times \{1 + (-)^{L_2 + \pi_2 + L_2' + \pi_2' - k_3}\} L_{k_1 k_2 k_3} (L_1 L_1' J_1 J_2) \end{aligned}$$

$$\times R_{k_3}^{1-1}(L_2 L_2' J_2 J_3) P_{k_1 k_2 k_3}^{0 \ 2}(\Omega_1, \Omega_2) \quad (52)$$

Finally, when the linear polarization of both γ -rays is measured, we have

$$\begin{aligned} W^{\xi_1 \xi_2}(\Omega_1, \Omega_2) &= \sum_{k_1} B_{k_1}(J_1) \sum_{\substack{L_1 \pi_1 \\ L_1' \pi_1'}} \frac{\Delta(L_1, L_1')}{2} \sum_{\substack{L_2 \pi_2 \\ L_2' \pi_2'}} \frac{\Delta(L_2, L_2')}{2} \\ &\times \sum_{q_1 q_1'} q_1^{\pi_1+1} q_1'^{\pi_1+1} \sum_{q_2 q_2'} q_2^{\pi_2+1} q_2'^{\pi_2+1} \sum_{k_2 k_3} L_{k_1 k_2 k_3}^{q_1 q_1'}(L_1 L_1' J_1 J_2) \\ &\times R_{k_3}^{q_2 q_2'}(L_2 L_2' J_2 J_3) P_{k_1 k_2 k_3}^{q_1 - q_1' \ q_2 - q_2'}(\Omega_1, \xi_1, \Omega_2, \xi_2) \quad (53) \end{aligned}$$

and the linear polarization-linear polarization triple correlation is

$$\begin{aligned} P_L^{(12)}(\Omega_1, \Omega_2) &= \frac{W^{0 \ 0}(\Omega_1, \Omega_2) + W^{\pi/2 \ \pi/2}(\Omega_1, \Omega_2) - W^{0 \ \pi/2}(\Omega_1, \Omega_2) - W^{\pi/2 \ 0}(\Omega_1, \Omega_2)}{W^{0 \ 0}(\Omega_1, \Omega_2) + W^{\pi/2 \ \pi/2}(\Omega_1, \Omega_2) + W^{0 \ \pi/2}(\Omega_1, \Omega_2) + W^{\pi/2 \ 0}(\Omega_1, \Omega_2)} \\ &= \frac{1}{W(\Omega_1, \Omega_2)} \sum_{k_1} B_{k_1}(J_1) \sum_{\substack{L_1 \pi_1 \\ L_1' \pi_1'}} (-)^{\pi_1'} \Delta(L_1, L_1') \sum_{\substack{L_2 \pi_2 \\ L_2' \pi_2'}} (-)^{\pi_2'} \Delta(L_2, L_2') \\ &\times \sum_{k_2 k_3} L_{k_1 k_2 k_3}^{1-1}(L_1 L_1' J_1 J_2) R_{k_3}^{1-1}(L_2 L_2' J_2 J_3) \{P_{k_1 k_2 k_3}^{2 \ 2}(\Omega_1, \Omega_2) \\ &\times [1 + (-)^{L_1 + \pi_1 + L_1' + \pi_1' - k_2} (-)^{L_2 + \pi_2 + L_2' + \pi_2' - k_3}] + P_{k_1 k_2 k_3}^{2-2}(\Omega_1, \Omega_2) \\ &\times [(-)^{L_1 + \pi_1 + L_1' + \pi_1' - k_2} + (-)^{L_2 + \pi_2 + L_2' + \pi_2' - k_3}]\} \quad (54) \end{aligned}$$

X. AN ARBITRARY NUMBER OF TRANSITIONS

The extension of the formalism for an arbitrary number of γ -ray transitions can be inferred from the study of three successive γ -transitions. The amplitude for this process is given by

$$A_{M_1 M_4}^{q_1 q_2 q_3}(\vec{k}_1, \vec{k}_2, \vec{k}_3) = \sum_{M_2 M_3} A_{M_1 M_2}^{q_1}(\vec{k}_1) A_{M_2 M_3}^{q_2}(\vec{k}_2) A_{M_3 M_4}^{q_3}(\vec{k}_3) \quad (55)$$

The quadruple correlation, for the case where the circular polarization of all three γ rays is observed, is given by

$$\begin{aligned} W^{q_1 q_2 q_3}(\Omega_1, \Omega_2, \Omega_3) &= \sum_{k_1} B_{k_1}(J_1) \sum_{\substack{L_1 \pi_1 \\ L_1' \pi_1'}} q_1^{\pi_1 + \pi_1'} \Delta(L_1, L_1') \\ &\times \sum_{\substack{L_2 \pi_2 \\ L_2' \pi_2'}} q_2^{\pi_2 + \pi_2'} \Delta(L_2, L_2') \sum_{\substack{L_3 \pi_3 \\ L_3' \pi_3'}} q_3^{\pi_3 + \pi_3'} \Delta(L_3, L_3') \\ &\times \sum_{k_2 k_3} L_{k_1 k_2 k_3}^{q_1}(L_1 L_1' J_1 J_2) \sum_{k_4 k_5} L_{k_3 k_4 k_5}^{q_2}(L_2 L_2' J_2 J_3) \\ &\times R_{k_5}^{q_3}(L_3 L_3' J_3 J_4) P_{k_1 k_2 k_3 k_4 k_5}(\Omega_1, \Omega_2, \Omega_3) \end{aligned} \quad (56)$$

where

$$\begin{aligned} P_{k_1 k_2 k_3 k_4 k_5}(\Omega_1, \Omega_3, \Omega_3) &= \frac{\hat{k}_5 \hat{k}_4}{\hat{k}_3} \frac{\hat{k}_3 \hat{k}_2}{\hat{k}_1} \\ &\times \sum_{K_1 K_2} (k_5 k_4; -K_1 K_1 - K_2 | k_3 - K_2) (k_3 k_2; -K_2 K_2 | k_1 0) \end{aligned}$$

$$\times D_{-k_1 0}^{k_5} (R_3) D_{k_1 k_2 0}^{k_4} (R_2) D_{k_2 0}^{k_2} (R_1) \quad (57)$$

By comparing this expression with Eq. (14) for a single γ -ray and Eq. (31) for two γ rays, a program for writing down the correlation for an arbitrary number of transitions can be detailed.

- (1) Beginning with the initial state $|J_1\rangle$ in the sequence, write a different k_i value for every nuclear level and every γ ray in the sequence, except for the last γ ray and the final nuclear state. Also if any of the γ transitions are unobserved, do not write a k_i value for this transition, and make the k_i values for the two nuclear states connected by this unobserved transition the same.
- (2) In the correlation formula, write down and sum over all of these k_i values, and insert the $B_{k_1}(J_1)$ coefficient for the initial state.
- (3) For every observed γ transition, write down the factor $\Delta(L_i, L_i')$ and sum over L_i, π_i, L_i', π_i' .
- (4) For every γ decay (except the last one) which connects the state $|J_i\rangle$ to the state $|J_{i+1}\rangle$ by multipoles L_i, L_i' , we insert a factor which depends on what we observe about the γ ray.

i) If we observe circular polarization, we insert the factor

$$L_{kk'k''}^{q_i} (L_i L_i' J_i J_{i+1}) q_i^{\pi_i + \pi_i'}$$

ii) If linear polarization is observed, we insert the factor

$$q_i^{\pi_i + 1} q_i'^{\pi_i' + 1} L_{kk'k''}^{q_i q_i'} (L_i L_i' J_i J_{i+1})$$

iii) If the direction only is observed, we insert the factor

$$L_{kk'k''} (L_i L_i' J_i J_{i+1}) \{1 + (-)^{L_i + \pi_i + L_i' + \pi_i' - k'}\}$$

iv) If the γ -ray is unobserved, we insert the factor

$$U_k(J_i, J_{i+1})$$

- (5) For the last observed γ -ray in the sequence, the above rules hold if $L_{kk'k''}^{q_i q_i'} (L_i L_i' J_i J_{i+1})$ is replaced by $R_k^{q_i q_i'} (L_i L_i' J_i J_{i+1})$.

The angular functions are defined as follows:

- (1) Starting with the last observed γ decay in the sequence and proceeding towards the first, insert the following factor for each γ ray

i) $D_{\kappa_i 0}^{k_i}(R_i)$ if either the circular polarization or the direction is observed.

ii) 1 if the γ is unobserved.

iii) $D_{\kappa_i q_i - q_i'}^{k_i}(R_i)$ if the linear polarization is observed.

- (2) For the first two D-matrices in this sequence, write a Clebsch-Gordan coefficient $(kk'; \kappa \kappa' | k'' \kappa'')$ to couple k for the second last γ decay to k' for the last decay (with the corresponding κ from the D-matrices) to k'' for the initial state in the second last decay. For each remaining D-matrix, write a Clebsch-Gordan coefficient to couple the k of the D-matrix to the last k in the preceding Clebsch-Gordan, to

give the k for the initial state of the transition. For the last Clebsch in the series, set the projection of the final k equal to zero.

- (3) For each Clebsch $(kk'; \kappa \kappa' | k'' \kappa + \kappa')$ insert the factor $\hat{k} \hat{k}' | \hat{k}''$ and finally sum over all the κ .

After completing this procedure, we are left with the angular correlation formula $W(\Omega_1, \Omega_2, \dots, \Omega_n)$. If polarizations are being measured, the polarization correlations $P(\Omega_1, \dots, \Omega_n)$ can be defined in the usual way.

REFERENCES

Rose, H.J. and Brink, D.M., 1967, Revs. Mod. Phys. 39, 306.

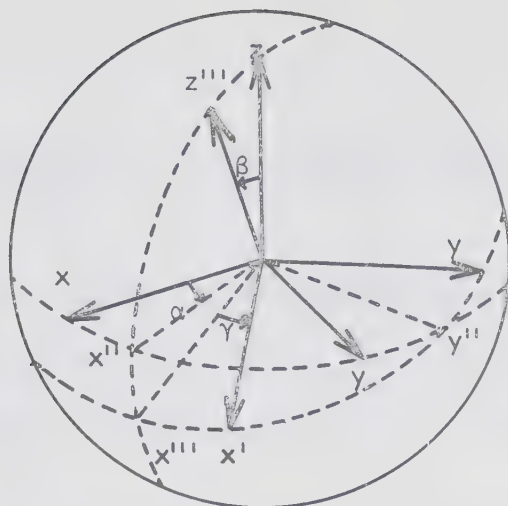


Figure 37. The Euler angles (α, β, γ) of the rotation R which takes the coordinate system $S(x, y, z)$ to $S'(x', y', z')$. This transformation is accomplished by a rotation of angle α about the z axis (to S''), followed by a rotation of angle β about the y'' axis (to S'), followed by a rotation of angle γ about the z''' axis (to S').

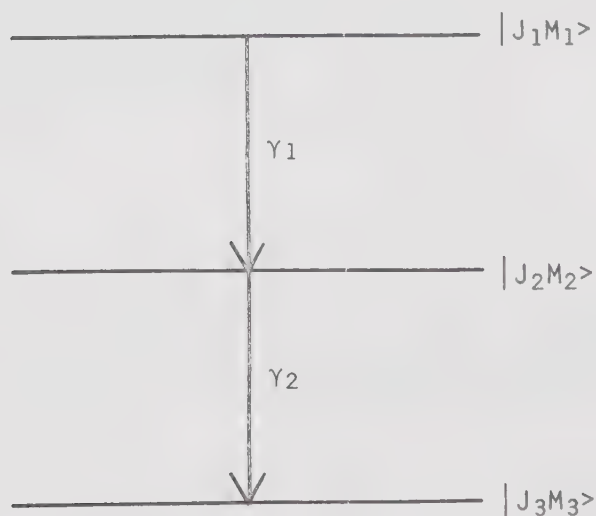


Figure 38. A schematic diagram of the γ ray cascade

$$|J_1 M_1\rangle \rightarrow |J_2 M_2\rangle \rightarrow |J_3 M_3\rangle$$

APPENDIX I γ -RAY ANGULAR CORRELATIONS

Consider the situation shown schematically in fig. 2, in which two γ rays are emitted sequentially. Using time-dependent perturbation theory, we can relate the amplitude for this process to that for a single γ decay.

We assume that the three nuclear states $\psi_i \equiv |J_i M_i\rangle$ ($i=1, 2, 3$) are eigenstates of a time-independent Hamiltonian \mathcal{H}_0

$$\mathcal{H}_0 \psi_i = E_i \psi_i \quad (\text{A1-1})$$

The total Hamiltonian for this system is $\mathcal{H} = \mathcal{H}_0 + \mathcal{H}_{\text{INT}}(t)$, where $\mathcal{H}_{\text{INT}}(t)$ is a time dependent interaction which induces transitions between the eigenstates ψ_i . The total wave function Ψ is a solution of the Schrödinger equation

$$\mathcal{H}\Psi = i\hbar \dot{\Psi} \quad (\text{A1-2})$$

We assume further that the states ψ_i form a complete orthonormal set for the system, and we can therefore expand the total wave function as

$$\Psi(t) = \sum_i a_i(t) \psi_i e^{-iE_i t/\hbar} \quad (\text{A1-3})$$

The square of the expansion coefficients $a_i(t)$ gives the probability

of finding the system in the state ψ_i at time t .

Substituting Eq. (3) into Eq. (2), and making use of the orthonormality of the wavefunctions ψ_i when integrated over all space coordinates, we arrive at the set of coupled differential

$$\begin{aligned} i\hbar \dot{a}_1(t) &= a_1(t)\mathcal{H}_{11} + a_2(t)\mathcal{H}_{12} e^{i\omega_1 t} + a_3(t)\mathcal{H}_{13} e^{i(\omega_1+\omega_2)t} \\ i\hbar \dot{a}_2(t) &= a_1(t)\mathcal{H}_{21} e^{-i\omega_1 t} + a_2(t)\mathcal{H}_{22} + a_3(t)\mathcal{H}_{23} e^{i\omega_2 t} \\ i\hbar \dot{a}_3(t) &= a_1(t)\mathcal{H}_{31} e^{-i(\omega_1+\omega_2)t} + a_2(t)\mathcal{H}_{32} e^{-i\omega_2 t} + a_3(t)\mathcal{H}_{33} \end{aligned} \quad (\text{A1-4})$$

where

$$\omega_1 = (E_1 - E_2)/\hbar$$

$$\omega_2 = (E_2 - E_3)/\hbar$$

$$\mathcal{H}_{ij} = \langle \psi_i | \mathcal{H}_{\text{INT}}(t) | \psi_j \rangle \quad (\text{A1-5})$$

The terms involving \mathcal{H}_{13} and \mathcal{H}_{31} describe transitions directly from the state ψ_1 to the state ψ_3 , and while such transitions may in fact occur, we are interested only in the cascade decay, and these terms may be excluded.

In order to solve the set of Eqs. (4), we assume that the interaction is turned on at $t = 0$, at which time the system is entirely in the state ψ_1 . We then have the boundary conditions

$$a_i(t = 0) = \delta_{i1} \quad (\text{A1-6})$$

We also assume that for a short time after $t = 0$, we can neglect the time dependence of the $a_i(t)$ on the right hand side of these equations. The second of these equations is then

$$i\hbar \dot{a}_2(t) = \mathcal{H}_{21}(t) e^{-i\omega_1 t} \quad (\text{A1-7})$$

If $\mathcal{H}_{21}(t)$ is a slowly varying function of time, we replace it with its value at $t = 0$, and can integrate (7) to get

$$a_2(t) = \frac{\mathcal{H}_{21}(0)}{\omega_1 \hbar} [e^{-i\omega_1 t} - 1] \quad (\text{A1-8})$$

Substituting this expression into the third of the Eq. (4) gives

$$i\hbar \dot{a}_3(t) = \frac{\mathcal{H}_{21}(0)}{\omega_1 \hbar} \mathcal{H}_{32}(t) e^{-i\omega_2 t} [e^{-i\omega_1 t} - 1] \quad (\text{A1-9})$$

which can be solved in a similar manner to give

$$a_3(t) = \frac{\mathcal{H}_{21}(0) \mathcal{H}_{32}(0)}{\omega_1 \hbar^2} \left| \frac{e^{-i(\omega_1+\omega_2)t} - 1}{\omega_1 + \omega_2} - \frac{e^{-i\omega_2 t} - 1}{\omega_2} \right| \quad (\text{A1-10})$$

Since we have explicitly removed any contribution from the direct transition $\psi_1 \rightarrow \psi_3$, the population of the state ψ_3 at any time t is a measure of the probability that the cascade transition has taken place. We therefore consider the term

$$|a_3(t)|^2 = \left| \frac{\mathcal{H}_{21}(0) \mathcal{H}_{32}(0)}{\hbar^2} \right|^2 \left| \frac{e^{-i(\omega_1+\omega_2)t} - 1}{\omega_1(\omega_1+\omega_2)} - \frac{e^{-i\omega_2 t} - 1}{\omega_1\omega_2} \right|^2 \quad (\text{A1-11})$$

Finally, we integrate (11) over all energies ω_1 and ω_2 of the photon states. This converts the second factor in the above to $2\pi t$, and the transition rate is

$$\begin{aligned}
 W &= \frac{d}{dt} |a_3(t)|^2 \\
 &\sim |\mathcal{H}_{21}(0) \mathcal{H}_{32}(0)|^2
 \end{aligned}
 \tag{A1-12}$$

apart from constant factors. The basic result is that the amplitude for the two-step process is just the product of the amplitudes for the individual decays.

APPENDIX 2 k SELECTION RULES

Consider the term in the triple correlation formula

$$\sum_{L_1, L_1'} \delta_{L_1}^{<\pi>} \delta_{L_1'}^{<\pi'>} L_{k_1 k_2 k_3} (L_1, L_1', J_1, J_2) \quad (A2-1)$$

Since L_1 and L_1' span the same range of values, this term cannot change when we interchange L_1 and L_1' . Making use of the well-known symmetry relations for the 9-j symbols and Clebsch-Gordan coefficients appearing in Eq. (30), we see that such an interchange introduces only a phase $(-)^{k_2+k_3-k_1}$, and we can then demand that $k_1 + k_2 + k_3$ be an even number.

A P P E N D I X B

C U P P L E - I

A DESCRIPTION OF CALCULATIONS IN THE

INTERMEDIATE COUPLING MODEL

C U P P L E - I

TITLE: CUPPLE-I

TYPE: Main

SOURCE LANGUAGE: FORTRAN IV (G)

ORIGIN: P.W. Green
Nuclear Research Centre
The University of Alberta

ABSTRACT: The purpose of this computer program is to calculate the energy eigenvalues and eigenfunctions, using the framework of the Intermediate Coupling model, for either a single particle coupled to the surface vibrations of an even-even core (for odd-A nuclei), or for two particles coupled to such a core (for even-even or odd-odd nuclei).

I ONE-PARTICLE CALCULATIONS - THEORETICAL FORMULATION

For a system composed of a single particle coupled to a collective core, the total Hamiltonian of the system can be expressed in the form

$$H_T = H_C + H_p + H_{INT} \quad (1)$$

where H_C is the Hamiltonian for the core, H_p is the particle Hamiltonian, and H_{INT} represents the interaction energy between the two systems.

The core is assumed to be capable of performing quadrupole oscillations, such that the nuclear surface can be described by

$$R(\theta, \phi) = R_0 [1 + \sum_{\mu} \alpha_{\mu}^* Y_2^{\mu}(\theta, \phi)] \quad (2)$$

where the α_{μ} are the dynamical variables of the collective motion. Provided that the deviations from a spherical shape are small, the collective Hamiltonian can be expressed in the form (Ch 54)

$$H_C = \frac{1}{2} \sum_{\mu} \{B |\dot{\alpha}_{\mu}|^2 + C |\alpha_{\mu}|^2\} \quad (3)$$

which is the Hamiltonian of a system of harmonic oscillators with frequency

$$\omega = \left(\frac{C}{B}\right)^{\frac{1}{2}} \quad (4)$$

The parameters B and C in (3) are, respectively, the collective mass and the nuclear deformability.

It is convenient to rewrite the core Hamiltonian (3) in terms of creation and annihilation operators (b_{μ}^{\dagger} and b_{μ}) for spin-2 phonons, which are defined by the equations

$$\begin{aligned} b_{\mu} &= \frac{1}{(2B\hbar\omega)^{\frac{1}{2}}} [B\omega\alpha_{\mu}^{\dagger} + i\pi_{\mu}] \\ b_{\mu}^{\dagger} &= \frac{1}{(2B\hbar\omega)^{\frac{1}{2}}} [B\omega\alpha_{\mu} - i\pi_{\mu}^{\dagger}] \end{aligned} \quad (5)$$

$$\text{where } \pi_{\mu} = B\dot{\alpha}_{\mu}^{\dagger}. \quad (6)$$

The core Hamiltonian then becomes

$$H_C = \sum_{\mu} (b_{\mu}^{\dagger} b_{\mu} + \frac{1}{2}) \hbar\omega \quad (7)$$

and has, as its eigenvectors, a series of states with energies

$$E_N = (N + \frac{5}{2}) \hbar\omega \quad (8)$$

N can be interpreted as the number of phonons associated with the particular state.

For a given single particle orbital, the particle Hamiltonian H_p is a constant, having as its eigenvalues the single particle energies of the average spherical potential.

The interaction Hamiltonian represents the energy due to the coupling between the extra particle and the quadrupole oscillations of the core. To first order in the α_μ , it can be written

$$H_{INT} = -k(r) \sum_{\mu} \alpha_{\mu}^* Y_2^{\mu}(\theta, \phi) \quad (9)$$

where (r, θ, ϕ) are the co-ordinates of the particle.

In calculating the matrix elements of (9), we will need the value of the radial matrix element

$$k \equiv \langle n'l' | k(r) | n\ell \rangle \quad (10)$$

which will depend, in general, on the quantum numbers n and ℓ describing the initial and final states of the particle. The dependence of k on these quantum numbers is not critical, however, and it will be assumed that k is a constant. Again, it is convenient to write the Hamiltonian in terms of phonon creation and annihilation operators,

$$H_{INT} = -\left(\frac{\pi}{5}\right)^{\frac{1}{2}} \hbar\omega_{\xi} \sum_{\mu} (-)^{\mu} [b_{-\mu}^{\dagger} + (-)^{\mu} b_{\mu}] Y_2^{\mu}(\theta, \phi) \quad (11)$$

where the strength of the interaction is characterized by the

dimensionless coupling parameter

$$\xi = \left(\frac{5}{2\pi\hbar\omega_C} \right)^{1/2} k \quad (12)$$

We shall work in an angular momentum representation. The basis states of the system are chosen as those of the non-interacting system

$$|NRj;IM\rangle = \sum_m (Rj;M-m \ m|IM) |NR \ M-m\rangle |jm\rangle \quad (13)$$

representing a particle of angular momentum j and z -projection m , coupled to a core state characterized by N phonons coupled to a core spin R , to give a state of total angular momentum I and projection M .

The eigenfunctions of the total Hamiltonian (1) will be linear combinations of these basis states, of the form

$$|E_I;IM\rangle = \sum_{NRj} A^{E_I}_{NRjI} (NRjI) |NRj;IM\rangle \quad (14)$$

The expansion coefficients $A^{E_I}_{NRjI} (NRjI)$ and the corresponding energy eigenvalues in Eq. (14) can be found by calculating the matrix elements of H_T , and diagonalizing the resulting matrix. In this representation, both the core Hamiltonian H_C and the particle Hamiltonian H_p have only diagonal matrix elements

$$\langle NRj;IM | H_C + H_p | NRj;IM \rangle = \left(N + \frac{5}{2} \right) \hbar\omega + \epsilon_j \quad (15)$$

where $\hbar\omega$ is the phonon energy and ϵ_j the single particle energy for the particle in orbital j .

The matrix elements of the interaction Hamiltonian are

$$\begin{aligned}
 \langle N'R'j'; l'M' | H_{INT} | NRj; lM \rangle \\
 = - \left(\frac{\pi}{5} \right)^{1/2} \hbar \omega_{\xi} \sum_{\mu} (R'j'; M'-m' \ m' | l'M') (Rj; M-m \ m | lM) (-)^{\mu} \\
 \times \langle N'R'M'-m' | b_{-\mu}^{\dagger} + (-)^{\mu} b_{\mu} | NRM-m \rangle \langle j'm' | Y_2^{\mu} | jm \rangle \quad (16)
 \end{aligned}$$

The Wigner-Eckart theorem* can be used to separate the dependence of the matrix elements on the magnetic quantum numbers

$$\begin{aligned}
 \langle N'R'M'-m' | b_{-\mu}^{\dagger} | NR \ M-m \rangle &= \frac{1}{R'} (R2; M-m \ -\mu | R'M'-m') \\
 &\times \langle N'R' || b^{\dagger} || NR \rangle \\
 \langle j'm' | Y_2^{\mu}(\theta, \phi) | jm \rangle &= \frac{1}{j'} (j2; m\mu | j'm') \langle j' || Y_2 || j \rangle \\
 \langle N'R'M'-m' | b_{\mu} | NR \ M-m \rangle &\equiv \langle NR \ M-m | b_{\mu}^{\dagger} | N'R' \ M'-m' \rangle \quad (17)
 \end{aligned}$$

where $j \equiv \sqrt{2j+1}$. The last line in the above is required because the Wigner-Eckart theorem can be used only with irreducible tensor operators. The creation operators b_{μ}^{\dagger} are irreducible tensors, but the annihilation operators b_{μ} are not.

* The definition of the Wigner-Eckart theorem used here is that of de Shalit and Talmi (Sh 63).

$$\langle j'M' | T_k^K | JM \rangle = \frac{1}{j'} (Jk; M\kappa | j'M') \langle j' || T_k || j \rangle$$

Because of this definition, our reduced matrix elements are a factor of j' larger than those of Choudhury (Ch 54) and Choudhury and O'Dwyer (Ch 67).

Using the techniques of Racah algebra, the sum of four Clebsch-Gordan coefficients reduces to

$$\delta_{11'} \delta_{MM'} \hat{R}' \hat{j}' W(R' j' R j; 12) (-)^{R' + j - 1} \quad (18)$$

and the complete term for H_{INT} is

$$\begin{aligned} & - \left(\frac{\pi}{5}\right)^{\frac{1}{2}} \hbar \omega \xi (-)^{R' + j - 1} \langle j' || Y_2 || j \rangle \{ \langle N' R' || b^\dagger || NR \rangle \\ & + (-)^{R' - R} \langle NR || b^\dagger || N' R' \rangle \} W(R' j' R j; 12) \delta_{11'} \delta_{MM'} \end{aligned} \quad (19)$$

It is now necessary to calculate the reduced matrix elements appearing in (19). The results for the spherical harmonics are given by several authors. We use that of de Shalit and Talmi (Sh 63)

$$\langle j' || Y_2 || j \rangle = \left(\frac{5}{4\pi}\right)^{\frac{1}{2}} \hat{j} \begin{pmatrix} j & 2 & -\frac{1}{2} & 0 \\ j' & -\frac{1}{2} \end{pmatrix} \frac{1}{2} [1 + (-)^{j + j'}] \quad (20)$$

To calculate the reduced matrix elements of the phonon creation operators b_μ^\dagger , it is convenient to introduce the coefficients of fractional parentage (cfp's) for an N-particle system. Using these coefficients, an N-phonon state can be expanded

$$\begin{aligned} |N\alpha RM\rangle &= \sum_{R_1 \alpha_1} [2^{N-1} (\alpha_1 R_1) 2 R] \{ 2^N \alpha R \} \sum_m (R_1 2; m M-m | RM) \\ &\times | (N-1) \alpha_1 R_1 m \rangle | 2 M-m \rangle \end{aligned} \quad (21)$$

where $[2^{N-1} (\alpha_1 R_1) 2 R] \{ 2^N \alpha R \}$ is the cfp, R_1 and R are the total angular momenta of the (N-1) and N particle systems respectively, and α_1 and α represent additional quantum numbers needed to completely

specify these states. We are concerned only with states for $N \leq 3$, and since these states are completely specified by the number of phonons N and the total angular momentum R , the quantum numbers α and α_1 will be suppressed.

Acting on this state with the annihilation operator b_μ gives

$$\begin{aligned} b_\mu |NRM\rangle &= \sqrt{N} \sum_{R_1} [2^{N-1}(R_1) 2R] \sum_m (R_1 2; m M-m | RM) \\ &\quad \times |N-1 R_1 m\rangle \delta_{\mu, M-m} \\ &= \sqrt{N} \sum_{R_1} [2^{N-1}(R_1) 2R] (R 2; M-\mu \mu | RM) |N-1 R_1 M-\mu\rangle \quad (22) \end{aligned}$$

where the factor \sqrt{N} comes from the fact that, for the annihilation operator acting on an N -particle state (Dw 67)

$$b_\mu |N\rangle = \sqrt{N} |N-1\rangle \quad (23)$$

We then consider the matrix element

$$\begin{aligned} \langle N'R'M' | b_\mu |NRM\rangle &\equiv \langle NRM | b_\mu^\dagger |N'R'M'\rangle \\ &= \sqrt{N} \sum_{R_1} [2^{N-1}(R_1) 2R] (R_1 2; M-\mu \mu | RM) \\ &\quad \times \delta_{N', N-1} \delta_{R', R_1} \delta_{M', M-\mu} \\ &= \sqrt{N} [2^{N-1}(R') 2R] (R' 2; M-\mu \mu | RM) \delta_{N', N-1} \delta_{M', M-\mu} \quad (24) \end{aligned}$$

Using the Wigner-Eckart theorem gives

$$\langle NRM | b_\mu^\dagger |N'R'M'\rangle = \frac{1}{R} (R' 2; M'\mu | RM) \langle NR || b^\dagger || N'R'\rangle \quad (25)$$

and comparing (24) and (25),

$$\langle NR || b^\dagger | N'R' \rangle = \sqrt{N} \hat{R} [2^{N-1} (R') 2R] \} 2^N R] \quad (26)$$

A list of the reduced matrix elements for $N \leq 3$ is given in Table XII.

II TWO PARTICLE CALCULATIONS - THEORETICAL FORMULATION

For a system composed of two particles coupled to a vibrating core, the total Hamiltonian is

$$H_T = H_C + H_p(1) + H_p(2) + H_{INT}(1) + H_{INT}(2) + H_{12} \quad (27)$$

The notation is the same as that used in Sect. I, with the indices 1 and 2 referring to the first and second particles respectively. The term H_{12} is the residual interaction between the two extra particles.

It is possible to diagonalize the total Hamiltonian (27) directly, in a manner analogous to that given in Sect. I, to obtain the eigenvalues and eigenvectors of the composite system. This procedure is often impractical, however, since it requires the diagonalization of very large matrices.

The sizes of the matrices involved can be substantially reduced if the problem is divided into two steps. One first finds the eigenfunctions for one of the particles (say, particle 1) coupled to the core, by diagonalizing the Hamiltonian

$$H_1 \equiv H_C + H_p(1) + H_{INT}(1) \quad (28)$$

It is reasonable to assume that those eigenfunctions of H_1 which lie very high in energy will not substantially affect the low-energy properties of the core plus two particle system, so one may then choose a subset of these eigenfunctions as a basis set for the two particle calculation, and diagonalize the total Hamiltonian to obtain the results for the complete system. This is the approach which we follow in this work.

The basis vectors for the two particle system are

$$|\alpha_1 J_1 j_2; IM\rangle = \sum_{m_2} (J_1 j_2; M-m_2 \ m_2 | IM) |\alpha_1 J_1 \ M-m_2\rangle |j_2 m_2\rangle \quad (29)$$

where α_1 is an additional quantum number to specify which state of spin J_1 we are considering. The states $|\alpha_1 J_1 \ M-m_2\rangle$, which are obtained by diagonalizing the Hamiltonian (28), are of the form

$$|\alpha_1 J_1 \ M-m_2\rangle = \sum_{NRj_1} B^{\alpha_1} (NRj_1 J_1) |NRj_1; J_1 \ M-m_2\rangle \quad (30)$$

The particle Hamiltonian $H_p(2)$ is diagonal in this representation, and has as its matrix elements the single particle energies for particle 2.

$$\langle \alpha_1 J_1 j_2; IM | H_p(2) | \alpha_1 J_1 j_2; IM \rangle = \epsilon_2 \quad (31)$$

H_1 is also diagonal, and has matrix elements equal to the energy of the state $|\alpha_1 J_1 \ M-m_2\rangle$. The only off-diagonal terms come from $H_{INT}(2)$ and H_{12} .

Considering $H_{INT}(2)$ first, we have

$$\begin{aligned} & \langle \alpha_1' J_1' j_2'; I' M' | H_{INT}(2) | \alpha_1 J_1 j_2; IM \rangle \\ &= -\left(\frac{\pi}{5}\right)^{1/2} \hbar \omega \xi_2 \sum_{m_2 m_2'} (J_1' j_2'; M'-m_2' \ m_2' | I' M') (J_1 j_2; M-m_2 \ m_2 | IM) \end{aligned}$$

$$\begin{aligned}
& \times \langle \alpha_1 'J_1 ' M'-m_2 ' | (-)^{\mu} b_{-\mu}^{\dagger} + b_{\mu} | \alpha_1 J_1 M-m_2 \rangle \\
& \times \langle j_2 'm_2 ' | Y_2^{\mu}(\Omega_2) | j_2 m_2 \rangle
\end{aligned} \quad (32)$$

The matrix element containing the boson creation and annihilation operators is expanded in terms of its component states to give

$$\begin{aligned}
& \sum_{\substack{NRj_1 \\ N'R'j_1'}} B^{*\alpha_1'}(N'R'j_1'J_1') B^{\alpha_1}(NRj_1J_1) \sum_{m_1m_1'} \langle j_1'm_1' | j_1m_1 \rangle \\
& \times (R'j_1'; M'-m_1'-m_2' m_1 | J_1'M'-m_2') (Rj_1; M-m_1-m_2 m_1 | J_1M-m_2) \\
& \times \langle N'R'M'-m_1'-m_2' | (-)^{\mu} b_{-\mu}^{\dagger} + b_{\mu} | NR M-m_1-m_2 \rangle
\end{aligned} \quad (33)$$

What follows now is just Racah algebra. The Wigner-Eckart theorem is again used to separate the dependence of the matrix elements on magnetic quantum numbers, and the sum of six Clebsch-Gordan coefficients reduces to two Racah coefficients. The final result for $H_{INT}(2)$ is

$$\begin{aligned}
& - \delta_{ll'} \delta_{MM'} \hat{J}_1 \hat{J}_1' (-)^{J_1-J_1'} \left(\frac{\pi}{5}\right)^{\frac{1}{2}} \hbar \omega_{\xi} \sum_{\substack{NR \\ N'R'}} \sum_{j_1} B^{*\alpha_1'}(N'R'j_1J_1') \\
& \times B^{\alpha_1}(NRj_1J_1) \{ \langle N'R' | | b^{\dagger} | | NR \rangle + (-)^{R'-R} \langle NR | | b^{\dagger} | | N'R' \rangle \} \\
& \times \langle j_2' | | Y_2 | | j_2 \rangle W(2R'J_1j_1; RJ_1') W(J_121j_2'; J_1'j_2)
\end{aligned} \quad (34)$$

This term is diagonal in the co-ordinates of the first particle (j_1), since the interaction does not involve particle 1.

Finally, we consider the residual interaction between the particles H_{12} .

$$\begin{aligned}
& \langle \alpha_1' J_1' j_2'; l' M' | H_{12} | \alpha_1 J_1 j_2; l M \rangle \\
&= \sum_{m_2 m_2'} \sum_{\substack{N' R' j_1' \\ NR j_1}} \sum_{m_1 m_1'} B^{\alpha_1' *} (N' R' j_1' J_1') B^{\alpha_1} (NR j_1 J_1) \\
&\times (J_1' j_2'; M' - m_2' \quad m_2' | l' M') (J_1 j_2; M - m_2 \quad m_2 | l M) \\
&\times (R' j_1'; M' - m_2' - m_1' \quad m_1' | J_1' M' - m_2') (R j_1; M - m_2 - m_1 \quad m_1 | J_1 M - m_2) \\
&\times \langle N' R' \quad M' - m_2' - m_1' | NR \quad M - m_2 - m_1 \rangle \langle j_1' m_1' | \langle j_2' m_2' | H_{12} | j_2 \quad m_2 \rangle | j_1 m_1 \rangle \quad (35)
\end{aligned}$$

which is diagonal in the core states $|NR \quad M - m_2 - m_1\rangle$. The interaction H_{12} must be a scalar and it is reasonable to write it as a sum of scalar products of two irreducible tensor operators, of the form

$$H_{12} = \sum_k \sum_K V_k (-)^K T_k^{-K}(1) T_k^K(2) \quad (36)$$

where the operator $T_k^{-K}(1)$ acts only on the co-ordinates of particle 1, and $T_k^K(2)$ acts only on the co-ordinates of particle 2. The parameter V_k describes the strength of the interaction. The matrix element in (35) can then be written

$$\begin{aligned}
& \sum_k V_k \frac{1}{\hat{j}_1' \hat{j}_2'} \langle j_1' || T_k(1) || j_1 \rangle \langle j_2' || T_k(2) || j_2 \rangle \\
& \times \sum_K (-)^K (j_1 k; m_1 - K | j_1' \quad m_1') (j_2 k; m_2 \quad K | j_2' m_2') \quad (37)
\end{aligned}$$

As before, the sum of six Clebsch-Gordan coefficients can be reduced using Racah algebra, and the result for H_{12} is

$$\delta_{ll'} \delta_{MM'} \sum_{NR} \sum_k V_k B^{\alpha_1' *} (NR j_1' J_1') B^{\alpha_1} (NR j_1 J_1) \langle j_1' || T_k(1) || j_1 \rangle$$

$$\begin{aligned}
& \times \langle j_2' || T_k(2) || j_2 \rangle (-)^k \hat{J}_1 \hat{J}_1' W(k j_1 J_1' R; j_1' J_1) \\
& \times W(J_1 k 1 j_2'; J_1' j_2) \quad (38)
\end{aligned}$$

A common choice for the residual interaction is a δ -function

$$H_{12} = V_0 \delta(\vec{r}_1 - \vec{r}_2) \quad (39)$$

It is more convenient to calculate the matrix elements of the δ -function interaction directly, since the multipole expansion contains an infinite number of terms. The result for H_{12} is

$$\begin{aligned}
& V_0 F_0 \delta_{NN'} \delta_{RR'} \delta_{II'} \delta_{MM'} \sum_{NR} \sum_{j_1 j_1'} B^{*\alpha_1'}(NR j_1' J_1') B^{\alpha_1}(NR j_1 J_1) \\
& \sum_L \hat{J} \hat{J}' \hat{j}_1 \hat{j}_1' \hat{j}_1 \hat{j}_2 \hat{j}_2' W(R j_1' 1 j_2'; J_1' L) W(R j_1 1 j_2; J_1 L) \\
& \times (j_1' j_2'; \frac{1}{2} - \frac{1}{2} | L 0) (j_1 j_2; \frac{1}{2} - \frac{1}{2} | L 0) \\
& F_0 = \frac{1}{4\pi} \int dr \frac{1}{r^2} R_{n_1' \ell_1'}^*(r) R_{n_2' \ell_2'}^*(r) R_{n_1 \ell_1}(r) R_{n_2 \ell_2}(r) \quad (40)
\end{aligned}$$

We again assume that the radial integral F_0 is independent of the quantum numbers n and ℓ and the strength of the δ -function interaction is described by the parameter

$$\eta \equiv V_0 F_0 \quad (41)$$

III PROGRAM DESCRIPTION

A) ONE PARTICLE CALCULATIONS

For one particle calculations, the parameters of the model are the phonon energy ($\hbar\omega$), the maximum number of phonons N , the single particle orbitals (ℓ, j), the single particle energies (ϵ_j), the total spin (I) and the coupling strength (ξ).

For each set of input data, the program first sets up a matrix describing all possible basis states, composed of all core states with N phonons or fewer, coupled to one of the single particle orbitals. This matrix is printed, with an identification number l for each basis state. For each total spin value l , the program scans the list of all basis states, and picks out those which can give rise to a state of spin l . Using this subset of basis states, the program then calculates the diagonal matrix elements, and the off-diagonal matrix elements (19) for $\xi = 1.0$. Finally, for each value of the interaction strength ξ , the program sets up the total Hamiltonian matrix, and diagonalizes it to find the eigenvalues and eigenvectors.

Output from the program begins with the matrix of basis states mentioned above. For each total spin value, a list of the identification numbers (l) of the subset of basis states used for the matrix is printed. Finally, for each ξ value, the eigenvalues are printed, along with the expansion coefficients $A^E(NRjl)$ of Eq. (14), if desired. The format of the output is self-explanatory.

The program also has the option of writing the results on unit 7, which is normally the card punch. This allows the results of a calculation to be used as input to another program. If this option is in effect, every calculation (specified by a total spin l and a coupling strength ξ) is assigned an identification number KM , which is printed just before the eigenvalues.

B) TWO PARTICLE CALCULATIONS

For two particles, the parameters describing the calculation are the single particle orbitals and energies of particle 2, the coupling

strength ξ_2 , the total spin I , the form and parameters of the two particle residual interaction, and the energies and expansion coefficients of the one-particle states (14), which in turn depend on the parameters listed in Sect. A.

The parameters of the one-particle states can be obtained from the punched output (on unit 7) from the one-particle calculation. The format is such that no rearrangement of these cards is required, and they may be used exactly as they are for input.

It is generally not necessary to use all of the one-particle eigenstates as basis states. Those which are required are indicated in the following manner.

One first indicates to the program how many data sets (each of which contains all of the eigenvectors for a given spin and ξ) it will be required to search. For each of these data sets, one then indicates the identification number (KM) for that data set, and how many (NBASE) states are to be included. The lowest (in energy) NBASE eigenvectors for this spin will be used. The only restrictions are that the list of identification numbers KM must be in increasing order (since it is not possible to backspace the input unit), and that the total number of one-particle states ($\sum \text{NBASE}$) must not exceed 40. Note that the eigenvalues and eigenvectors are read from input unit 4.

After all the data has been input, the calculations proceed in the same manner as for the one-particle case, and the output is identical in format.

IV PROGRAM INPUT

Excluding the input from unit 4 discussed above, all other input to the program comes from unit 5 (generally the card reader). The input cards are in the form

```
IC,(DUM(J), J=1,7)      FORMAT (I2,8X,7F10.0).
```

IC is a (two digit) control integer, specifying the meaning to be attached to the dummy variables DUM, and perhaps also specifying the data to be entered on the succeeding cards. Table XIII contains a list of the options.

All of the input data is remembered by the program. That is, all of the data associated with a certain value of IC, once it has been entered, will be used in all further calculations, until another card with the same value of IC is read.

All input data is copied to the line printer. At the end of each input data set (indicated by an IC = 10 card), the current values of all relevant parameters are checked for obvious errors. If any errors are found, the calculations are aborted, and the program returns to get more input. This process continues until no errors are found in the current data values, at which time calculations proceed.

V HELPFUL HINTS

1) Although it is possible to make unit 7 the card punch and unit 4 the card reader, this procedure is not recommended. It is easier (and safer) to assign these units to a magnetic tape or disc file.

2) For the two particle residual interaction (Eq.(36)), the form of the tensor operators $T_k(1)$ and $T_k(2)$ has not been specified in the current version of the program. This can be done by modifying the function subprograms T1K(K) and T2K(K) such that for a given value of K, T1K returns the value of the reduced matrix element $\langle j_1' || T_k(1) || j_1 \rangle$ and T2K returns the value $\langle j_2' || T_k(2) || j_2 \rangle$.

REFERENCES

- Ch 54 D.C. Choudhury, Matt. Fys. Medd. Dan. Vid. Selsk. 28, No. 4 (1954)
- Ch 67 D.C. Choudhury and T.F. O'Dwyer, Nucl. Phys. A93 (1967) 300
- Dw 67 T.F. O'Dwyer, Ph. D. Thesis, Polytechnic Institute of Brooklyn (1967) unpublished
- Sh 63 A. de Shalit and I. Talmi, Nuclear Shell Theory (Academic Press, New York) (1963)

TABLE XII

Reduced matrix elements for the boson
creation operators.

N	R	N'	R'	$(\langle NR b^\dagger N'R' \rangle)^2$
1	2	0	0	5
2	0	1	2	2
2	2	1	2	10
2	4	1	2	18
3	2	2	0	7
3	0	2	2	3
3	2	2	2	20/7
3	3	2	2	15
3	4	2	2	99/7
3	2	2	4	36/5
3	3	2	4	* 6
3	4	2	4	90/7
3	6	2	4	39

* The presence of an asterisk preceding a number indicates that the reduced matrix element is given by the negative square root of that number.

TABLE XIII

Input Cards for CUPPLE - I

IC	DUM(J) J = ?	NAME	REMARKS
-1	-	-	Causes program to exit
0	-	-	Ignored
01	-	-	The remainder of this card is ignored. The program then expects a card containing a descriptive TITLE in (20A4) format.
02	1	IWHICH	IWHICH = 1 for one particle calculations IWHICH = 2 for two particle calculations <u>FOR IWHICH = 1</u>
	2	NFONON	Maximum number of phonons $0 \leq \text{NFONON} \leq 3$
	3	EFONON	The phonon energy $\hbar\omega$ (MeV) <u>FOR IWHICH = 2</u>
	2	NSET	The number of data sets (each containing the eigenvalues and eigenfunctions for core states with a given J_1) which will be read from unit 4. The program then expects NSET data cards, each of which must have IC=0, with the following information on each card.
	1	ID	The data set ID number (KM)
	2	NBASE	The number of states of spin J_1 , to be included as core states. The lowest energy NBASE states will be used.
			Restrictions $1 \leq \text{NSET} \leq 10$ $\sum_i \text{NBASE}_i \leq 40$

IC	DUM(J) J = ?	NAME	
03	1	NPART	The number of single particle orbitals allowed for the particle ($1 \leq \text{NPART} \leq 4$) The program then expects NPART data cards, each with IC=0, containing the following information for each orbital.
	1	N1(I)	The radial quantum number n_i
	2	PARTL(I)	The orbital angular momentum ℓ_i
	3	PARTJ(I)	The total angular momentum $j_i = \ell_i \pm \frac{1}{2}$
	4	PARTE(I)	The single particle energy ϵ_i
04	1	XIMIN	The minimum value for the coupling strength ξ
	2	XISTP	The increment in ξ
	3	XIMAX	The maximum value of ξ
			Calculations for each spin will be done for values of ξ from XIMIN to XIMAX, in increments of XISTP. For one value of ξ only, make XISTP = 0, and XIMIN = XIMAX
05	1	LPUNCH	=1 Results will be punched on cards =0 Punched output will be suppressed
	2	LFULL	Should be 0 always. LFULL = 1,2 provides two levels of full print, which are useful for checking out the program, but should not be used otherwise.
	3	LCOEFF	=1 Print (and punch if LPUNCH = 1) both the eigenvalues and expansion coefficients of the eigenstates. =0 Print (and punch) only eigenvalues
	4	KMSTRT	Only needed if LPUNCH = 1. The starting ID number for punched output. Subsequent data sets are numbered sequentially.
	5	MAXDIA	Maximum number of diagonalizations
	6	MAXRNK	The maximum matrix rank (≤ 50)

IC	DUM(J) J = ?	NAME	REMARKS
06	1	KLIMIT	For IWHICH = 2 only. The two particle residual interaction is taken as a multipole expansion, and terms up to and including $k = \text{KLIMIT}$ are to be considered. $0 \leq \text{KLIMIT} \leq 6$.
	2	VPN(1)	V_k for $k = 0$
	3	VPN(2)	V_k for $k = 1$ etc.
07	1	NSPIN	Number of total spin value l for which calculations will be done. $1 \leq \text{NSPIN} \leq 6$
	2	RSPIN(1)	First l -value
	3	RSPIN(2)	Second l -value etc.
08	1	XDELT	For IWHICH = 2 only. The two particle interaction is taken as a delta function. This entry is the parameter $\eta = V_0 F_0$ describing the strength of this interaction.
09	-		Not used
10	-		End of input. Check the current value of all parameters, and if no errors are found, begin calculation.

B30073